INTERACTION NOTES

NOTE 474

MARCH 1989

Equivalent Polarizabilities of Apertures with Depth

Larry K. Warne, Terry E. Koontz, and Kenneth C. Chen

Sandia National Laboratories, Albuquerque, NM 87185

ABSTRACT

Simple approximate formulas are given for the equivalent polarizabilities of a narrow slot aperture having depth. The length of the slot is assumed to be much larger than its width. The special case, where the length is also much larger than the slot depth, is treated by means of an equivalent antenna radius. This equivalent antenna radius is shown to be useful in describing not only the dominant axial polarizability but also the transverse polarizabilities. The equivalent antenna radius is also shown to generalize existing polarizability formulas for hatch–type apertures. Approximate formulas for the slot aperture are also constructed which hold for all depths. Simple, somewhat heuristic, arguments are initially used to derive the approximate polarizability formulas. A more rigorous derivation follows along with numerical calculations and comparisons.

I. INTRODUCTION

Equivalent polarizabilities of apertures in an infinitesimally thin conducting plane have been widely used in the EMP community to treat aperture penetration problems [1]. The aperture dimensions are assumed to be small compared to the wavelength. The finite thickness of the conducting plane (aperture depth) has a large effect on these polarizabilities if it is larger than one of the aperture dimensions. The effect of aperture depth will be illustrated for slot apertures in this paper.

The paper, for the most part, concentrates on the rectangular slot aperture of length $\ell = 2h$, depth d, and width w, such that

$$\ell >> w \ . \tag{1}$$

The Thick case implies that the added condition,

$$\ell >> d \ , \tag{2}$$

also holds. The Thick case can be treated by introducing an equivalent antenna radius of the slot [2]. The equivalent antenna radius is also useful in describing the transverse polarizabilities of the slot [3]. A brief derivation of the axial magnetic polarizability, for the Thick case, is given in Sections II – V.

Sections II and VI give a brief derivation of the transverse polarizabilities.

Section V discusses the use of the equivalent radius in existing hatch aperture polarizability formulas to incorporate depth for the Thick case.

Sections VII through X discuss the Deep case

$$\ell, d >> w \quad . \tag{3}$$

Approximations for the axial magnetic polarizability are constructed which are actually shown to hold for

$$0 \leq d < \infty \quad . \tag{4}$$

Polarizabilities at both the incident side and transmitted side of the slot are constructed throughout.

II. HEURISTIC DERIVATION OF POLARIZABILITIES FOR THE THICK CASE

The axial magnetic polarizability is now estimated for the Thick case. Consider. first, the case where the depth is zero. Figure 1 depicts the electric surface current on the incident side, $y < 0$, of the slot. The short circuit magnetic field on the surface is assumed to be polarized in the axial direction H_z^{sc}. The radius ρ_o is defined such that

$$\frac{w}{2} << \rho_o << \ell \ . \tag{5}$$

An approximate transmission line circuit model can be constructed to describe the voltage along the slot as shown in Figure 2. The x component K_x^{sc} of the short circuit surface current density,

$$\underline{K}^{sc} = \underline{n} \times \underline{H}^{sc} \ , \tag{6}$$

acts as the distributed source. The distributed inductance per unit length of the slot is given approximately by

$$L \approx \frac{1}{4}\left[\frac{2\pi\mu_o}{\ell n(\frac{\ell}{w/4})}\right] \ . \tag{7}$$

A heuristic explanation of (7) is now given. Figure 1 shows that the short circuit surface current is diverted by the slot, so that locally (closer than a distance ρ_o) it flows axially around the slot. From a heuristic point of view, all of the diverted surface current can be taken to flow axially within a chosen outer radius of the order of the slot length. The appropriate questions then become: how can the inductance per unit length be determined, and what is the proper choice of outer radius?

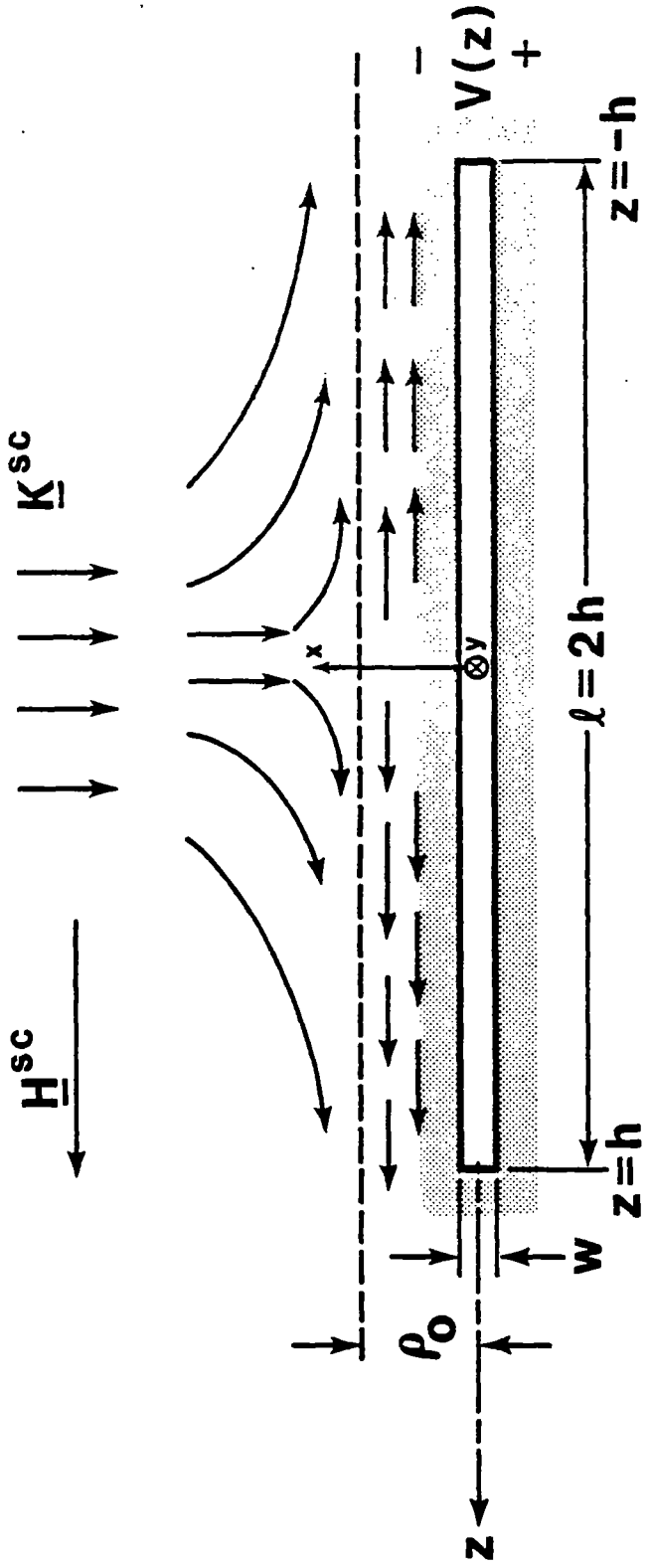

Figure 1. Low frequency electric surface current on the incident side of a narrow slot in a Thin perfectly conducting plane.

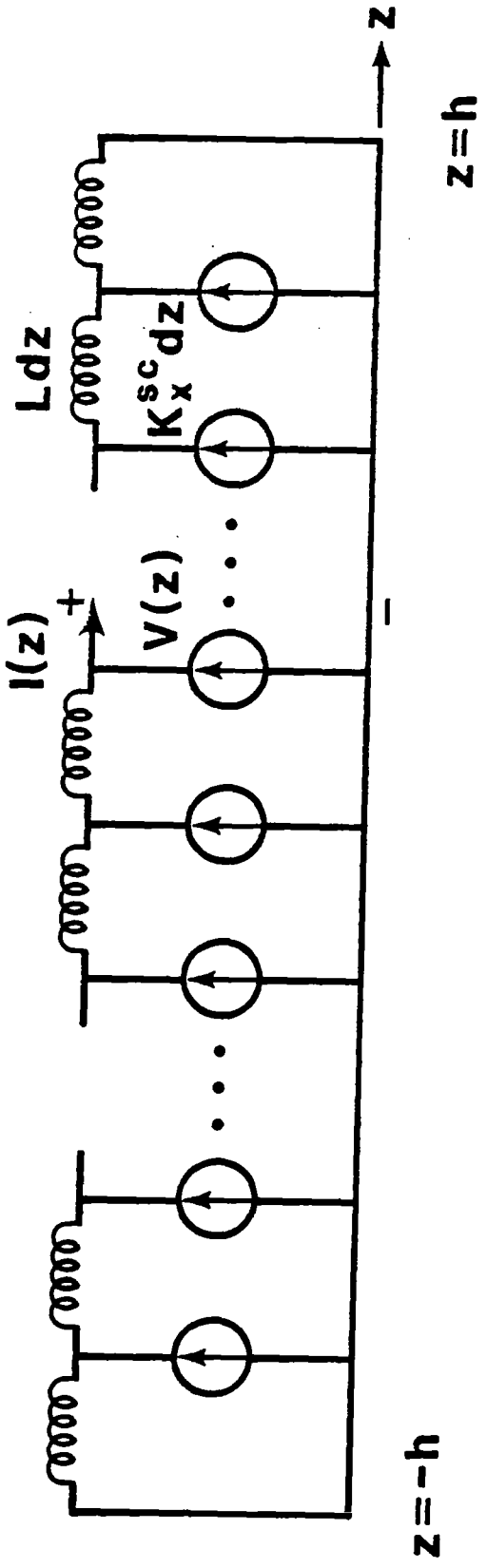

Figure 2. Low frequency transmission line model for slot voltage and axial current.

The inductance per unit length can be found by consideration of Figure 3. The quantity in brackets in (7) is the capacitance per unit length, with $\epsilon_o \to \mu_o$, of a coax of outer radius ℓ and inner radius w/4 (see Figure 3). The factor of one quarter in (7) arises from the relations between the electric and magnetic problems shown in Figure 3 (this is of course the usual factor arising in Babinet's principle). Note that the magnetic field which leaves the slot at position z reenters the slot at position $-z$. This heuristic picture takes the magnetic field leaving the slot (magnetic conductor at inner equivalent radius w/4) at position z to be purely radial, terminating on a perfect magnetic conductor at the outer radius of order ℓ. The return field is purely radial inward (from this outer magnetic conductor to the inner equivalent radius) at position $-z$.

The inner radius w/4 is, of course, the usual equivalent radius of a slot aperture in a Thin plane (or a conducting strip of width w). The outer radius ℓ is of correct order but is nevertheless somewhat arbitrary. This choice of outer radius corresponds to the zero order Hallén solution of the integral equation for the slot [2] (As is well known, and will be seen in section V, this choice of outer radius is somewhat too large, giving too small an inductance (7) and thus too small a polarizability.).

If the slot is shorted at its center, the Norton equivalent current in the x direction is

$$I^{sc} = h\, K_x^{sc} = -h\, H_z^{sc} \quad . \tag{8}$$

The Norton equivalent inductance of the slot at its center is

$$L_{slt} = L\, h\, \frac{1}{2} \quad , \tag{9}$$

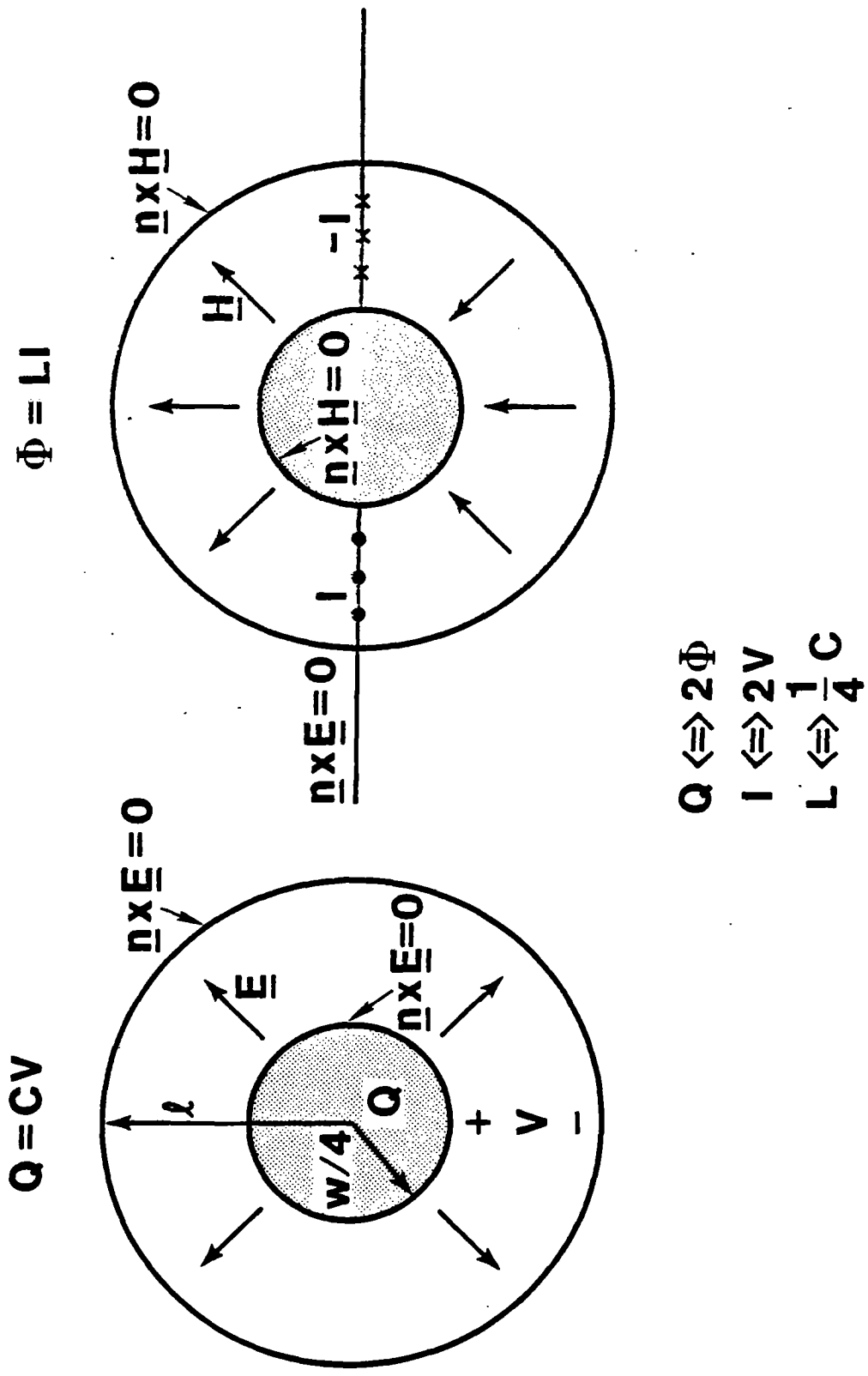

Figure 3. Transverse electrostatic field in a coax and approximate complementary magnetostatic field in the slot cross section with heuristic outer magnetic conductor.

where the factor of one half accounts for the parallel combination of the two inductances (inductance from $-h < z < 0$ and inductance from $h > z > 0$).

The center voltage is given by (time convention $e^{-i\omega t}$ is used throughout)

$$V(0) = -i\omega L_{slt} I^{sc} \quad . \tag{10}$$

Note that by use of Faraday's law, $V(0)/(-i\omega)$ equals the total magnetic flux passing through half the slot ($h > z > 0$) in the positive y direction Φ_{tot}.

The slot inductance per unit length (7) can be written as the parallel combination

$$L = \frac{1}{1/L_{dist} + 1/L_{near}} \quad , \tag{11}$$

where

$$L_{near} \approx \frac{1}{4} \frac{2\pi\mu_o}{\ell n(\frac{\rho_o}{w/4})} \tag{12}$$

and

$$L_{dist} \approx \frac{1}{4} \frac{2\pi\mu_o}{\ell n(\frac{\ell}{\rho_o})} \tag{13}$$

are the inductances per unit length of the near or local region (inside ρ_o) and the distant or nonlocal region (outside ρ_o). Note that the heuristic nature of (7) results from the heuristic nature of (13). The local contribution (12) is rigorously meaningful because the current is flowing axially when ρ_o is sufficiently small compared to ℓ.

When the depth is not zero, the radius ρ_o is introduced in each half space as shown in the cross section of Figure 4. Figure 5 illustrates the added parallel interior branch for current flow. The slot inductance per unit length now becomes

$$L = \frac{1}{1/L_{dist} + 1/L_{near} + 1/L_{intr}} , \tag{14}$$

where the interior inductance per unit length is

$$L_{intr} \approx \frac{w}{d} \mu_o . \tag{15}$$

The interior inductance (15) has been taken as approximately the uniform field result. The exterior contributions (12) and (13) have been taken as approximately the Thin slot values.

The result (14) may also be written as

$$L \approx \frac{1}{4} \left[\frac{2\pi\mu_o}{\ell n(\ell/a)} \right] , \tag{16}$$

where

$$a \approx \frac{w}{4} e^{-\frac{\pi d}{2w}} . \tag{17}$$

Note that the heuristic quantity L_{dist} does not influence the choice of the equivalent radius (17), and because of this, (17) is rigorous. The approximate symbol in (17) has been used to denote the fact that the small fringing corrections near the edges of the slot, for $d > 0$, have not been included.

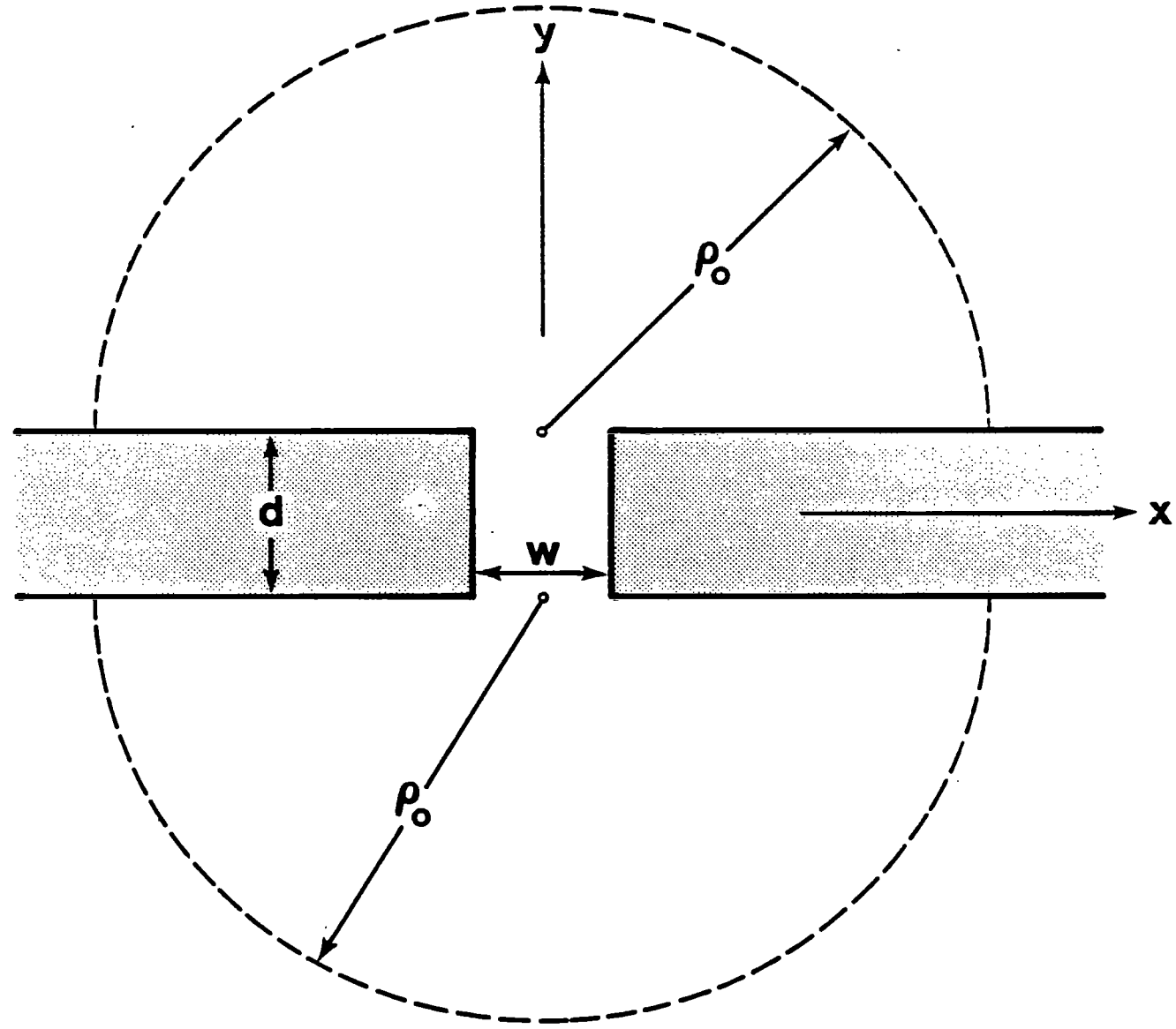

Figure 4. Cross section of a narrow slot in a Thick plane. The quantity $\rho_o >> d,w$ defines the boundary between the local and nonlocal regions.

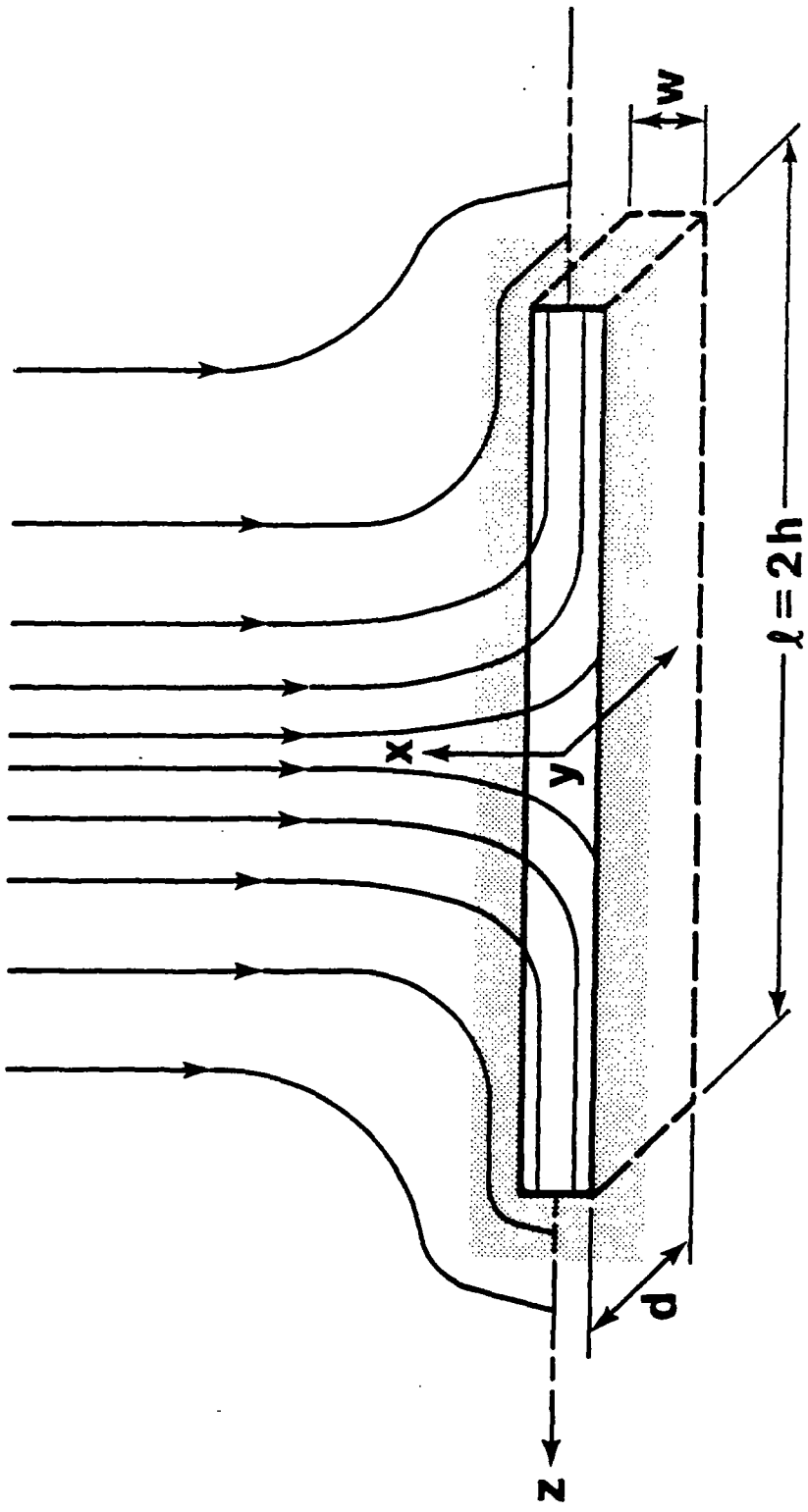

Figure 5. Low frequency electric surface current on the incident side (and interior) of a narrow slot in a Thick perfectly conducting plane.

The magnetic field of the aperture can be determined from

$$\underline{H} = -\nabla\varphi_m \ , \tag{18}$$

where for a magnetic dipole (in the far zone of the aperture r >> h) the magnetic scalar potential is given by

$$\varphi_m = \frac{\underline{m} \cdot \underline{r}}{4\pi r^3} \ . \tag{19}$$

The magnetic dipole moment $\underline{m}$ is given in terms of the magnetic polarizability by

$$\underline{m} = -2\, \underline{\alpha}_m \cdot \underline{H}^{sc} \ , \tag{20}$$

where $\underline{H}^{sc}$ is the short circuit magnetic field at the aperture. The relation (20) is used on the shadow or transmitted side of the aperture. The minus sign in (20) is dropped on the illuminated or incident side of the aperture.

The magnetic dipole moment can be found from the magnetic charge density ρ_m as

$$\underline{m} = \frac{1}{\mu_o} \int_V \underline{r}\, \rho_m \, dV \ , \tag{21}$$

where $\underline{r}$ is the position vector and the volume V contains the magnetic charge. Applying (21) to the transmitted or shadow side of the slot it becomes

$$m_z = \frac{1}{\mu_o} \int_{-h}^{h} z \cdot q_m^+(z)\, dz \ , \qquad (22)$$

where $q_m^+(z)$ is the equivalent magnetic charge per unit length on the y = + d/2 side of the aperture. This magnetic charge can be determined from the voltage along the slot V(z) by means of

$$\frac{dV}{dz} = i\omega \frac{1}{2} q_m^+ \ , \qquad (23)$$

where the factor of one half arises from the fact that q_m^+ is defined so as to include the image charge in the ground plane at y = + d/2. Equation (23) can be found by applying Faraday's law to a closed contour of length dz and width w on the y = + d/2 face of the slot. The voltage distribution from Figure 2 is given by

$$V(z) = V(0)(1 - z^2/h^2) \ . \qquad (24)$$

Using (20), (22), (23), and (24) we obtain

$$\alpha_{m,zz} \approx \frac{\ell^2}{3\mu_o} L_{slt} \approx \frac{\pi \ell^3}{24\ \ell n(\ell/a)} \ , \qquad (25)$$

where (9) and (16) have been used to define L_{slt}.

The axial polarizability in the Thick case can also be determined from existing formulas for the Thin (d = 0) case. For example, an approximation for the axial polarizability component $\alpha_{m,zz}$ due to a slot aperture in a Thin plane (d = 0) can be found [1] as

$$\alpha_{m,zz} \approx \frac{\pi}{24} \frac{\ell^3}{\ell n(4\ell/w) - 1} \cdot \tag{26}$$

To obtain a slightly more accurate approximation than (25) for the axial polarizability of a slot in a Thick plane we simply replace w/4 in (26) by the equivalent radius (17). yielding

$$\alpha_{m,zz} \approx \frac{\pi}{24} \frac{\ell^3}{\ell n(\ell/a) - 1} \cdot \tag{27}$$

The axial polarizability, (25) or (27), holds approximately on both sides of the aperture in the Thick case.

The electric field of the aperture can be determined from

$$\underline{E} = -\nabla\varphi \ , \tag{28}$$

where for an electric dipole (in the far zone of the aperture r >> h) the electric scalar potential is given by

$$\varphi = \frac{\underline{p} \cdot \underline{r}}{4\pi\epsilon_o r^3} \cdot \tag{29}$$

The electric dipole moment $\underline{p}$ is given in terms of the electric polarizability by

$$\underline{p} = 2\,\epsilon_o\,\underline{\alpha}_e \cdot \underline{E}^{sc} \ , \tag{30}$$

where $\underline{E}^{sc}$ is the short circuit electric field at the aperture. The relation (30) is used on

the shadow or transmitted side of the aperture. A minus sign is introduced on the right of the equals sign in (30) on the illuminated or incident side of the aperture.

The transverse components of the polarizability tensors $\alpha_{m,xx}$ and $\alpha_{e,yy}$ for the slot will now be estimated. The transverse components for a Thin plane (d = 0) are given [1] by

$$\alpha_{m,xx} = \alpha_{e,yy} = \frac{\pi}{16} w^2 \ell \ . \tag{31}$$

The result (31) may be viewed on a per unit length basis. The end effects may be ignored and the problem treated as two dimensional in the slot cross section. The polarizability per unit length of the slot (or line polarizability) is $\frac{\pi}{16} w^2$. The magnetic and electric scalar potentials satisfy Laplace's equation

$$\nabla^2(\varphi_m, \varphi) = 0 \ . \tag{32}$$

Interior to the slot $(-\frac{d}{2} < y < \frac{d}{2})$ the potentials satisfy the boundary conditions

$$\frac{\partial}{\partial x}\varphi_m^< = 0 \ , \ x = \pm \frac{w}{2} \ , \tag{33}$$

$$\frac{\partial}{\partial y}\varphi^< = 0 \ , \ x = \pm \frac{w}{2} \ , \tag{34}$$

where $\varphi_m^<$ and $\varphi^<$ denote the potentials interior to the slot. The appropriate solutions thus take the form

$$\varphi_m^< = \sum_{n=1}^{\infty} A_n \cos\frac{n\pi}{w}(x + w/2)\, e^{\pm \frac{n\pi}{w} y} \ , \tag{35}$$

$$\varphi^{<} = \sum_{n=1}^{\infty} B_n \sin\frac{n\pi}{w}(x + w/2)\, e^{\pm \frac{n\pi}{w} y} \quad . \qquad (36)$$

(Actually only the n odd terms will be present due to the symmetry of the slot and the short circuit fields about x = 0). The interior solutions $\varphi_m^{<} = A_o y$ and $\varphi^{<} = B_o x$ are excluded at every z location by the transverse nature of the incident fields and the symmetry of the slot about x = 0 (this symmetry is needed to rule out end contributions). The transverse polarizabilities are therefore expected to exhibit an exponential decay $e^{-\frac{\pi}{w}d}$ on the shadow or transmitted side of the slot relative to the illuminated or incident side. Furthermore, if a sketch is made of the transverse field lines near the incident face of the slot, it is clear that presence of the depth gives rise to only a slight decrease in the scattered fields or the dipole moments (contrary to the axial or longitudinal case where there is a large decrease in the axial dipole moment). The following approximate formulas thus appear reasonable

$$\alpha^{-}_{m,xx} = \alpha^{-}_{e,yy} \approx \pi \left(\frac{w}{4}\right)^2 \ell \ , \text{ incident side} \ , \qquad (37)$$

$$\alpha^{+}_{m,xx} = \alpha^{+}_{e,yy} \approx \pi \left[\frac{w}{4} e^{-\frac{\pi d}{2w}}\right]^2 \ell \ , \text{ transmitted side} \ . \qquad (38)$$

The formula (38) is, perhaps, better justified by the rigorous relation [3] between the equivalent antenna radius and the transverse dipole moments of a narrow slot aperture having depth

$$\alpha^{+}_{m,xx} = \alpha^{+}_{e,yy} = \pi a^2 \ell \ , \qquad (39)$$

where the polarizabilities in (39) are those on the transmitted side of the aperture, and

the approximate result (17) can be used for a. The approximation (37), on the incident side, and (38), on the transmitted side, will be rigorously justified later in this paper.

III. INTEGRAL EQUATION FOR MAGNETIC CHARGE PER UNIT LENGTH IN THICK CASE

A somewhat more general derivation [2] of the integral equation, for the magnetic charge per unit length at the faces of a slot in a Thick plane, is now given.

The static magnetic field can be determined from the Maxwell equations

$$\nabla \times \underline{H} = 0 \ , \tag{40}$$

$$\nabla \cdot \underline{B} = \rho_m \ , \tag{41}$$

and the constitutive relation

$$\underline{B} = \mu_o \underline{H} \ , \tag{42}$$

where ρ_m is again the magnetic volume charge density. Equation (40) implies that the magnetic field can be determined from a scalar potential (18). Substituting (18) into (41) and (42) yields a Poisson equation for φ_m with solution

$$\varphi_m(\underline{r}) = \frac{1}{\mu_o} \int_V \frac{\rho_m(\underline{r}')}{4\pi |\underline{r} - \underline{r}'|} dV' \ . \tag{43}$$

The slot faces at $y = \pm \frac{d}{2}$ can be shorted provided that the appropriate amount of surface magnetic charge σ_m is placed on the conductors by means of

$$\sigma_m = \underline{n} \cdot (\underline{H}_2 - \underline{H}_1) \ . \qquad (44)$$

The unit vector $\underline{n}$ is normal to the surface between regions 1 and 2 and points from 1 to 2.

The boundary ρ_o shown in Figure 4 partitions the region surrounding the metal into local ($\rho < \rho_o$) and nonlocal ($\rho > \rho_o$) regions. The magnetic scalar potential in the nonlocal exterior region is given approximately by

$$\varphi_m^{>}(\rho,z) = \frac{1}{\mu_o} \int_{-h}^{h} \frac{q_m^{\pm}(z')}{4\pi R} dz' \ , \ y \gtrless \pm \frac{d}{2} \ , \qquad (45)$$

where $R = \sqrt{\rho^2 + (z - z')^2}$, ρ and z are the usual cylindrical coordinates measured from the center of each slot face ($x = 0$, $y = \pm \frac{d}{2}$), $q_m^{\pm}$ is the total magnetic charge per unit length at each of the two slot faces (note that $q_m^{\pm}$ is assumed to include the image magnetic charge in the conducting plane at $y = \pm \frac{d}{2}$), and $\varphi_m^{>}$ denotes the exterior nonlocal potential.

An axial magnetic field H_z^{inc} is assumed to impinge on the slot from the half space $y < -\frac{d}{2}$. If the slot is shorted, the short circuit field in the incident half space $y < -\frac{d}{2}$ is given by

$$H_z^{sc} = 2\, H_z^{inc} \ . \qquad (46)$$

The integral form of (40) is

$$\oint_C \underline{H} \cdot \underline{d\ell} = 0 \ . \tag{47}$$

Applying (47) to the contour C shown in Figure 6 yields

$$[H_z^{>}(\rho_o^-,z) + H_z^{sc}]\, dz - H_z^{>}(\rho_o^+,z)\, dz + dI_{\rho_o} = 0 \ . \tag{48}$$

The quantity dz is a differential of axial length and dI_{ρ_o} is a differential of local axial current

$$I_{\rho_o} = \int_{C_{\ell cs}} \underline{H} \cdot \underline{d\ell} \ , \tag{49}$$

in the axial direction (the contour $C_{c\ell s}$ is the cross–section part of C with the largest z value in Figure 6). The quantity $H_z^{>}$ is the nonlocal exterior axial magnetic field

$$H_z^{>} = -\frac{\partial}{\partial z} \varphi_m^{>} \ , \tag{50}$$

and the notation $\rho_o^{\pm}$ indicates which particular half space, $y \gtrless \pm \frac{d}{2}$, is being considered.

The Thick case ($\ell >> w,d$) imposes the approximate condition

$$q_m^+(z) \approx -\, q_m^-(z) \ . \tag{51}$$

Using (51) in (45), from (50) we obtain the relation

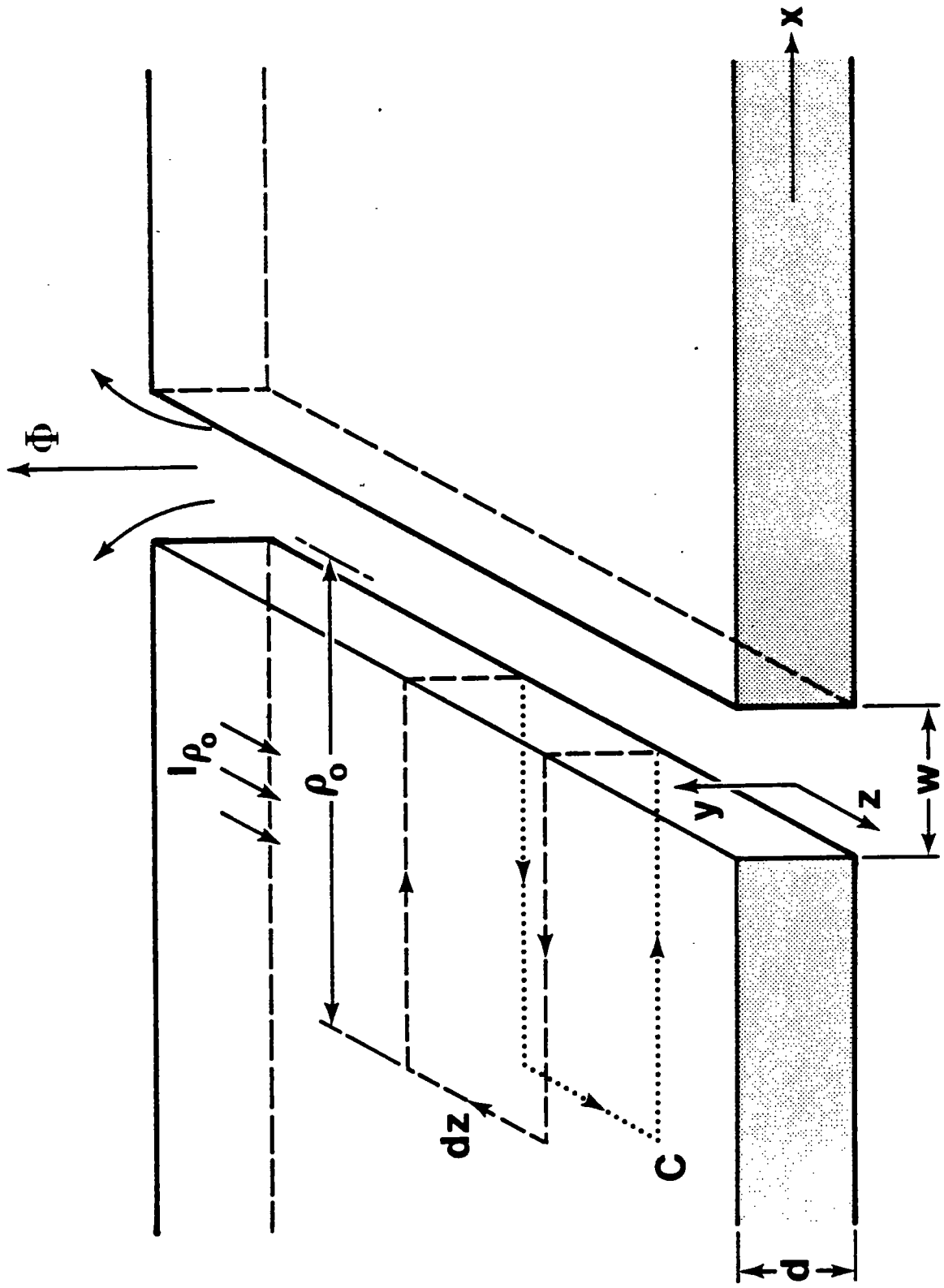

Figure 6. Portion of a Thick slot defining contour C for application of Ampere's law.

$$H_z^{>}(\rho_o^+,z) = -H_z^{>}(\rho_o^-,z) \quad . \tag{52}$$

Inserting (52) into (48), and integrating with respect to z, we obtain

$$\varphi_m^{>}(\rho_o^-,z) - \tfrac{1}{2} I_{\rho_o} = -\varphi_m^{inc}(z) = z\, H_z^{inc} \,, \tag{53}$$

where the integration constant has been dropped because each term in (53) is odd with respect to z (note $q_m^{\pm}(-z) = -q_m^{\pm}(z)$).

The total magnetic flux per unit length in the positive y direction is denoted by $\bar{\Phi}$. where

$$\bar{\Phi}(z) = \pm \tfrac{1}{2} q_m^{\pm}(z) \quad . \tag{54}$$

The local current I_{ρ_o} can be related to the magnetic charge per unit length q_m^{-} by means of the relation

$$L_{\rho_o} I_{\rho_o} = \bar{\Phi} \,, \tag{55}$$

where L_{ρ_o} is the local inductance per unit length.

The local inductance per unit length is taken to have the form

$$L_{\rho_o} = \frac{\pi \mu_o}{2\ \ell n(\rho_o/a)} \,, \tag{56}$$

where a is a constant (the equivalent antenna radius) to be determined.

Let us define

$$R_o = \sqrt{\rho_o^2 + (z - z')^2} \quad . \tag{57}$$

If we exclude the small regions near the ends of the slot ($h - |z| >> \rho_o$), then the following approximations in $\varphi_m^{>}(\rho_o^{-},z)$ can be made:

$$\int_{-h}^{h} \frac{q_m^{-}(z')}{R_o}\, dz' \approx \int_{-h}^{h} \frac{q_m^{-}(z') - q_m^{-}(z)}{|z - z'|}\, dz' + q_m^{-}(z) \int_{-h}^{h} \frac{dz'}{R_o} \quad , \tag{58}$$

$$\int_{-h}^{h} \frac{dz'}{R_o} \approx \ell n[4(h^2 - z^2)] - 2\, \ell n\, \rho_o \quad . \tag{59}$$

Inserting (58), (59), (54), (45), (55), and (56) into (53) gives Hallén's integral equation

$$\frac{1}{\mu_o} \int_{-h}^{h} \frac{q_m(z')}{4\pi R_a}\, dz' = -\varphi_m^{inc}(z) = z\, H_z^{inc} \quad , \tag{60}$$

where $q_m^{-}(z) = q_m(z)$ and $R_a = \sqrt{a^2 + (z - z')^2}$.

IV. EQUIVALENT RADIUS FOR THICK CASE

The equivalent antenna radius will now be evaluated by means of the solution of the magnetostatic field problem in the cross section by conformal mapping. The Schwarz–Christoffel transformation will be used to map the region surrounding the conductors in the $z = x + iy$ plane of Figure 4 to the upper half of a $z_1 = x_1 + iy_1$ plane. The appropriate transformation is [4]

$$z = C_1 \int_1^{z_1} \frac{\sqrt{(1 - z_1^2)(1 - p^2 z_1^2)}}{z_1^2} dz_1 + \frac{w}{2} - i\frac{d}{2} , \tag{61}$$

where the principal branch of each linear factor in the square root is to be taken. The constant p is evaluated by solving the transcendental equation

$$2\frac{d}{w} = -\frac{2\,E(p') - (1 + p^2)K(p')}{2\,E(p) - (1 - p^2)K(p)} , \tag{62}$$

where the complete elliptic integrals of the first and second kinds are defined by

$$K(p) = \int_0^{\pi/2} \frac{d\theta}{\sqrt{1 - p^2 \sin^2\theta}} , \tag{63}$$

$$E(p) = \int_0^{\pi/2} \sqrt{1 - p^2 \sin^2\theta}\, d\theta , \tag{64}$$

and

$$p' = \sqrt{1 - p^2} \ . \tag{65}$$

The constant C_1 can be found from p and

$$\frac{w}{2C_1} = (1 - p^2)K(p) - 2E(p) \ . \tag{66}$$

Figure 7 shows a plot [4] of p and $-C_1/w$. The asymptotic result,

$$p \sim 4/e^{(2 + \pi d/w)} \ , \frac{d}{w} >> 1 \ , \tag{67}$$

is also shown. The parameter p is unity when $d/w = 0$. The quantity $-C_1/w$ ranges between 1/4 when $d/w = 0$ and $1/\pi$ when $d/w = \infty$.

The magnetostatic field may be determined from (18) and the magnetostatic potential

$$\varphi_m = -\frac{1}{\mu_o} \text{Re } W \ , \tag{68}$$

where Re denotes the real part and the complex potential W is given by

$$W = \frac{\overline{\Phi}}{\pi} \ell n(z_1/a_1) \ , \tag{69}$$

where $\overline{\Phi}$ is the magnetic flux per unit length passing through the slot in the positive y direction and a_1 is an arbitrary real constant. Figure 8 shows the local magnetic field distribution.

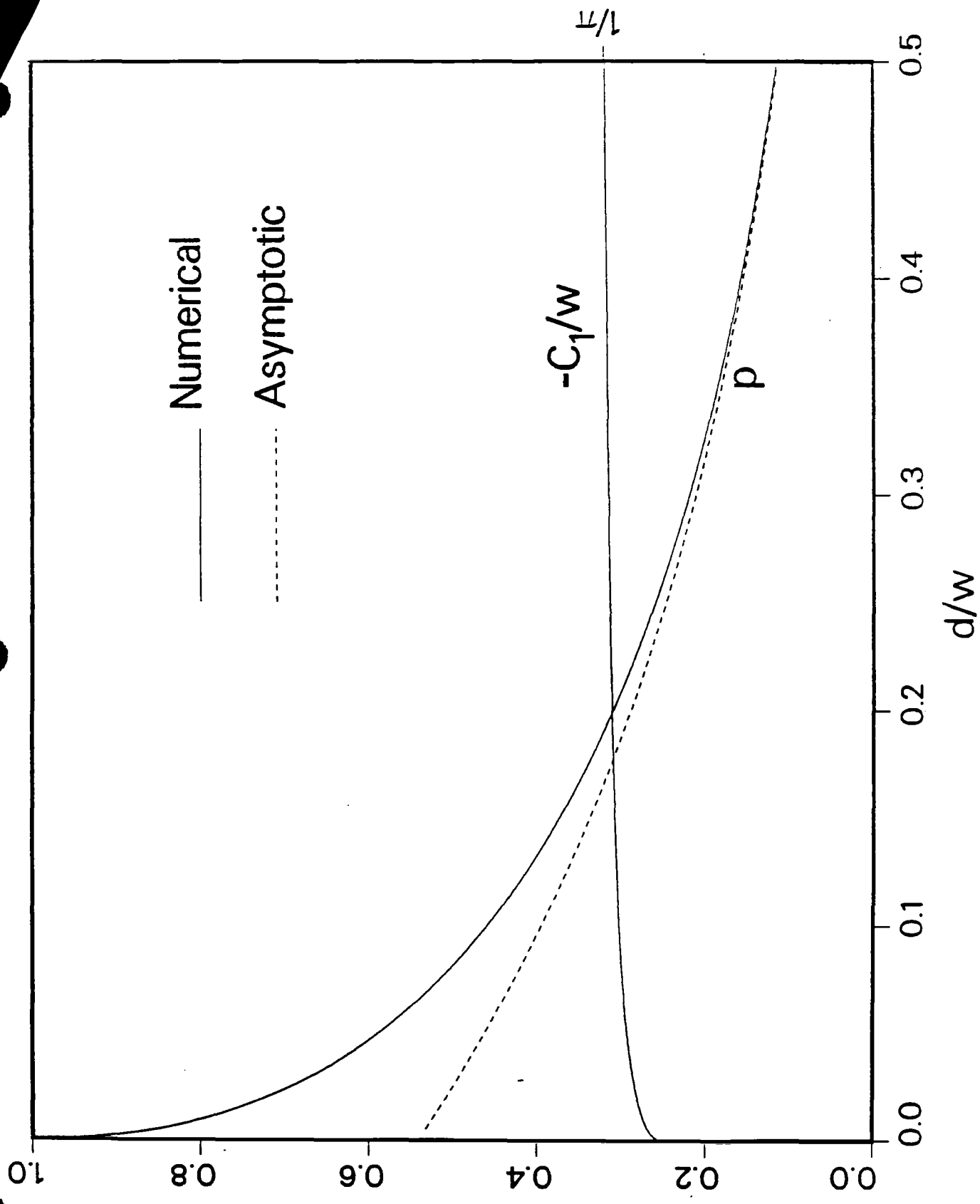

Figure 7. Thick slot conformal mapping parameters p and $-C_1/w$. The solid curves are numerical solutions of the transcendental equation.

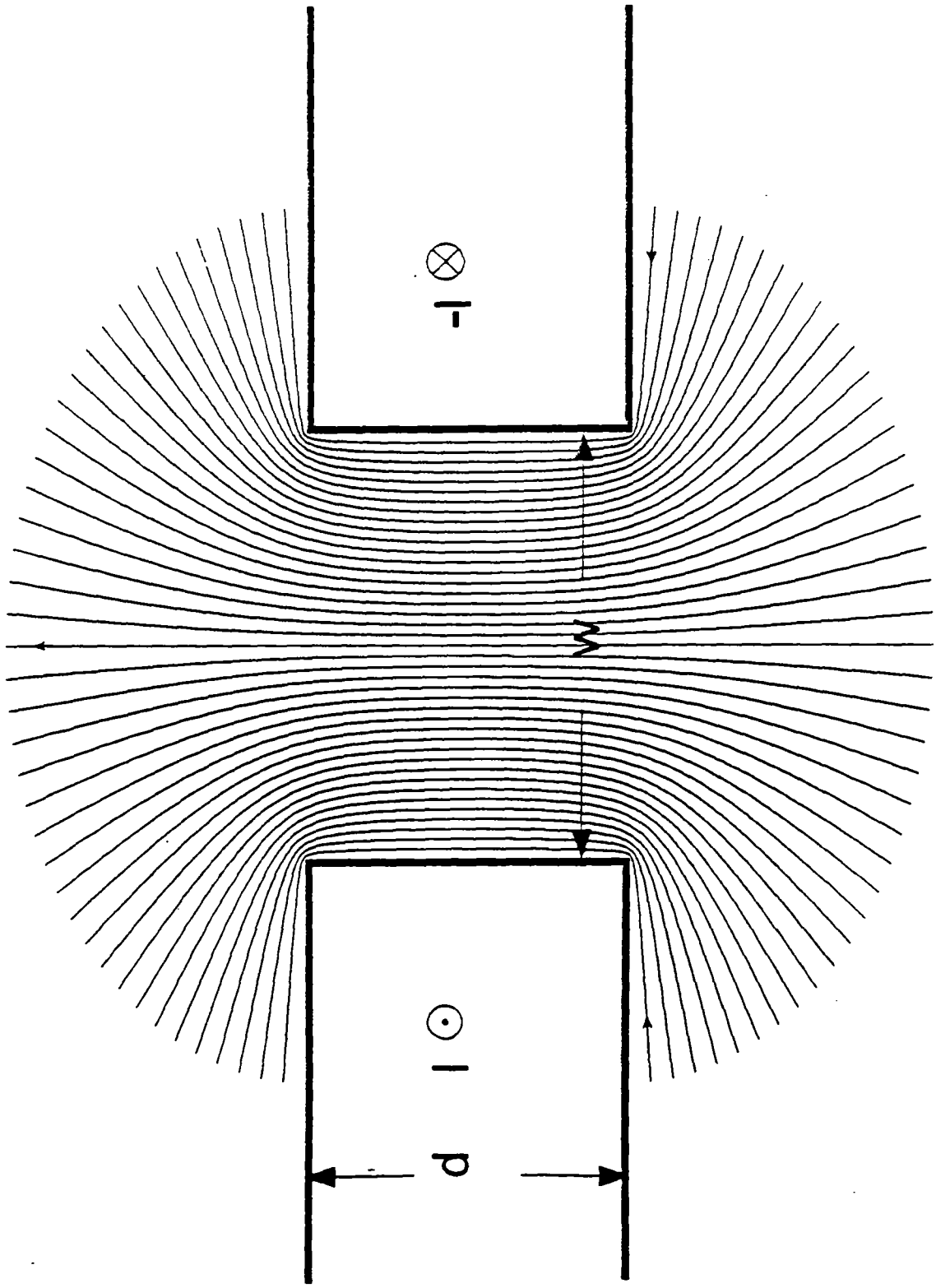

Figure 8. The local magnetostatic field in the cross section of a Thick slot when excited by a longitudinal magnetic field.

From (18), the local current (49) can be written as

$$I_{\rho_o} = -[\varphi_m(z = -\rho_o + i\frac{d}{2}) - \varphi_m(z = -\rho_o - i\frac{d}{2})] \quad . \tag{70}$$

Using (68) and (69), this becomes

$$I_{\rho_o} = \frac{\Phi}{\mu_o \pi} \ell n \left[\frac{z_1(-\rho_o + i\frac{d}{2})}{z_1(-\rho_o - i\frac{d}{2})}\right] \quad . \tag{71}$$

Expanding (61) for $\rho_o >> w$ we obtain the asymptotic forms

$$z_1 \sim \frac{\rho_o}{pC_1} \quad , z = -\rho_o + i\frac{d}{2} \quad , \tag{72}$$

$$z_1 \sim \frac{C_1}{\rho_o} \quad , z = -\rho_o - i\frac{d}{2} \quad . \tag{73}$$

Inserting (72) and (73) into (71) gives

$$I_{\rho_o} = \frac{\Phi}{\mu_o \pi} \ell n \left[\frac{\rho_o^2}{C_1^2 p}\right] \quad . \tag{74}$$

Comparison of (74) with (55) yields the local inductance per unit length (56) with equivalent radius

$$a = -C_1 / \bar{p} \quad . \tag{75}$$

The limiting forms for p and $-C_1/w$ yield the limiting forms for a

$$a \to \frac{w}{4} \ , \frac{d}{w} \to 0 \ , \tag{76}$$

$$a \sim \frac{2}{\pi} w \ / \ e^{(1 + \frac{\pi d}{2w})} \ , \frac{d}{w} >> 1 \ . \tag{77}$$

The approximate form (17) can be obtained by taking the parallel combination of the Thin limit (d = 0, a = w/4) of (56) and the uniform field interior result (15)

$$a \approx \frac{w}{4} e^{-\frac{\pi d}{2w}} \ . \tag{78}$$

Figure 9 shows a comparison between the Very Thick slot (d >> w) field lines and the composite Thin slot exterior field – uniform interior field lines.

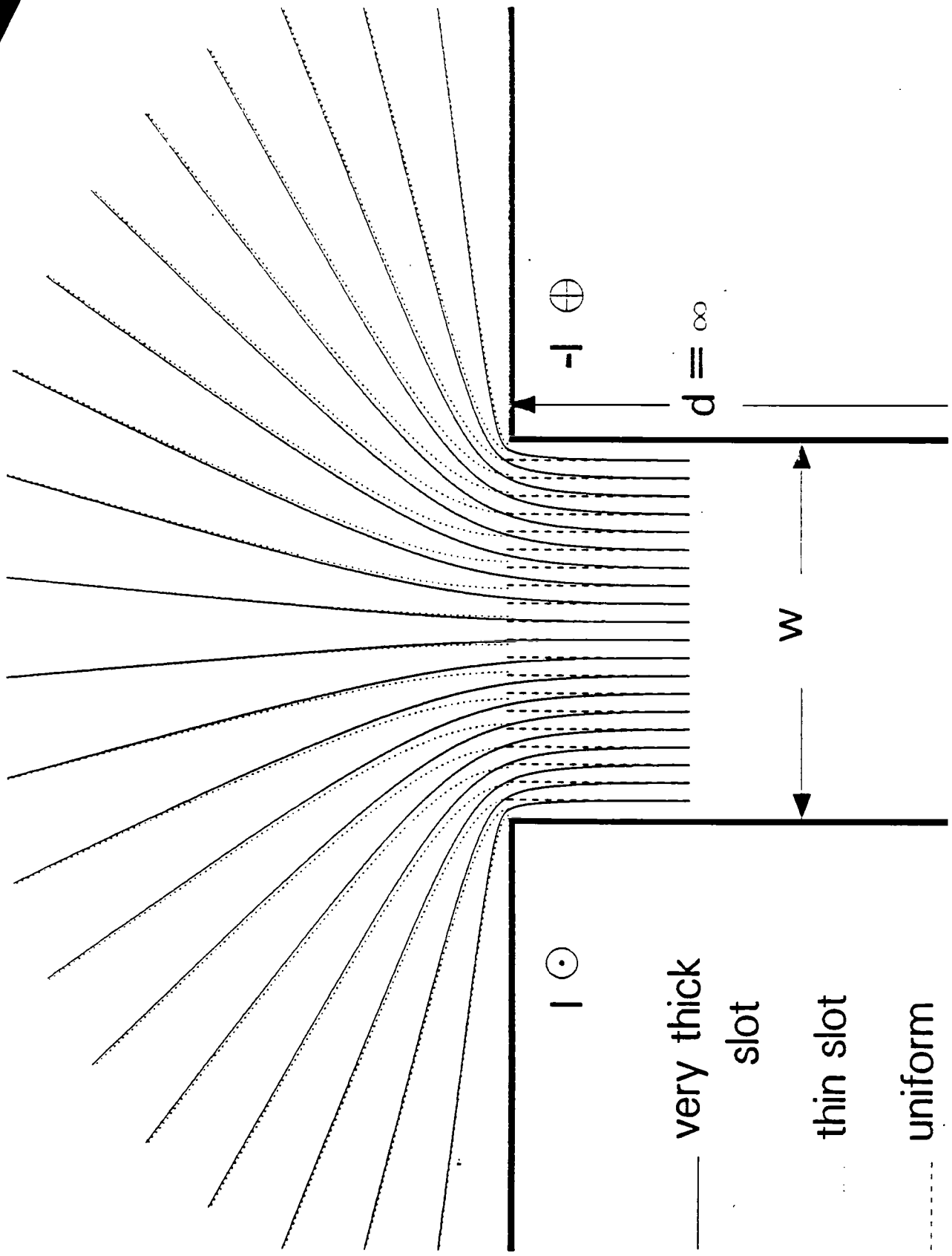

Figure 9. The local magnetostatic field in the cross section of a Very Thick slot (solid curves), Thin slot (dotted curves), and uniform field (dashed curves), when excited by a longitudinal magnetic field.

V. AXIAL POLARIZABILITY FOR THICK CASE

The derivation of the first order Hallén results for the axial polarizability given in [2] (for the complementary conducting tube see [5]) will now be briefly reviewed. Figure 10 illustrates the axial magnetic dipole moments of the slot in a Thick plane.

Replacing ρ_o by a in the approximations (58) and (59), equation (60) becomes

$$[\Omega + \ell n(1 - \frac{z^2}{h^2})]q_m(z) + \int_{-h}^{h} \frac{q_m(z') - q_m(z)}{|z - z'|} dz'$$

$$\approx 4\pi\mu_o z H_z^{inc} \quad , \tag{79}$$

where the antenna fatness parameter is

$$\Omega = 2\ \ell n(2h/a) \quad . \tag{80}$$

The approximate antenna fatness parameter, when (78) is used for a, has the simple form

$$\Omega_{ap} = 2\ \ell n(4\ell/w) + \pi\, d/w \quad . \tag{81}$$

Figure 11 shows the ratio of (81) to (80) with the true equivalent radius (75). The error in using (81) is thus quite small. In fact, using the asymptotic result (77) in (80) yields

$$\Omega - \Omega_{ap} \sim 2\ \ell n(\frac{\pi e}{8}) = 0.13 \quad , \frac{d}{w} >> 1 \quad . \tag{82}$$

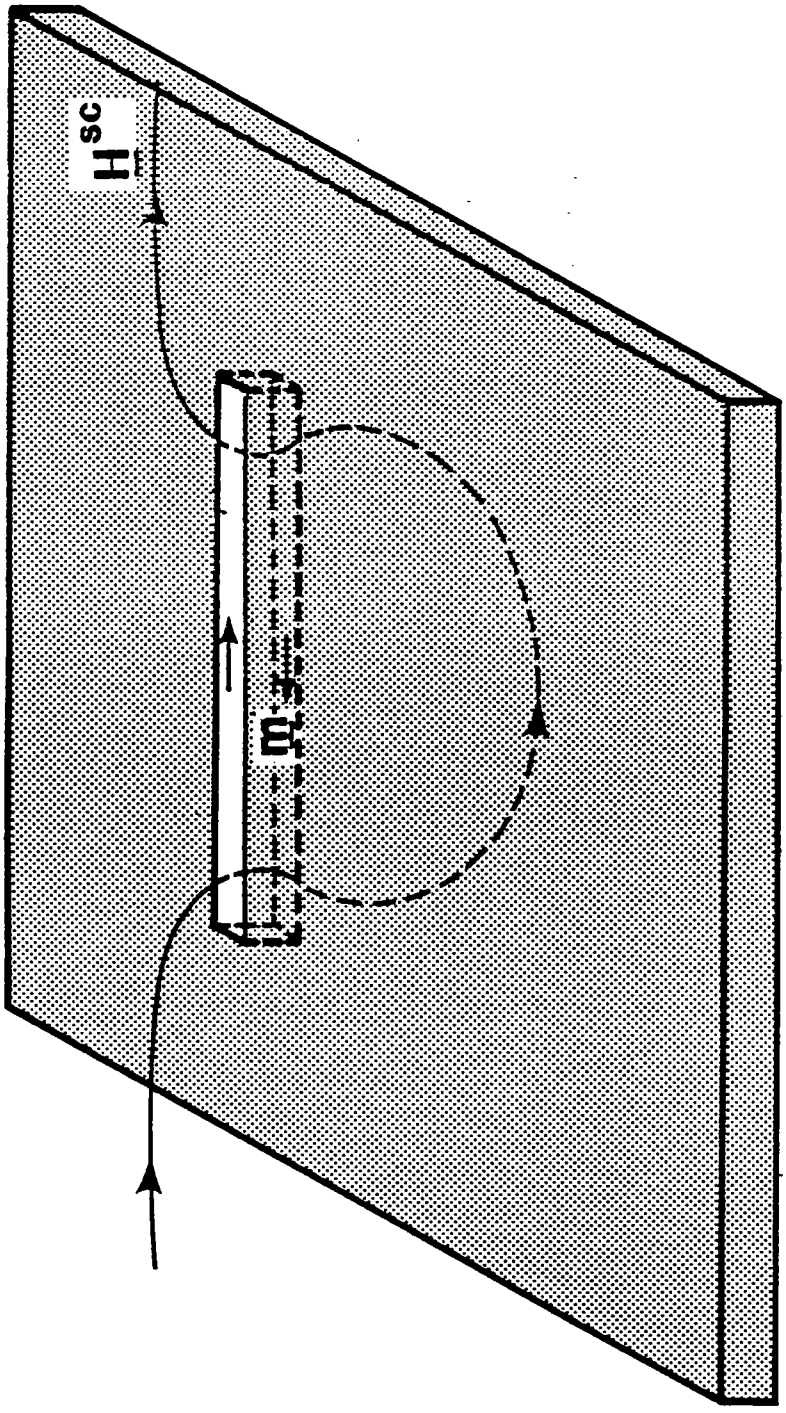

Figure 10. Longitudinal or axial magnetostatic field penetration of the Thick slot. The incident and transmitted magnetic dipole moments are depicted.

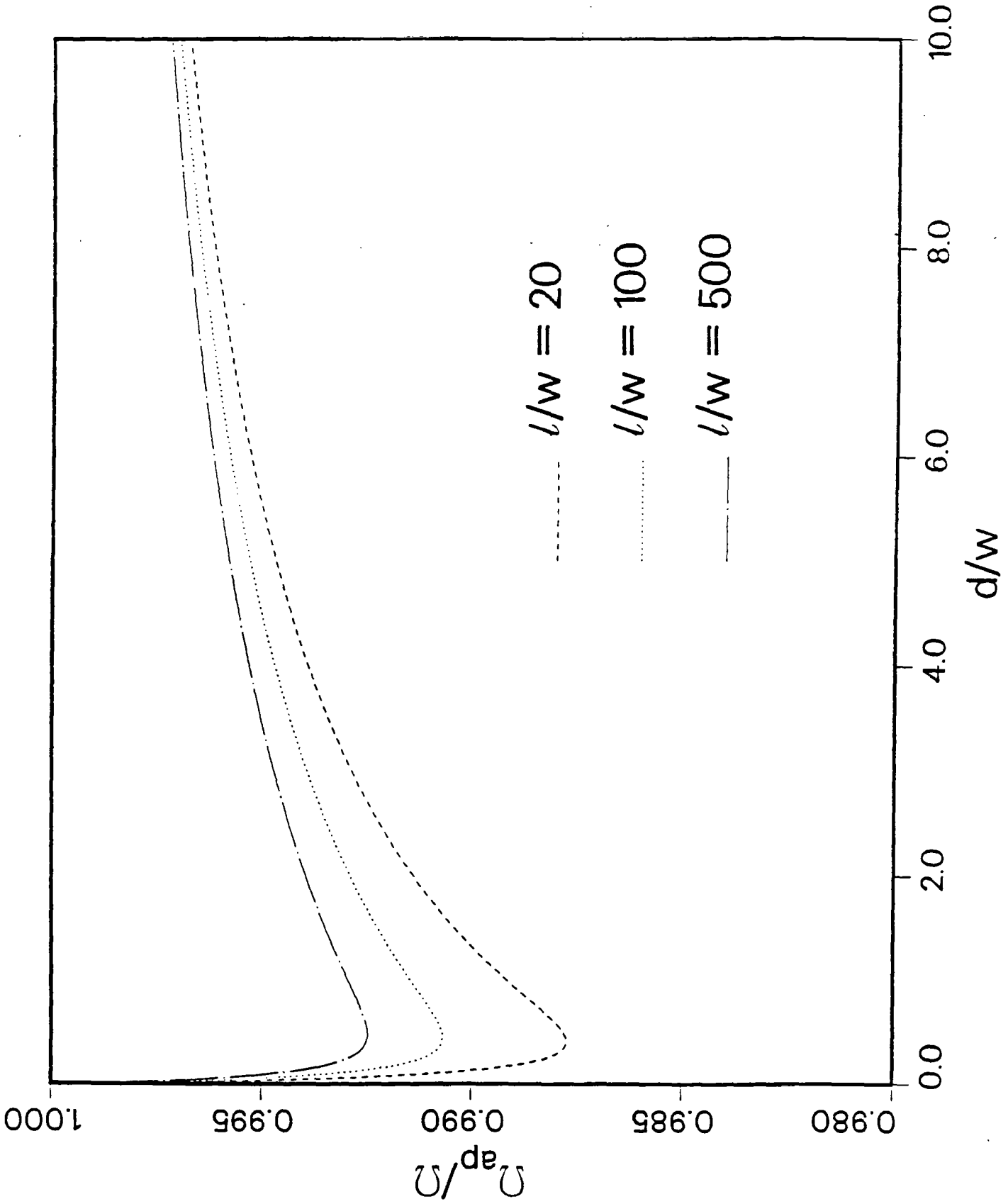

Figure 11. A comparison of antenna fatness parameters when evaluated by means of the approximate equivalent radius Ω_{ap} and exact equivalent radius Ω.

Taking Ω as a large parameter in (79), the equation may be iterated to yield the first order (away from the end points) solution

$$q_m(z) \sim \frac{4\pi\mu_o}{\Omega} H_z^{inc} z\left[1 + \frac{2}{\Omega} - \frac{1}{\Omega}\ell n(1 - \frac{z^2}{h^2})\right] . \tag{83}$$

Expanding (45) in the far zone $r >> h$ gives

$$\varphi_m^{>} \sim \mp \frac{z}{4\pi\mu_o r^3} \int_{-h}^{h} q_m(z')z'dz' \quad , y \gtrless \pm \frac{d}{2} . \tag{84}$$

Inserting (83) for q_m in (84) gives

$$\varphi_m \sim \mp \frac{h^3 H_z^{sc} z}{6r^3(\frac{\Omega}{2} + \ell n\ 2 - \frac{7}{3})} \quad , y \gtrless \pm \frac{d}{2} , \tag{85}$$

where terms of order $1/\Omega$ in the parentheses have been dropped. Comparison of (85) with (19) and (20) yields the axial polarizability

$$\alpha_{m,zz} \sim \frac{\ell^3 \pi}{24\ (\frac{\Omega}{2} + \ell n\ 2 - \frac{7}{3})} . \tag{86}$$

The difference between the first order result (86) and the approximation (27) is the first order constant $\frac{7}{3} - \ell n\ 2 \approx \frac{5}{3}$ in the denominator of (86) versus unity in (27). The expansion parameter $\Omega - 2$, in the denominator of (27), is consistent with the use of Schelkunoff's average biconical admittance (impedance in the case of an antenna [6]). The asymptotically correct result (86) is expected to give better results for the large Ωs

associated with Thick slots.

To give some feel for the accuracy of (86) versus (27) we will give a numerical solution of (60). It is more convenient to work with a quantity y_m related to the magnetic charge per unit length by means of

$$\frac{\partial}{\partial z} y_m = q_m \ , \tag{87}$$

where we require $y_m(z)$ to satisfy the boundary conditions

$$y_m(\pm h) = 0 \ . \tag{88}$$

Note that y_m is proportional to the axial magnetic current of the slot (voltage). Integration by parts in (60), followed by application of the operator $\frac{\partial}{\partial z}$, yields the integro–differential equation

$$\frac{\partial^2}{\partial z^2} \int_{-h}^{h} \frac{y_m(z')}{R_a} dz' = 4\pi\mu_o H_z^{inc} \ . \tag{89}$$

The quantity y_m is now expanded as

$$y_m(z) = \sum_{n=-N}^{N} y_{mn} F_n(z) \ , \tag{90}$$

where y_{mn} are coefficients to be determined, and the basis functions are

$$F_n(z) = \frac{z - z_{n-1}}{z_n - z_{n-1}} \ , z_{n-1} \leq z < z_n \ ,$$

$$= \frac{z_{n+1} - z}{z_{n+1} - z_n} \ , z_n \leq z < z_{n+1} \ , \qquad (91)$$

$$= 0 \ , \text{otherwise} \ .$$

Inserting (90) into (89), and applying the operator

$$\int_{-h}^{h} F_n(z) \, dz \ ,$$

we obtain the system of equations

$$\sum_{n=-N}^{N} y_{mn} \, G_{jn} = 4\pi\mu_o H_z^{inc} \, H_j \ , \ j = -N,...,0, ...,N \ , \qquad (92)$$

where

$$G_{jn} = \int_{-h}^{h} F_j(z) \, \frac{\partial^2}{\partial z^2} \int_{h}^{h} F_n(z') \, \frac{dz'}{R_a} \ , \qquad (93)$$

$$H_j = \int_{-h}^{h} F_j(z) \, dz \ . \qquad (94)$$

The axial magnetic polarizability is determined from

$$\alpha_{m,zz} = -\frac{1}{4\mu_o H_z^{inc}} \int_{-h}^{h} y_m(z)\, dz \ . \qquad (95)$$

Inserting (90) into (95) yields

$$\alpha_{m,zz} = -\frac{1}{4\mu_o H_z^{inc}} \sum_{j=-N}^{N} y_{mj}\, H_j \ . \qquad (96)$$

Integration by parts in (93) yields

$$G_{jn} = \frac{A_n(z_{j-1}) - A_n(z_j)}{z_j - z_{j-1}} + \frac{A_n(z_{j+1}) - A_n(z_j)}{z_{j+1} - z_j} \ , \qquad (97)$$

where

$$A_n(z) = \int_{-h}^{h} \frac{F_n(z')}{R_a}\, dz' \ . \qquad (98)$$

Integration of (98) and (94) can be carried out in closed form by elementary means.

Because $y_m(-z) = y_m(z)$, if the points z_n are chosen symmetrically, such that $z_{-n} = -z_n$, then $y_{m,-n} = y_{mn}$. The system (92) thus becomes

$$\sum_{n=0}^{N} y_{mn} \frac{\epsilon_n}{2} \epsilon_j (G_{jn} + G_{j,-n})$$

$$= 4\pi\mu_o H_z^{inc} \epsilon_j H_j \ , \ j = 1,\ldots,N \ , \qquad (99)$$

where $\epsilon_n = 1$ if $n = 1$, and $\epsilon_n = 2$ if $n \geq 1$. Noting then that $F_{-j}(-z) = F_j(z)$, and therefore $H_{-j} = H_j$, the polarizability becomes

$$\alpha_{m,zz} = \frac{-1}{4\mu_o H_z^{inc}} \sum_{j=0}^{N} \epsilon_j \, y_{mj} \, H_j \ . \qquad (100)$$

Because $G_{jn} = G_{nj}$, and furthermore with $z_{-n} = -z_n$, $G_{-j,-n} = G_{jn}$, the system in (99) is symmetrical. We will use uniform spacing

$$z_n = n \, \Delta \ , \ n = -N,...,0,...,N \ , \qquad (101)$$

where $\Delta = h/(N + 1)$.

Figures 12 – 14 show the polarizabilities determined from the Galerkin method (100) (solid curve), the approximation using $\Omega - 2$ (27) (dotted curve), and the Hallén zero order result (25) (dashed curve), all normalized by the first order result (86), denoted by $\alpha^{FO}_{m\,,\,zz}$. When viewing these curves, note that the parameter N should be constrained so that the basis function length $\Delta >> a$ (Note that the approximation of taking the charge to reside along a zero radius filament, (45) and (60), breaks down if too high an accuracy solution $\Delta \to 0$ is attempted for a fixed value of a.). From a practical point of view, if say $\Delta > 4a$, the filament approximation is reasonable. Thus, similar to asymptotic expansions, only a certain amount of accuracy in the magnetic charge per unit length, for a given Ω, can be expected. It is clear from Figures 13 and 14 that the first order asymptotic result is very accurate for $\Omega > 20$. Furthermore, Figure 12 indicates that the first order result is more accurate than the $\Omega - 2$ approximation or the zero order asymtotic result for $\Omega > 10$. Thus the first order result appears to be useful for Thick slots. Indeed, Vainshtein [7] has shown, by considering the solution of a

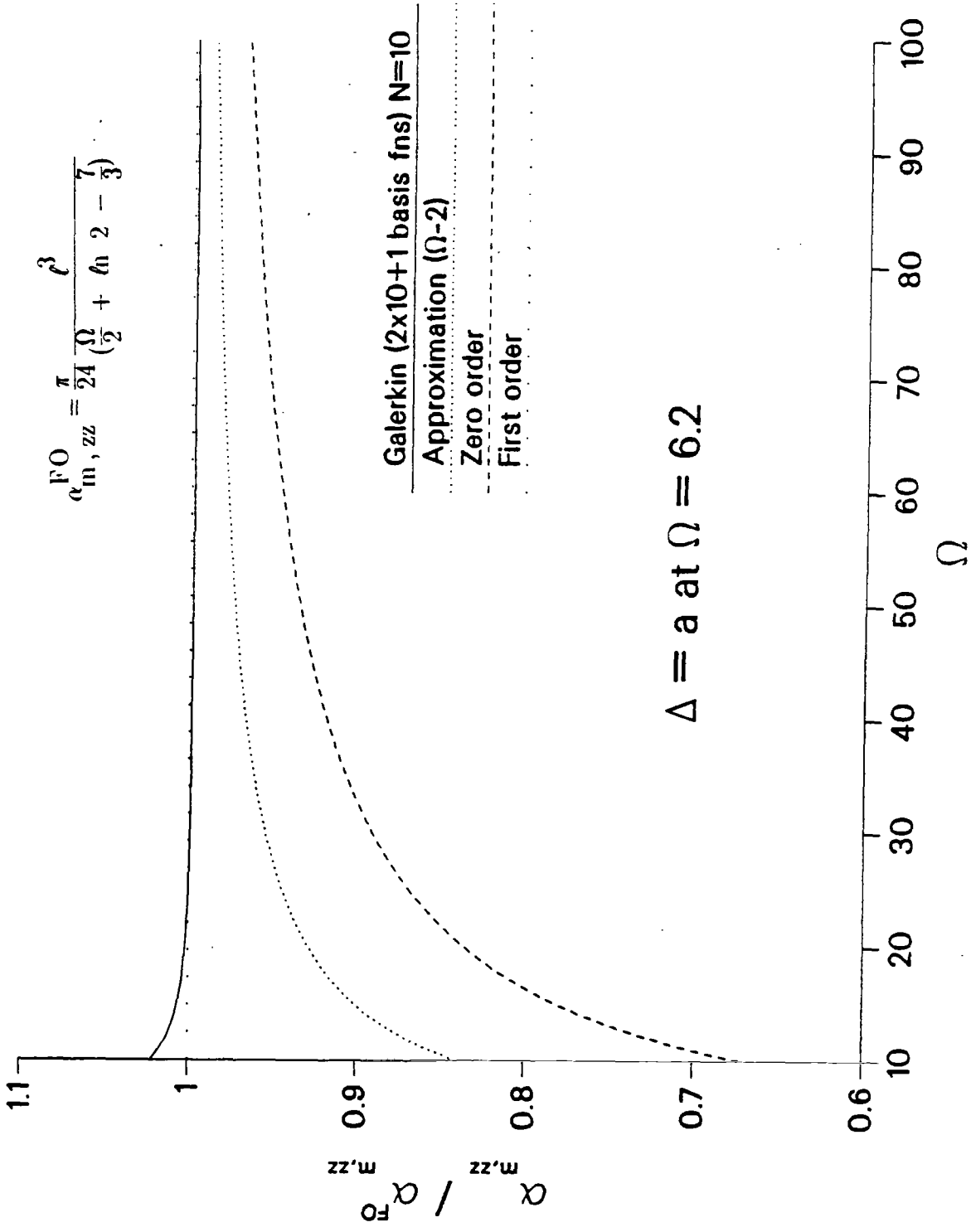

Figure 12. Polarizabilities determined from the solution of Hallén's integral equation by the Galerkin solution with N = 10 (solid curve), first order Hallén solution (widely spaced dotted curve), zero order Hallén solution (dashed curve), and an approximation based on the expansion parameter $\Omega - 2$. All curves are normalized by the first order Hallén result.

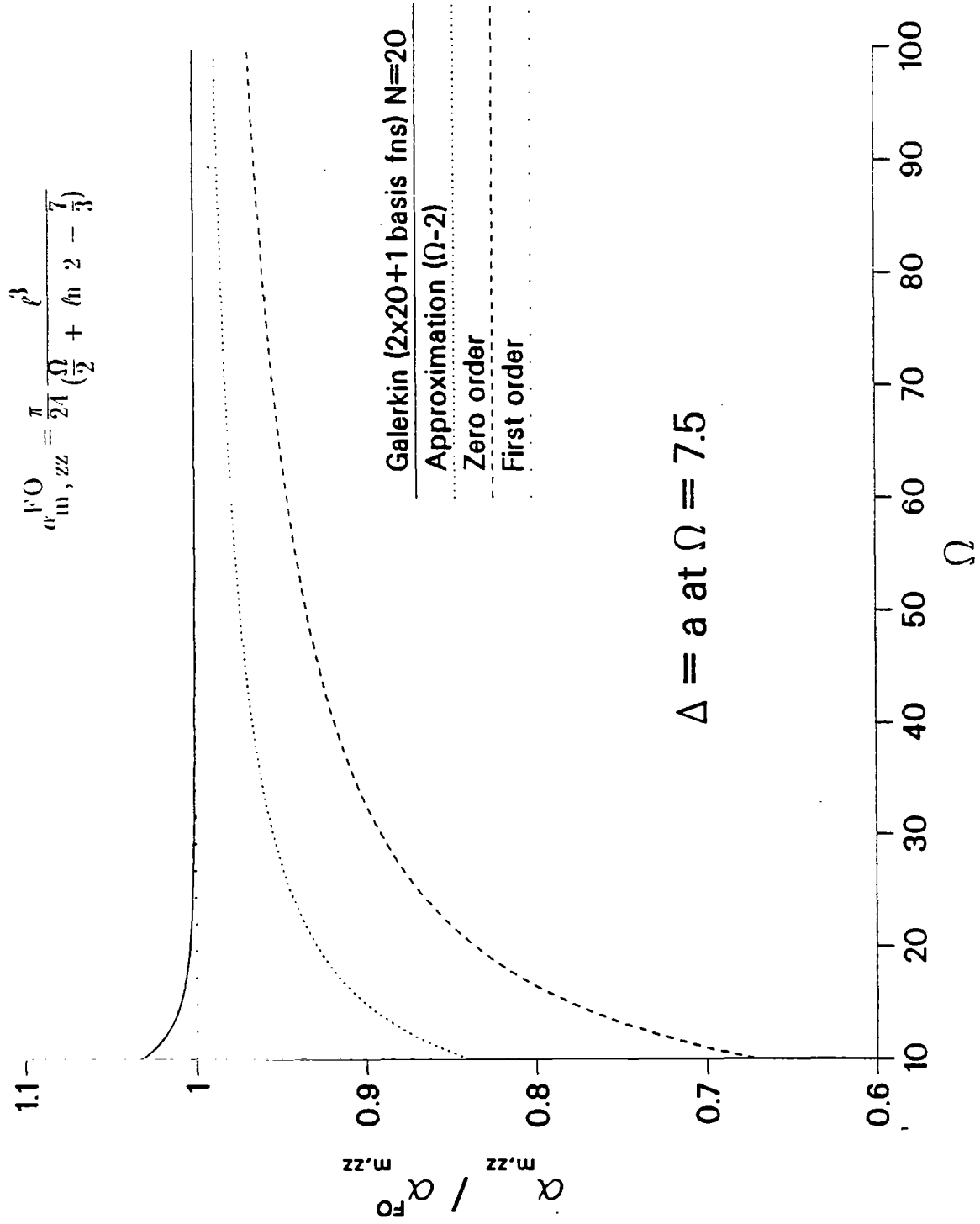

Figure 13. Same as Figure 12 except N = 20 in the Galerkin solution.

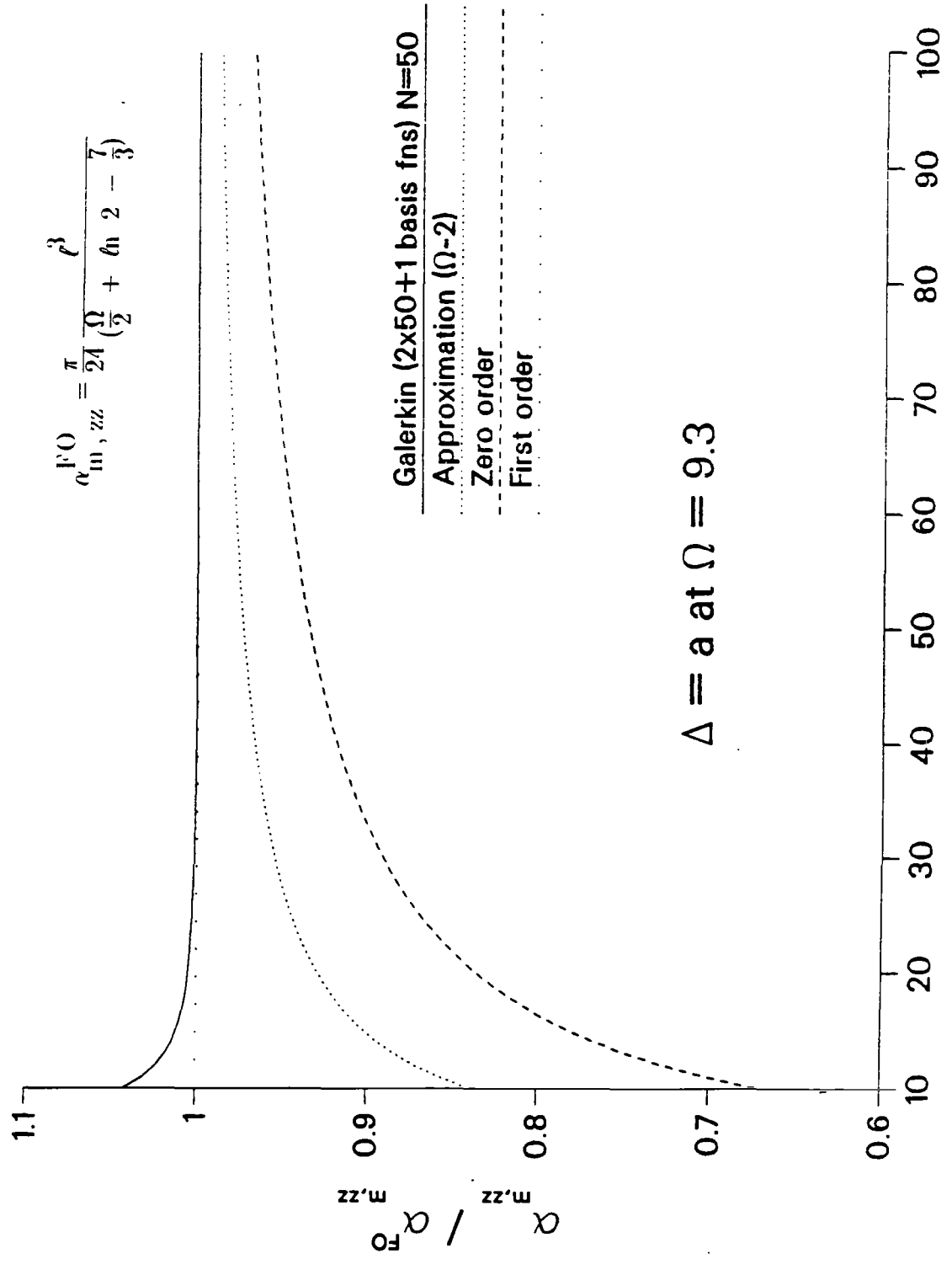

Figure 14. Same as Figure 12 except N = 50 in the Galerkin solution.

tubular cylinder via a global Chebyshev basis set, that the first order result for the polarizability is accurate for $\Omega \geq 6$. Note that the difference between the numerical or Galerkin value and the first order value (unity) at the left end of Figures 12 and 13 (Ω = 10) is in agreement with the numerical data given in [7].

Figure 15 shows the result from the first order formula (86), normalized by (86) evaluated for zero depth (denoted by $\alpha^{\circ}_{m,zz}$), for various parameters. Because of the small errors introduced by the approximation (81) for the fatness parameter, the approximate equivalent radius (78) will be used in all these curves. The strong influence of the depth on the polarizabilities in the Thick case is clearly illustrated. Note that the polarizability formula (86) holds on both sides of the slot for the Thick case ($\ell >>$ d,w).

Figure 16, taken from [1], shows various types of hatch apertures in Thin (d = 0) planes. Figure 17 gives a table, from [1], showing approximations for the polarizabilites. Figure 18 shows the same table with the formulas now generalized to include depth. To be consistent with the notation in [1], g is the hatch aperture width and Δ denotes plane thickness (this should not be confused with the basis function length in (101)). Note that the hinges on the hatch aperture are taken to be unmodified by the thickness of the plane (Furthermore, the approximate Thin hinge inductance, contained in the formulas of the table, was assumed to be unmodified by the thickness of the plane. A more rigorous treatment of the hinges, and experimental determination of hinge properties, would be very useful.). Thus the concept of an equivalent radius, (75) or approximately (78), for the Thick slot, yields simple generalizations for existing Thin slot hatch aperture polarizability formulas.

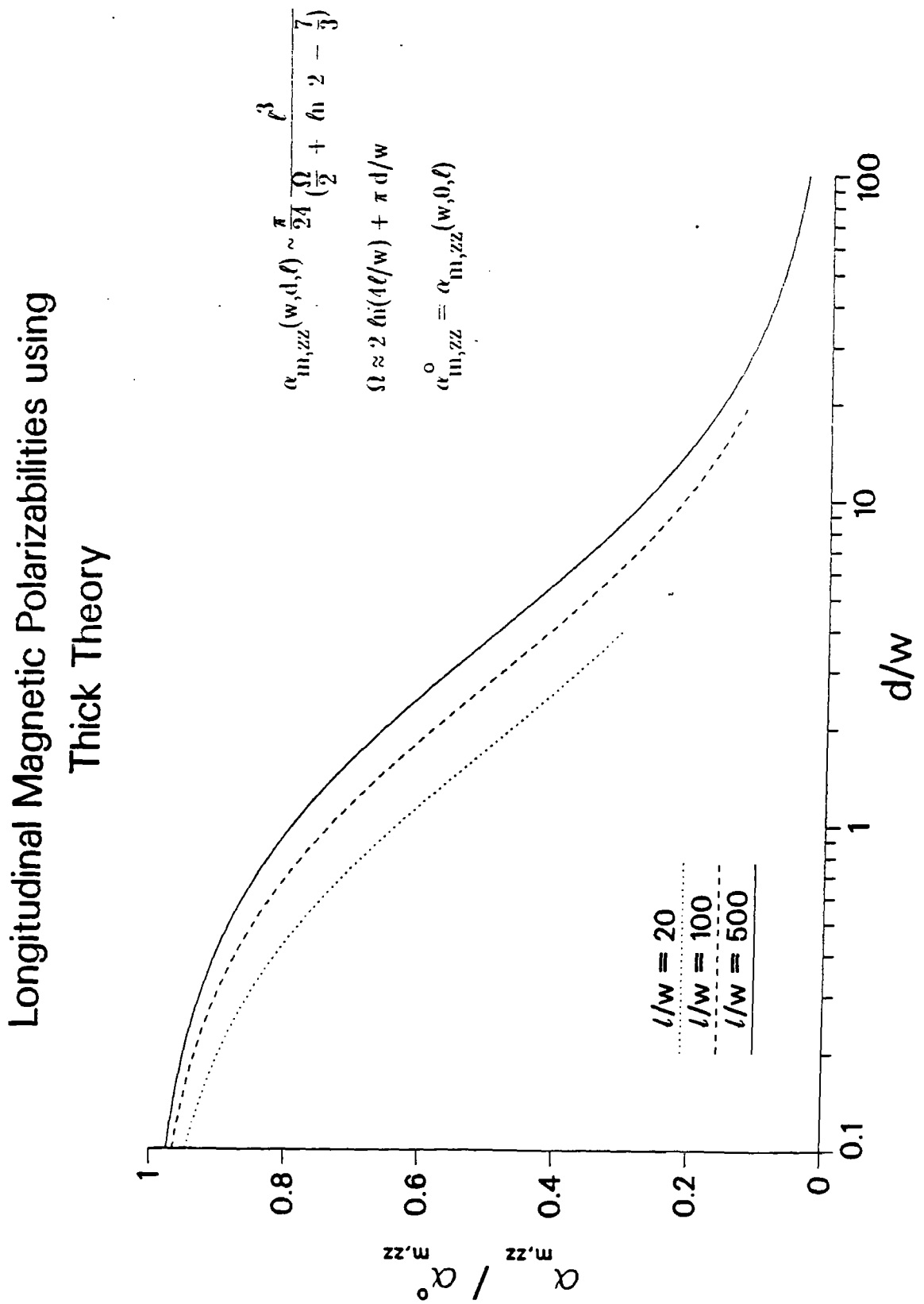

Figure 15. Longitudinal magnetic polarizabilities for the Thick case determined from the first order solution. The curves are normalized by the first order solution for zero depth, and thus depend only on the parameters ℓ/w and d/w.

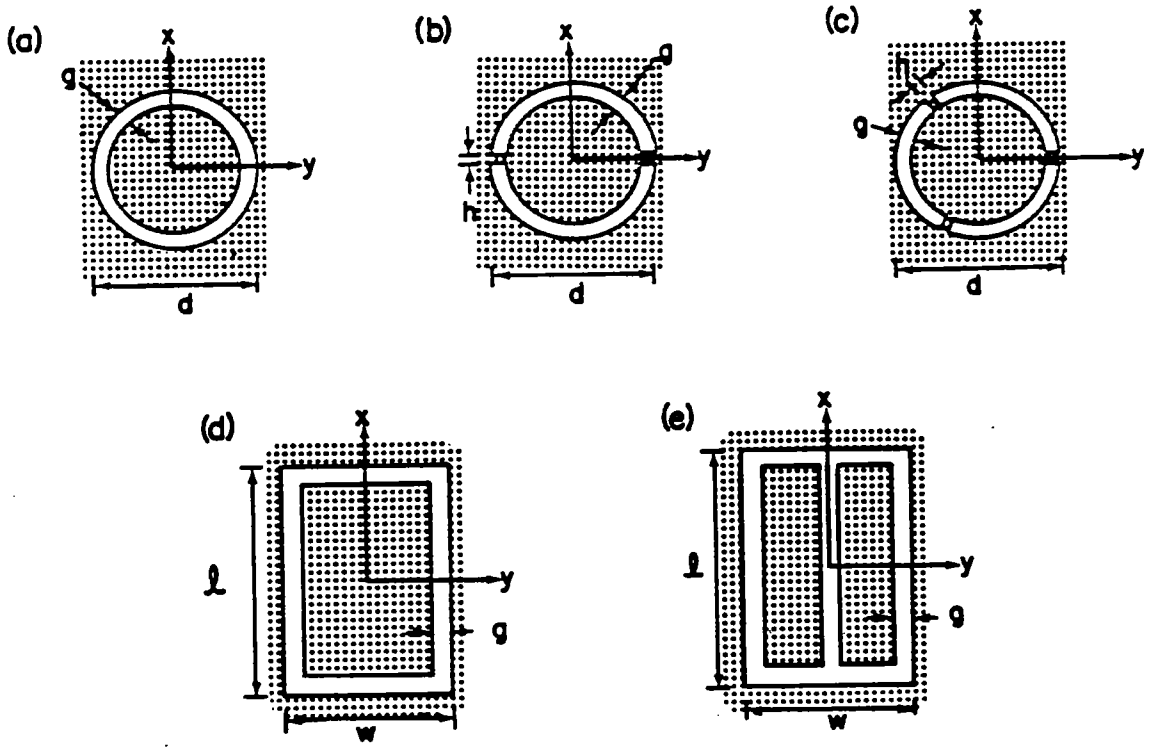

Fig. 106. Hatch apertures.

Figure 16. Examples of various hatch apertures in Thin conducting planes taken from [1].

Table 15. POLARIZABILITIES OF HATCH APERTURES

Aperture	α_e	$\alpha_{m,xx}$	$\alpha_{m,yy}$
Fig. 106a	$\frac{\pi^2}{32}\frac{d^3}{\ell n(16\ d/g)-2}$	$\frac{\pi^2}{16}\frac{d^3}{\ell n(16\ d/g)-2}$	$\frac{\pi^2}{16}\frac{d^3}{\ell n(16\ d/g)-2}$
Fig. 106b	$\frac{\pi^2 d^3}{16\Omega}\frac{s^2\mu\epsilon}{s^2\mu\epsilon+128h/(\pi\Omega dg^2)}$	$\frac{\pi^2 d^3}{8\Omega}\left[1-\frac{8/\pi^2}{1+\Omega g^2/(8\pi dh)}\right]$	$\frac{\pi^2}{16}\frac{d^3}{\ell n(16\ d/g)-2}$
Fig. 106c	$\frac{\pi^2 d^3}{16\,\Omega}\frac{s^2\mu\epsilon}{s^2\mu\epsilon+192h/(\pi\Omega dg^2)}$	$\frac{\pi^2 d^3}{8\Omega}\left[1-\frac{27/(4\pi^2)}{1+9\Omega g^2/(64\pi dh)}\right]$	$\frac{\pi^2 d^3}{8\Omega}\left[1-\frac{27/(4\pi^2)}{1+9\Omega g^2/(64\pi dh)}\right]$
Fig. 106d	$\frac{\pi}{4}\frac{\ell^2 w}{(1+\ell/w)\ell n[4(\ell+w)/g]}$	$\frac{\pi}{12}\frac{\ell^3[1+3(w/\ell)]}{\ell n[4(\ell+w)/g]}$	$\frac{\pi}{12}\frac{w^3[1+3(\ell/w)]}{\ell n[4(\ell+w)/g]}$
Fig. 106e	$\frac{\pi}{4}\frac{\ell^2 w}{(1+\ell/w)\ell n[4(\ell+w)/g]}$	$\frac{\pi}{24}\frac{\ell^3[8/3+7(w/\ell)+2(w/\ell)^2]}{\ell n[4(\ell+w)/g]}$	$\frac{\pi}{12}\frac{w^3[1+3(\ell/w)]}{\ell n[4(\ell+w)/g]}$

Note: $\Omega = 2[\ell n(16d/g) - 2]$

Figure 17. Table of hatch aperture polarizabilities from [1] corresponding to the examples in Figure 16.

Table 15. POLARIZABILITIES OF HATCH APERTURES

Aperture	α_e	$\alpha_{m,xx}$	$\alpha_{m,yy}$
Fig. 106a	$\frac{\pi^2}{32}\frac{d^3}{\ln(4\,d/a)-2}$	$\frac{\pi^2}{16}\frac{d^3}{\ln(4\,d/a)-2}$	$\frac{\pi^2}{16}\frac{d^3}{\ln(4\,d/a)-2}$
Fig. 106b	$\frac{\pi^2 d^3}{16\Omega}\frac{s^2\mu\varepsilon}{s^2\mu\varepsilon+128h/(\pi\Omega dg^2)}$	$\frac{\pi^2 d^3}{8\Omega}\left[1-\frac{8/\pi^2}{1+\Omega g^2/(8\pi dh)}\right]$	$\frac{\pi^2}{16}\frac{d^3}{\ln(4\,d/a)-2}$
Fig. 106c	$\frac{\pi^2 d^3}{16\,\Omega}\frac{s^2\mu\varepsilon}{s^2\mu\varepsilon+192h/(\pi\Omega dg^2)}$	$\frac{\pi^2 d^3}{8\Omega}\left[1-\frac{27/(4\pi^2)}{1+9\Omega g^2/(64\pi dh)}\right]$	$\frac{\pi^2 d^3}{8\Omega}\left[1-\frac{27/(4\pi^2)}{1+9\Omega g^2/(64\pi dh)}\right]$
Fig. 106d	$\frac{\pi}{4}\frac{\ell^2 w}{(1+\ell/w)\ln[(\ell+w)/a]}$	$\frac{\pi}{12}\frac{\ell^3[1+3(w/\ell)]}{\ln[(\ell+w)/a]}$	$\frac{\pi}{12}\frac{w^3[1+3(\ell/w)]}{\ln[(\ell+w)/a]}$
Fig. 106e	$\frac{\pi}{4}\frac{\ell^2 w}{(1+\ell/w)\ln[(\ell+w)/a]}$	$\frac{\pi}{24}\frac{\ell^3[8/3+7(w/\ell)+2(w/\ell)^2]}{\ln[(\ell+w)/a]}$	$\frac{\pi}{12}\frac{w^3[1+3(\ell/w)]}{\ln[(\ell+w)/a]}$

Note: $\Omega = 2[\ln(4d/a) - 2]$

$a = \frac{g}{4}\, e^{-\frac{\pi\Delta}{2g}}$

Figure 18. Simple generalization of these formulas to the Thick case using equivalent radius a. Note, to conform with notation in [1], g is the hatch aperture width and Δ is the plane thickness.

VI. TRANSVERSE POLARIZABILITIES FOR THICK CASE

Following Kaden [4] the conformal mapping solution of Section IV will be used to derive the transverse polarizabilities. The three dimensional character of the problem will be considered after the line polarizabilities (or polarizabilities per unit length) have been obtained.

Two expansions of the transformation (61) are needed. The first is related to (73), and involves $|z| \to \infty$, $\text{Im } z \leq -d/2$ (where $z = x + iy$). Expansion of (61) for $|z_1| - 0$ yields

$$z_1 \sim -\frac{C_1}{z}, \quad |z| \to \infty, \ \text{Im } z \leq -d/2 . \tag{102}$$

The second result is related to (72), and involves $|z| \to \infty$, $\text{Im } z \geq d/2$. Expansion of (61) for $|z_1| \to \infty$ yields

$$z_1 \sim -\frac{z}{pC_1} + C_2 + \frac{pC_1}{2z}\left(1 + \frac{1}{p^2}\right),$$

$$|z| \to \infty, \ \text{Im } z \geq d/2 , \tag{103}$$

where the constant C_2 is given by

$$C_2 = -\int_{1/p}^{\infty} \frac{\sqrt{(z_1^2 - 1)(z_1^2 - 1/p^2)} - z_1^2}{z_1^2}\, dz_1 + \frac{1}{p} + \frac{w + id}{2pC_1} . \tag{104}$$

To be consistent with Kaden [4] the incident wave in this section will be taken to impinge on the slot from the $y > d/2$ half space, contrary to the previous sections. The final results will be independent of this choice.

The short circuit transverse magnetic field is x directed and constant H_x^{sc}. The magnetic field can be determined from a magnetic scalar potential by means of (18). This scalar potential can be found from a complex potential W by means of

$$\varphi_m = -\frac{1}{\mu_o} \operatorname{Re} W \quad . \tag{105}$$

The complex potential represents a uniform field in the z_1 plane

$$W = A\, z_1 \quad , \tag{106}$$

where the constant A can be found by using the first term of (103) as

$$A = -\mu_o H_x^{sc} p C_1 \quad . \tag{107}$$

The third term of (103) gives the contribution from the magnetic line dipole moment of the slot on the incident side

$$\varphi_m = \frac{\underline{m} \cdot \underline{\rho}}{2\pi\rho^2} \quad , \tag{108}$$

where $\underline{\rho}$ is the position vector in the cross section, and from $m_x = 2\, \bar{\alpha}_{m,xx}\, H_x^{sc}$, see (20), the incident magnetic line polarizability is given by

$$\alpha^{-}_{m,xx} = \frac{1}{2}(1 + p^2)\,\pi C_1^2 \text{ , incident side .} \qquad (109)$$

The expansion (102) when inserted into (106) gives the magnetic line dipole moment on the transmitted side of the slot, yielding (108) with dipole moment $m_x = -2\,\alpha^{+}_{m,xx} H_x^{sc}$. and line polarizability

$$\alpha^{+}_{m,xx} = \pi\, pC_1^2 \text{ , transmitted side .} \qquad (110)$$

The result (110) can be written as

$$\alpha^{+}_{m,xx} = \pi\, a^2 \text{ , transmitted side ,} \qquad (111)$$

where a is the equivalent radius (75). This relation has been shown to be true for general slot cross sections [3].

The transverse electric short circuit field is taken to be y directed and constant E_y^{sc}. The fields are determined from the electric scalar potential by means of (28). The scalar potential can be found from a complex potential W as

$$\varphi = \text{Im } W \ . \qquad (112)$$

The complex potential again represents a uniform field in the z_1 plane and is given by (106). The amplitude constant A is again found from the first term of (103) as

$$A = E_y^{sc} pC_1 \ . \qquad (113)$$

The third term of (103) gives the electric line dipole moment contribution on the incident

side of the slot

$$\varphi = \frac{\underline{p} \cdot \underline{\rho}}{2\pi\epsilon_o \rho^2} \ , \tag{114}$$

where from $p_y = -2\epsilon_o \alpha^-_{e,yy} E^{sc}_y$, the electric line polarizability $\alpha^-_{e_{yy}}$ on the incident side is again given by (109). On the transmitted side the expansion (102) shows that the electric line dipole moment $p_y = 2\epsilon_o \alpha^+_{e_{yy}} E^{sc}_y$ again has an electric line polarizability given by (110).

Making use of the limiting values for p and $-C_1/w$ discussed in Section IV, we obtain, on the incident side, the asymptotic formulas

$$\alpha^-_{m,xx} = \alpha^-_{e,yy} = \tfrac{1}{2}(1 + p^2)\, \pi C_1^2 \ , \text{ incident side} \ , \tag{115}$$

$$\sim \pi \left(\frac{w}{4}\right)^2 , \frac{d}{w} << 1 \ , \tag{116}$$

$$\sim \frac{w^2}{2\pi} , \frac{d}{w} >> 1 \ , \tag{117}$$

and a useful uniformly valid approximation

$$\alpha^-_{m,xx} = \alpha^-_{e,yy} \approx \pi \left(\frac{w}{4}\right)^2 , \text{incident side} \ . \tag{118}$$

Similarly on the transmitted side we obtain the asymptotic formulas

$$\alpha^+_{m,xx} = \alpha^+_{e,yy} = \pi a^2 \ , \text{ transmitted side} \ , \tag{119}$$

$$\sim \pi \left(\frac{w}{4}\right)^2 , \frac{d}{w} << 1 \ , \tag{120}$$

$$\sim \frac{4}{\pi} w^2 e^{-(2 + \pi d/w)} , \frac{d}{w} >> 1 \ , \tag{121}$$

and a useful uniformly valid approximation

$$\alpha^+_{m,xx} = \alpha^+_{e,yy} \approx \pi \left[\frac{w}{4} e^{-\frac{\pi d}{2w}}\right]^2 \text{ , transmitted side .} \tag{122}$$

The three dimensional point polarizabilities can be found from (115) – (122) simply by multiplying by the slot length ℓ. The small regions near the ends of the slot, where the field is perturbed from the two dimensional distribution, do not contribute significantly to the polarizabilities because the slot is narrow and Thick ($\ell >>$ d,w).

Figures 19 and 20 show the transverse field distributions with dipoles on the transmitted side depicted.

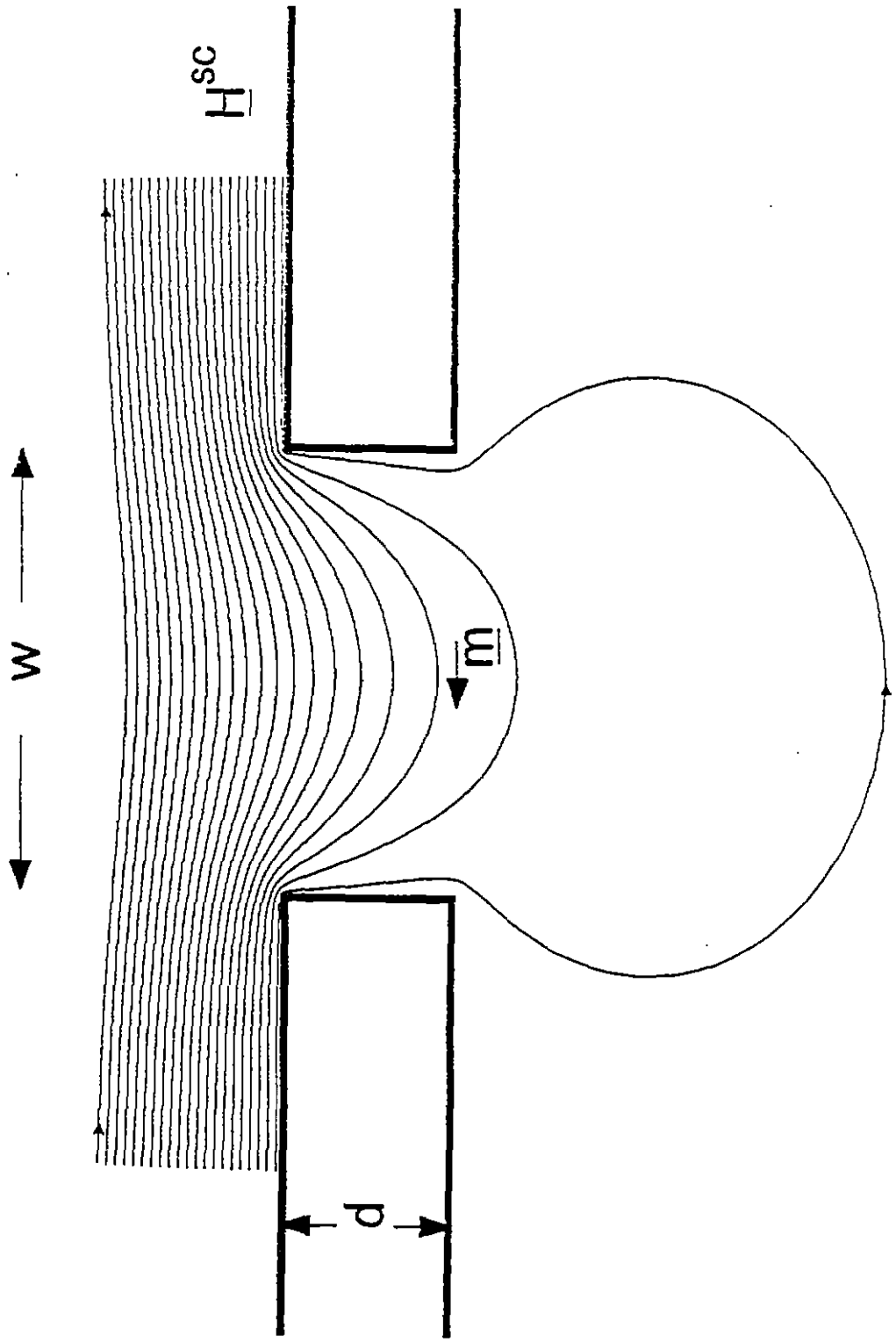

Figure 19. Transverse magnetic field penetration of the Thick slot.

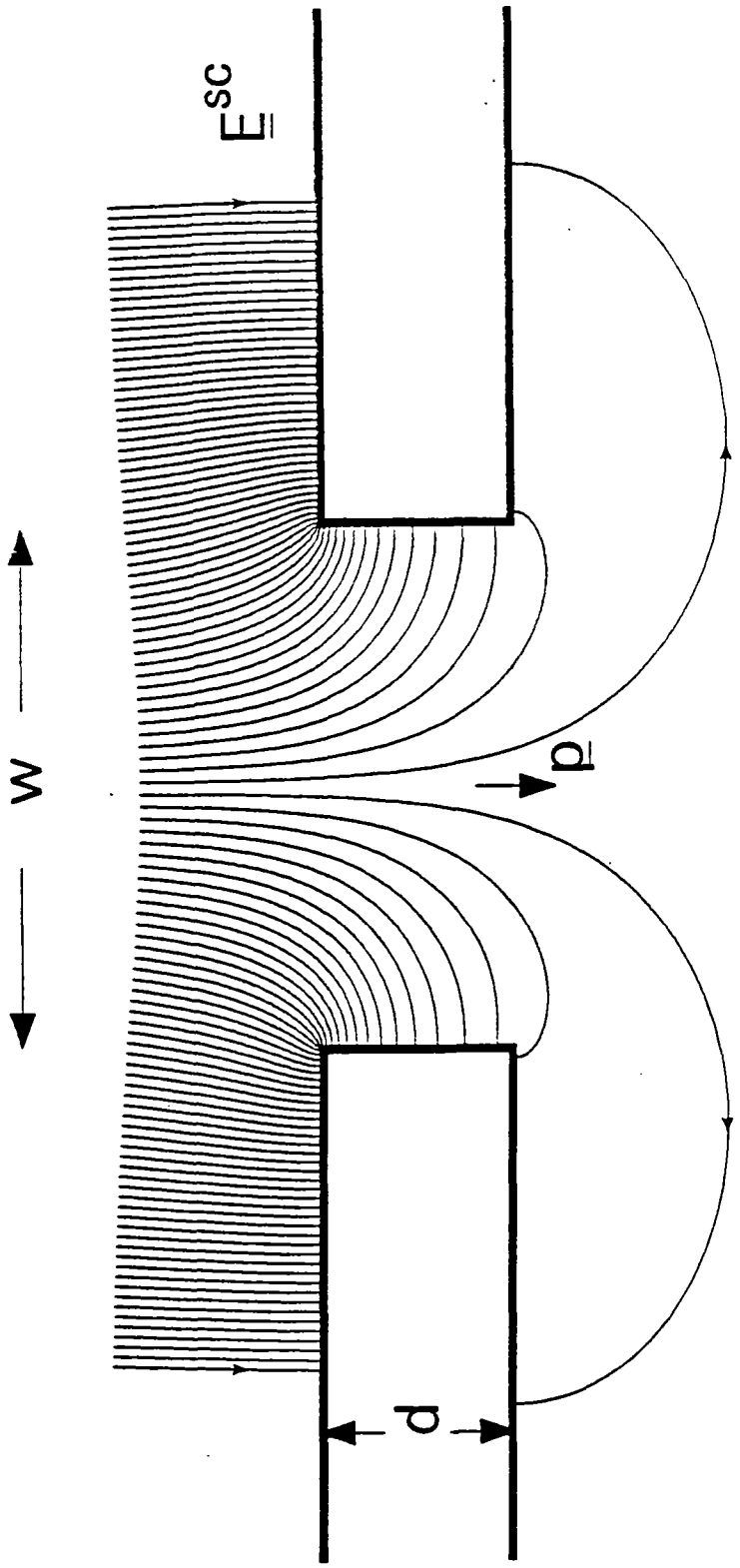

Figure 20. Transverse electric field penetration of the Thick slot.

VII. HEURISTIC DERIVATION OF AXIAL POLARIZABILITIES FOR DEEP CASE

The geometry is shown in Figure 21. The field is incident from $y < -\frac{d}{2}$. The magnetic field is derivable from (18), where the potential satisfies Laplace's equation (32) and the boundary conditions

$$\frac{\partial}{\partial z}\varphi_m^< = 0, z = \pm h \ . \tag{123}$$

The interior fields and hence potential will be taken uniform in x. Because H_y is odd in z, the interior potential can be written as

$$\varphi_m^< = \sum_{m,odd} \sin \frac{m\pi}{\ell} z \left[A_m e^{\frac{m\pi}{\ell} y} + B_m e^{-\frac{m\pi}{\ell} y} \right] \ . \tag{124}$$

The y directed magnetic flux per unit length $\Phi^{\pm}$ in the Deep case will be different at $y = \pm \frac{d}{2}$. This magnetic flux per unit length is related to the magnetic charge per unit length, as viewed from the exterior of the slot, by means of

$$\Phi^{\pm} = \pm \frac{1}{2} q_m^{\pm} \ , \tag{125}$$

where again the magnetic charge per unit length includes the image in the $y = \pm \frac{d}{2}$ ground planes. From (124) we must have

$$H_y^< = -\frac{\partial}{\partial y}\varphi_m^< = B_y/\mu_o = \Phi^{\pm}/(w\mu_o) \ , y = \pm \frac{d}{2} \ . \tag{126}$$

In Section II it was noted that the voltage along a slot in a Thin (d = 0) or Thick

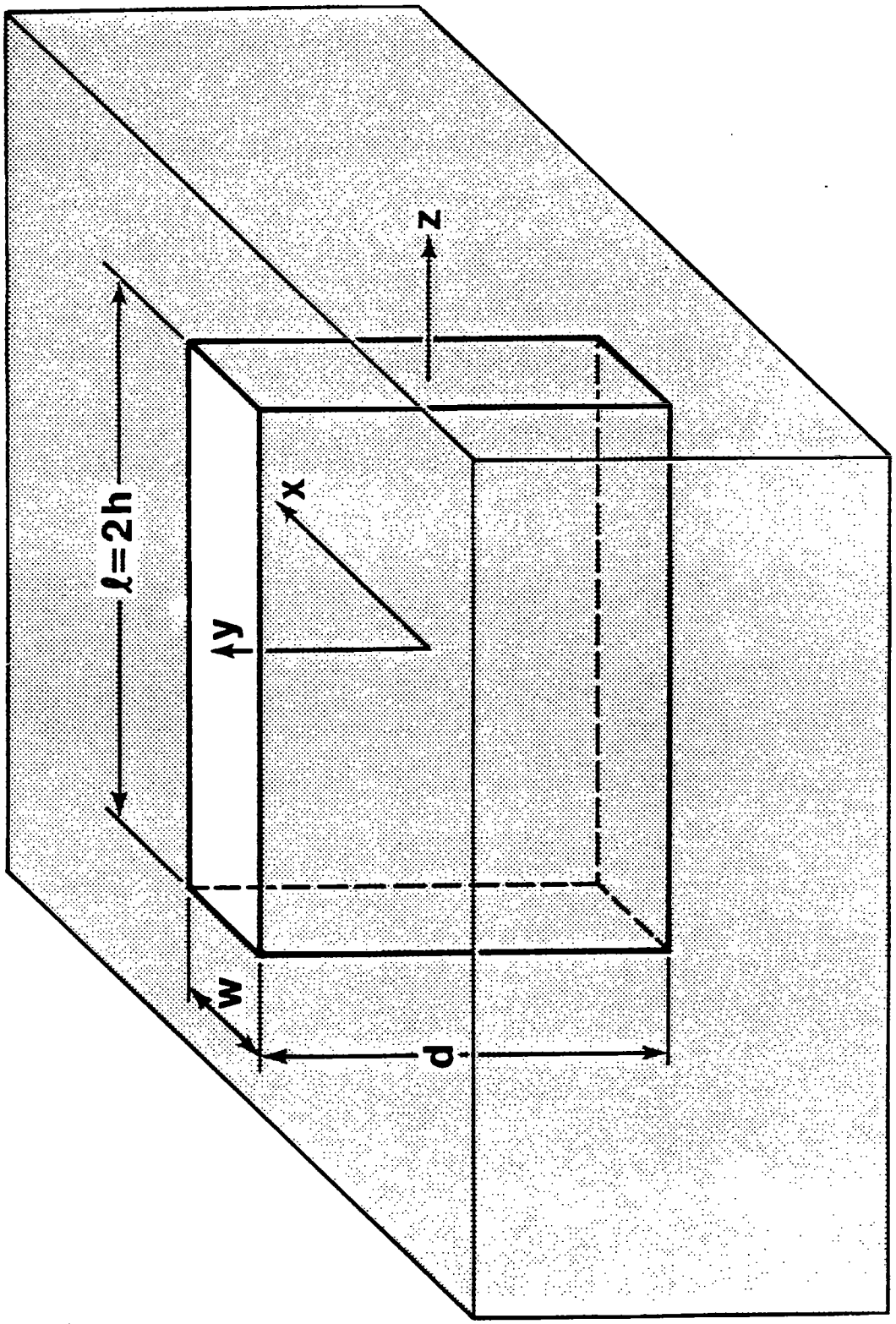

Figure 21. Geometry of the Deep slot.

($\ell >> d$) plane can be modeled by means of a transmission line of the form shown in Figure 2. The current I(z) is the z directed electric current on the $x < 0$ conductor. The continuity equation for the current is

$$\frac{\partial}{\partial z} I = K_x^{sc} \quad . \tag{127}$$

For the Deep problem the current on the interior walls is not uniform in y, nor is it purely axial, but it is described by the potential (124). Equation (127) must therefore be generalized to the continuity equations

$$\frac{\partial}{\partial z} I^{+} = K_y^{<} = \frac{\partial}{\partial z} \varphi_m^{<} \, , \; y = + \frac{d}{2} \quad , \tag{128}$$

$$\frac{\partial}{\partial z} I^{-} = -K_y^{<} + K_x^{sc} = - \frac{\partial}{\partial z} \varphi_m^{<} - H_z^{sc} \, , \; y = - \frac{d}{2} \quad , \tag{129}$$

where $I^{\pm}$ denotes the exterior z directed current on the $x < 0$ conductor for $y = \pm \frac{d}{2}$ and $K_y^{<}$ is the interior surface current density on the $x < 0$ conductor.

The usual relation between the flux per unit length and the current on a transmission line is in this case

$$\Phi^{\pm} \approx L \, I^{\pm} \quad , \tag{130}$$

where

$$L \approx \frac{1}{2} \left[\frac{2 \pi \mu_o}{\ell n \left(\frac{\ell}{w/4} \right)} \right] \quad . \tag{131}$$

The inductance per unit length (131) is twice (7) because it now applies to only one side of the exterior half plane. Integrating (128) and (129) with respect to z and using (130) yields

$$\Phi^{+}/L = \varphi_m^{<}(y = \tfrac{d}{2}) , \tag{132}$$

and

$$-\Phi^{-}/L = \varphi_m^{<}(y = -\tfrac{d}{2}) + z\, H_z^{sc} . \tag{133}$$

Finally using (126) we arrive at the impedance conditions

$$\frac{\partial}{\partial y}\varphi_m^{<} = -\frac{L}{w\mu_o}\varphi_m^{<} , y = +\frac{d}{2} , \tag{134}$$

and

$$\frac{\partial}{\partial y}\varphi_m^{<} = \frac{L}{w\mu_o}(\varphi_m^{<} + zH_z^{sc}) , y = -\frac{d}{2} . \tag{135}$$

Solving for A_m and B_m yields the representation

$$\varphi_m^{<} = -\frac{4\ell^2}{w\pi^2} H_z^{sc} \sum_{m,\text{odd}} \frac{1}{m^2} \sin(\tfrac{m\pi}{\ell}z)$$

$$\frac{\left[\frac{2m\pi\mu_o}{L}\cosh\{\frac{m\pi}{\ell}(\frac{d}{2} - y)\} + 2\frac{\ell}{w}\sinh\{\frac{m\pi}{\ell}(\frac{d}{2} - y)\}\right]}{\left[\frac{2m\pi\mu_o}{L}\sinh(\frac{m\pi}{2\ell}d) + 2\frac{\ell}{w}\cosh(\frac{m\pi}{2\ell}d)\right]\left[\frac{2m\pi\mu_o}{L}\cosh(\frac{m\pi}{2\ell}d) + 2\frac{\ell}{w}\sinh(\frac{m\pi}{2\ell}d)\right]} . \tag{136}$$

Applying (21) at both slot faces yields the dipole moments

$$m_z = \frac{1}{\mu_o} \int_{-h}^{h} z\, q_m^{\pm}(z)\, dz = \mp 2\, \alpha_{m,zz}^{\pm}\, H_z^{sc} \ , \tag{137}$$

where the second equality follows from equation (20). Using (125), (126), and (136) in (137) yields the polarizabilities

$$\alpha_{m,zz}^{-} = \frac{8\ell^3}{\pi^3} \sum_{m,\text{odd}} \frac{1}{m^3} \left[\frac{2m\pi\mu_o}{L} + 2\frac{\ell}{w} \coth\left(\frac{m\pi}{2\ell} d\right) \right.$$

$$\left. + \frac{2m\pi\mu_o}{L} + 2\frac{\ell}{w} \tanh\left(\frac{m\pi}{2\ell} d\right) \right]^{-1} \ , \tag{138}$$

$$\alpha_{m,zz}^{+} = \frac{16\ell^4}{\pi^3 w} \sum_{m,\text{odd}} m^3 \left[\frac{2m\pi\mu_o}{L} \sinh\left(\frac{m\pi}{2\ell} d\right) + 2\frac{\ell}{w} \cosh\left(\frac{m\pi}{2\ell} d\right) \right]^{-1}$$

$$\left[\frac{2m\pi\mu_o}{L} \cosh\left(\frac{m\pi}{2\ell} d\right) + 2\frac{\ell}{w} \sinh\left(\frac{m\pi}{2\ell} d\right) \right]^{-1} \ . \tag{139}$$

Note that the exterior inductance per unit length L can be written as

$$L \approx \frac{2\pi\mu_o}{\Omega_o} \ , \tag{140}$$

where the exterior fatness parameter is defined by

$$\Omega_o = 2\, \ell n(\ell/a_o) \approx 2\, \ell n(4\ell/w) \ , \tag{141}$$

and the exterior equivalent radius is approximately $a_o \approx w/4$.

Because of the rapid convergence of the summations in (138) and (139) the first term of each yields a good approximation for the polarizability

$$\bar{\alpha}_{m,zz} \approx \frac{8\ell^3}{\pi^3}\left[\frac{1}{\Omega_o + 2\frac{\ell}{w}\coth(\frac{\pi d}{2\ell})} + \frac{1}{\Omega_o + 2\frac{\ell}{w}\tanh(\frac{\pi d}{2\ell})}\right], \quad (142)$$

$$\alpha^+_{m,zz} \approx \frac{16\ell^4/(\pi^3 w)}{\left[\Omega_o \sinh(\frac{\pi d}{2\ell}) + 2\frac{\ell}{w}\cosh(\frac{\pi d}{2\ell})\right]\left[\Omega_o \cosh(\frac{\pi d}{2\ell}) + 2\frac{\ell}{w}\sinh(\frac{\pi d}{2\ell})\right]}. \quad (143)$$

Two limits of (142) and (143) will now be taken. First the Very Deep limit $\frac{d}{\ell} >> 1$ yields the results

$$\bar{\alpha}_{m,zz} \approx \frac{16\ell^3}{\pi^3(\Omega_o + 2\frac{\ell}{w})}, \quad (144)$$

$$\alpha^+_{m,zz} \approx \frac{64\ell^4 e^{-\pi d/\ell}}{\pi^3 w(\Omega_o + 2\frac{\ell}{w})^2}. \quad (145)$$

If the exterior inductance is ignored by taking it large $L \to \infty$ (we can equivalently take $\Omega_o \to 0$) in (144) and (145) we obtain the simplified results

$$\bar{\alpha}_{m,zz} \approx \frac{8\ell^2 w}{\pi^3}, \quad (146)$$

$$\alpha^+_{m,zz} \approx \frac{16\ell^2 w}{\pi^3} e^{-\pi d/\ell}. \quad (147)$$

The results (146) and (147) correspond to the magnetic charge at both ends of an open

circuited waveguide driven by a uniform current at one end and including only the dominant mode TE_{10}.

The Thick limit $\frac{d}{\ell} << 1$ of (142) and (143) yields

$$\alpha^{-}_{m,zz} \approx \alpha^{+}_{m,zz} \approx \frac{8\ell^3/\pi^3}{\Omega_o + \pi \frac{d}{w}} \approx \frac{8\ell^3}{\pi^3 \Omega} , \qquad (148)$$

where the fatness paramter is given by $\Omega = 2\ \ell n(\ell/a)$ and the approximate equivalent radius a is (17). Comparing (148) and (25) reveals a factor of $96/\pi^4 \approx 0.986$ discrepancy between them. This factor results from including only one term in (138) and (139). If the coth term in (138) is dropped and the approximation $\tanh(\frac{m\pi}{2\ell}d) \approx m\frac{\pi d}{2\ell}$ is used in the second term, then the resulting sum

$$\sum_{m,odd} \frac{1}{m^4} = \frac{\pi^4}{96} , \qquad (149)$$

corrects the discrepancy. The error incurred in the Thick limit, when only one term is included, is obviously quite small. The error incurred in the Very Deep limit, on the incident side, when only one term is included, is slightly larger because the sum in (138) then takes the form of a sum of $\frac{1}{m^3}$ (typically $\frac{2\ell}{w\Omega_o} >> 1$). The error incurred in the Very Deep limit, on the transmitted side, when only one term is included, is of course negligible since all higher order modes experience larger exponential attenuation.

VIII. INTEGRAL EQUATION FOR MAGNETIC CHARGE PER UNIT LENGTH IN DEEP CASE

The integral equation can be obtained by taking the static limit of results in [2], however, we will instead generalize the procedure used in Section III. We assume that the dimensions satisfy (3) in this section.

Figure 22 shows a portion of the slot and contours $C_{\pm}$ where (47) will be applied. It is assumed that $d_o << \ell$ where $y_o = \frac{d}{2} - d_o$. The field is again incident from the $y < -\frac{d}{2}$ half space. The contour C_- yields

$$[H_z^{>}(\rho_o^-,z) + H_z^{sc}]\, dz - H_z^{<}(-y_o,z)\, dz + dI^-_{\rho_o,d_o} = 0 \ , \qquad (150)$$

and the contour C_+ yields

$$- H_z^{>}(\rho_o^+,z)\, dz + H_z^{<}(y_o,z)\, dz + dI^+_{\rho_o,d_o} = 0 \ , \qquad (151)$$

where $dI^{\pm}_{\rho_o,d_o}$ is a differential of the local axial current

$$I^{\pm}_{\rho_o,d_o} = \int_{C^{\pm}_{c\ell s}} \underline{H} \cdot \underline{d\ell} \ , \qquad (152)$$

in the axial direction (the contours $C^{\pm}_{c\ell s}$ are the cross–section parts of $C^{\pm}$ with the largest z value in Figure 22). The quantity $H_z^{<}$ is now interpreted as the nonlocal interior axial magnetic field. From (18) the axial magnetic field can be found as

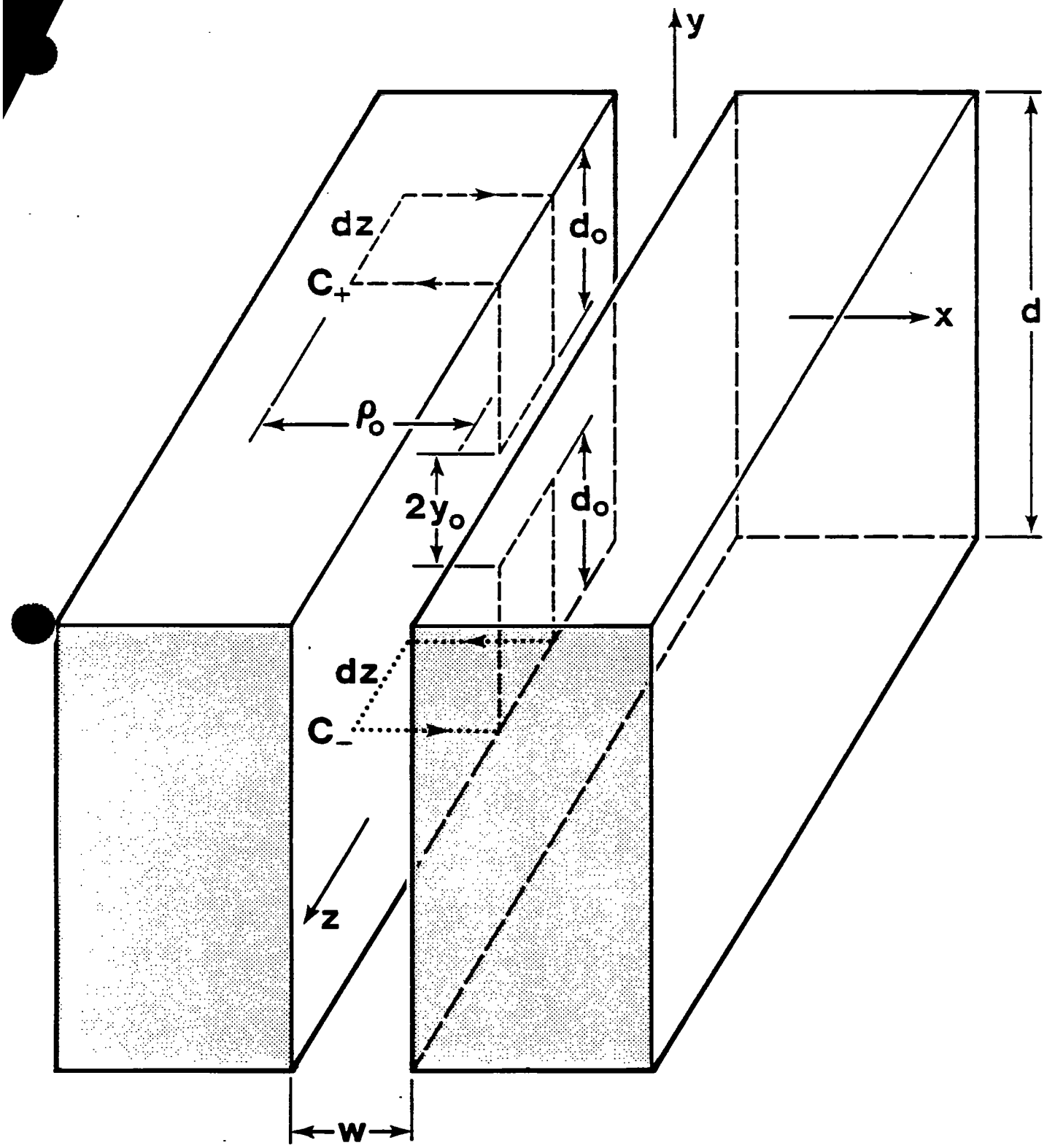

Figure 22. Portion of Deep slot with contours $C_{\pm}$ defined for application of Ampere's law.

$$H_z = -\frac{\partial}{\partial z}\varphi_m \ . \tag{153}$$

Integrating (150) and (151) with respect to z yields

$$\varphi_m^{>}(\rho_o^-,z) + \varphi_m^{sc}(z) - \varphi_m^{<}(-y_o,z) - I^-_{\rho_o,d_o} = 0 \ , \tag{154}$$

$$\varphi_m^{>}(\rho_o^+,z) - \varphi_m^{<}(y_o,z) + I^+_{\rho_o,d_o} = 0 \ , \tag{155}$$

where $\varphi_m^{sc}(z) = -z\,H_z^{sc}$, $\varphi_m^{>}$ is given by (45), and $\varphi_m^{<}$ now denotes the nonlocal interior potential (note all terms in the above two equations will be taken as odd in z). The local axial current is related to the magnetic flux per unit length by means of

$$L^{\pm}_{\rho_o,d_o} I^{\pm}_{\rho_o,d_o} = \Phi^{\pm} \ , \tag{156}$$

where $L^{\pm}_{\rho_o,d_o}$ are local inductances per unit length at the incident and transmitted sides of the slot. They will be taken to have the form

$$L^{\pm}_{\rho_o,d_o} = \frac{\pi\mu_o}{\ell n(\rho_o/a_o^{\pm}) + \pi\frac{d_o}{w}} \ , \tag{157}$$

where $a_o^{\pm}$ are equivalent antenna radii to be determined.

The potential $\varphi_m^{<}$ satisfies Laplace's equation, is taken to be uniform in x, and satisfies the boundary conditions

$$\frac{\partial}{\partial z}\varphi_m^< = 0 \, , \, z = \pm h \, , \tag{158}$$

$$-\mu_o w \frac{\partial}{\partial y}\varphi_m^< = \overline{\Phi}^{\pm} = \pm \frac{1}{2} q_m^{\pm} \, , \, y = \pm \frac{d}{2} \, . \tag{159}$$

The nonlocal interior potential can thus be written as

$$\varphi_m^< = -\frac{1}{\pi\mu_o w} \int_{-h}^{h} \sum_{m=1}^{\infty} \frac{1}{m} \operatorname{csch}(m\pi d/\ell) \cos\frac{m\pi}{\ell}(z + h) \cos\frac{m\pi}{\ell}(z' + h)$$

$$\left[q_m^+(z') \cosh\frac{m\pi}{\ell}(\frac{d}{2} + y) + q_m^-(z') \cosh\frac{m\pi}{\ell}(\frac{d}{2} - y)\right] dz' \, . \tag{160}$$

Inserting (160) into (154) and (155) yields

$$\varphi_m^>(\rho_o^-,z) + \varphi_m^{sc}(z) - I_{\rho_o,d_o}^- + \frac{1}{\pi\mu_o w} \int_{-h}^{h} \sum_{m=1}^{\infty} \frac{1}{m} \operatorname{csch}(m\pi d/\ell) \cos\frac{m\pi}{\ell}(z' + h)$$

$$\cos\frac{m\pi}{\ell}(z + h) \left[q_m^+(z') \cosh(\frac{m\pi}{\ell}d_o) + q_m^-(z') \cosh\frac{m\pi}{\ell}(d - d_o)\right] dz' = 0 \, , \tag{161}$$

$$\varphi_m^>(\rho_o^+,z) + I_{\rho_o,d_o}^+ + \frac{1}{\pi\mu_o w} \int_{-h}^{h} \sum_{m=1}^{\infty} \frac{1}{m} \operatorname{csch}(m\pi d/\ell) \cos\frac{m\pi}{\ell}(z + h) \cos\frac{m\pi}{\ell}(z' + h)$$

$$\left[q_m^+(z') \cosh\frac{m\pi}{\ell}(d - d_o) + q_m^-(z') \cosh(\frac{m\pi}{\ell}d_o)\right] dz' = 0 \, . \tag{162}$$

The approximations

$$\cosh(\tfrac{m\pi}{\ell}d_o) \approx 1 \ , \tag{163}$$

$$\cosh\tfrac{m\pi}{\ell}(d - d_o) \approx \cosh(\tfrac{m\pi}{\ell}d) - \tfrac{m\pi}{\ell}d_o \sinh(\tfrac{m\pi}{\ell}d) \ , \tag{164}$$

along with the identity [8]

$$\sum_{m=1}^{\infty} \cos\tfrac{m\pi}{\ell}(z + h) \cos\tfrac{m\pi}{\ell}(z' + h) = \tfrac{\ell}{2}[\delta(z - z') - \tfrac{1}{\ell}] \ , \tag{165}$$

will now be used in (161) and (162). Furthermore, the approximations (58) and (59) yield the result

$$\frac{1}{\mu_o}\int_{-h}^{h} \frac{q_m^{\pm}(z')}{4\pi R_o}\,dz' + \frac{\ell n(\rho_o/a_o^{\pm})}{2\pi\mu_o} q_m^{\pm}(z) \approx \frac{1}{\mu_o}\int_{-h}^{h} \frac{q_m^{\pm}(z')}{4\pi R_{a_o^{\pm}}}\,dz' \ , \tag{166}$$

where R_o is given by (57) and

$$R_{a_o^{\pm}} = \sqrt{(a_o^{\pm})^2 + (z - z')^2} \ . \tag{167}$$

Using (45), (163), (164), (165), and (166) in (161) and (162) yields

$$\frac{1}{\mu_o}\int_{-h}^{h} \frac{q_m^{-}(z')}{4\pi R_{a_o^{-}}}\,dz' + \frac{1}{\pi\mu_o w}\int_{-h}^{h} \sum_{m=1}^{\infty} \frac{1}{m} \cos\tfrac{m\pi}{\ell}(z + h) \cos\tfrac{m\pi}{\ell}(z' + h)$$

$$\left[q_m^{+}(z') \operatorname{csch}(\tfrac{m\pi}{\ell}d) + q_m^{-}(z') \coth(\tfrac{m\pi}{\ell}d)\right] dz' = z\, H_z^{sc} \ , \tag{168}$$

$$\frac{1}{\mu_o}\int_{-h}^{h}\frac{q_m^{+}(z')}{4\pi R_{a_o^{+}}}\,dz' + \frac{1}{\pi\mu_o w}\int_{-h}^{h}\sum_{m=1}^{\infty}\frac{1}{m}\cos\frac{m\pi}{\ell}(z+h)\cos\frac{m\pi}{\ell}(z'+h)$$

$$\left[q_m^{+}(z')\coth(\frac{m\pi}{\ell}d) + q_m^{-}(z')\,\mathrm{csch}(\frac{m\pi}{\ell}d)\right]dz' = 0\,. \qquad (169)$$

These are the desired integral equations.

In the case where the slot is symmetric in the depth, $a_o^{-} = a_o^{+} = a_o$, (168) and (169) may be decoupled by letting

$$q_m^{\pm} = q_m^{e} \mp q_m^{o}\ , \qquad (170)$$

where q_m^{e} and q_m^{o} denote the even and odd parts of the magnetic charge per unit length with respect to the depth y. We thus obtain

$$\frac{1}{\mu_o}\int_{-h}^{h}\frac{q_m^{e}(z')}{4\pi R_{a_o}}\,dz' + \frac{1}{\pi\mu_o w}\int_{-h}^{h}q_m^{e}(z')\sum_{m=1}^{\infty}\frac{1}{m}\coth(\frac{m\pi}{2\ell}d)\cos\frac{m\pi}{\ell}(z+h)$$

$$\cos\frac{m\pi}{\ell}(z'+h)\,dz' = -\varphi^{inc}(z) = z\,H_z^{inc}\ , \qquad (171)$$

$$\frac{1}{\mu_o}\int_{-h}^{h}\frac{q_m^{o}(z')}{4\pi R_{a_o}}\,dz' + \frac{1}{\pi\mu_o w}\int_{-h}^{h}q_m^{o}(z')\sum_{m=1}^{\infty}\frac{1}{m}\tanh(\frac{m\pi}{2\ell}d)\cos\frac{m\pi}{\ell}(z+h)$$

$$\cos\frac{m\pi}{\ell}(z'+h)\,dz' = -\varphi_m^{inc}(z) = z\,H_z^{inc}\,. \qquad (172)$$

Note that because $q_m^{\pm}(z)$, $q_m^{e}(z)$, and $q_m^{o}(z)$ are odd with respect to z, only the odd terms in the summations contribute.

In the Thick limit $\frac{d}{\ell} << 1$, $q_m^{\pm} \approx \mp q_m^{o}$, and thus (172) alone must be solved. In the Very Deep limit $\frac{d}{\ell} >> 1$, (168) and (169) should be used instead of (171) and (172). Note that in the Very Deep limit, the $\operatorname{csch}(\frac{m\pi}{\ell}d)$ term in (168) may be ignored and $\coth(\frac{m\pi}{\ell}d)$ may be replaced by unity yielding

$$\frac{1}{\mu_o}\int_{-h}^{h}\frac{q_m^{-}(z')}{4\pi R_{a_o}^{-}}\,dz' + \frac{1}{\pi\mu_o w}\int_{-h}^{h} q_m^{-}(z')\sum_{m=1}^{\infty}\frac{1}{m}\cos\frac{m\pi}{\ell}(z+h)\cos\frac{m\pi}{\ell}(z'+h)\,dz'$$

$$\sim -\varphi_m^{sc}(z) = z\,H_z^{sc}\ . \qquad (173)$$

Furthermore, in the Very Deep limit (169) becomes

$$\frac{1}{\mu_o}\int_{-h}^{h}\frac{q_m^{+}(z')}{4\pi R_{a_o}^{+}}\,dz' + \frac{1}{\pi\mu_o w}\int_{-h}^{h} q_m^{+}(z')\sum_{m=1}^{\infty}\frac{1}{m}\cos\frac{m\pi}{\ell}(z+h)\cos\frac{m\pi}{\ell}(z'+h)\,dz'$$

$$\sim -\frac{2e^{-\pi d/\ell}}{\pi\mu_o w}\sin(\tfrac{\pi}{\ell}z)\int_{-h}^{h} q_m^{-}(z')\sin(\tfrac{\pi}{\ell}z')\,dz'\ . \qquad (174)$$

IX. EQUIVALENT RADIUS FOR DEEP CASE

The quantity a_o can be found by taking $d >> w$ and extracting the uniform field contribution to a in Section IV. However, we briefly determine it by means of the simple direct solution to the slot in a Very Thick ($d >> w$) plane [2].

The geometry is shown in Figure 23. Note that the origin has been shifted to the corner of the metal originally at $x = -w/2$, $y = -d/2$. The transformation which maps the region surrounding the conductors into the upper half of a z_1 plane is [2], [9]

$$\frac{z}{w} = \frac{1}{\pi}(\arctan \zeta - \zeta) , \quad \zeta = \sqrt{z_1^2 - 1} , \tag{175}$$

where the arctangent is defined by

$$\arctan \zeta = \frac{\pi}{2} + \frac{1}{2i} \ell n\left[\frac{i\zeta + 1}{i\zeta - 1}\right] , \tag{176}$$

and the principal branch of each linear factor in the square root and logarithm are to be taken.

The magnetostatic field is determined from (18) and (68) with the complex potential in this case given by

$$W = -\frac{\overline{\Phi}}{\pi} \ell n(z_1/a_1) , \tag{177}$$

where a_1 is an arbitrary real constant. The current $\overline{I}_{\rho_o, d_o}$ is determined from applying (152) as

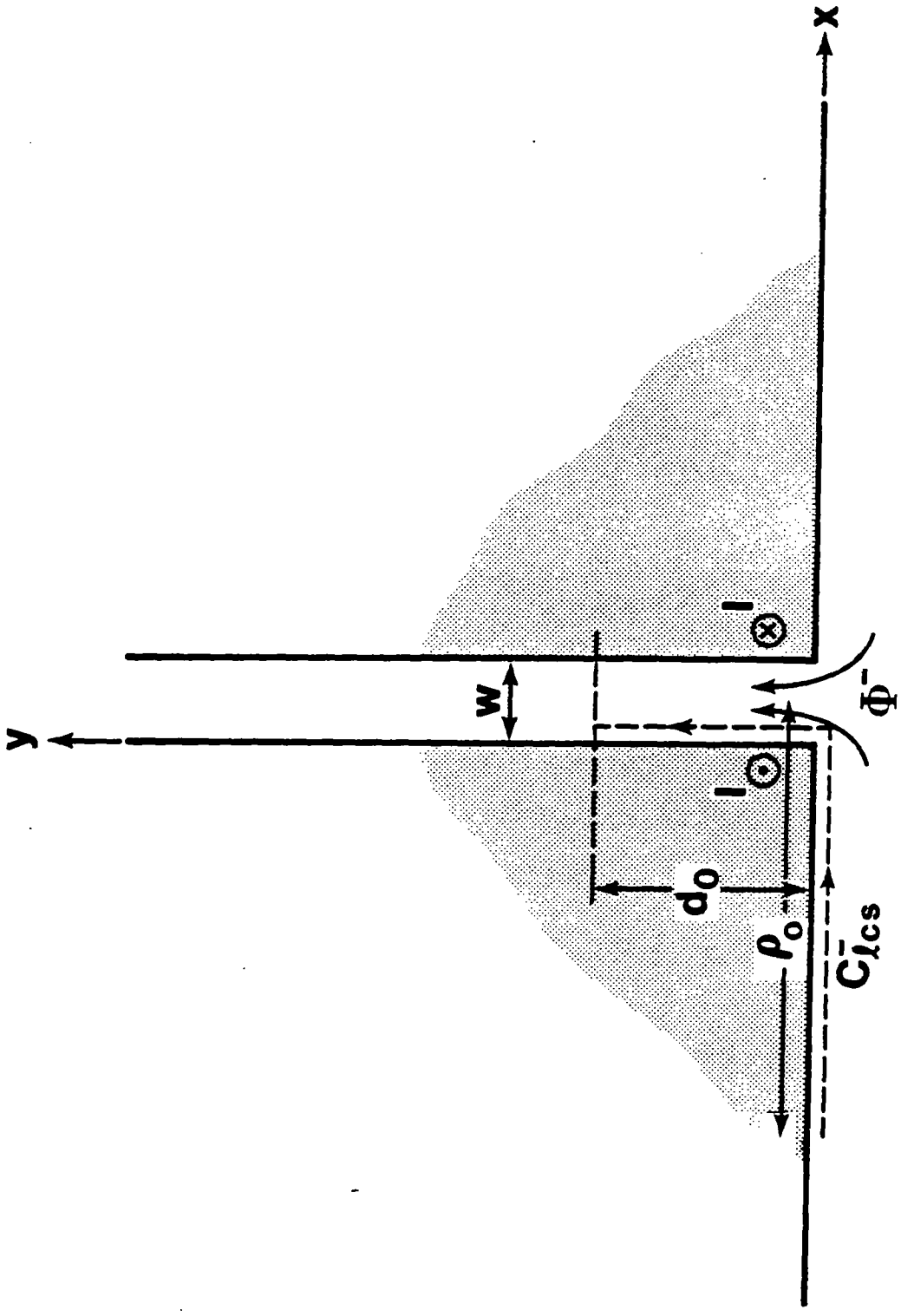

Figure 23. Incident edge of Deep slot for evaluation of local axial current and inductance.

$$I^{-}_{\rho_o,d_o} = \varphi_m(-\rho_o) - \varphi_m(id_o) \ , \tag{178}$$

where the arguments of φ_m are the complex locations in the cross-section z plane of Figure 23.

The transformation (175) can be expanded for ρ_o, $d_o >> w$ as

$$z_1 \sim \pi \frac{\rho_o}{w} \ , \ z = -\rho_o \ , \tag{179}$$

$$z_1 \sim 2\, e^{-\pi d_o/w} - 1 \ , \ z = id_o \ . \tag{180}$$

Using (179) and (180) in (68), (177), and (178), yields

$$I^{-}_{\rho_o,d_o} = \bar{\Phi}^{-}/L_{\rho_o,d_o} \ , \tag{181}$$

where

$$L_{\rho_o,d_o} = \frac{\pi\mu_o}{\ell n(\rho_o/a_o) \ + \ \pi \ d_o/w} \ , \tag{182}$$

and the equivalent radius is

$$a_o = \frac{2w}{\pi e} \approx \frac{w}{4.27} \ . \tag{183}$$

Of course, by symmetry $I^{+}_{\rho_o,d_o}$ and $\bar{\Phi}^{+}$ are also related by (181).

If we consider (172) in the Thick limit $\frac{d}{\ell} << 1$, by taking $\tanh(\frac{m\pi}{2\ell}d) \approx m\frac{\pi d}{2\ell}$ and

using (165) we obtain

$$\frac{1}{\mu_o}\int_{-h}^{h}\frac{q_m^o(z')}{4\pi R_{a_o}}\,dz' + \frac{\ell n\left(e^{\frac{\pi d}{2w}}\right)}{2\pi\mu_o}\,q_m^o(z) = -\varphi_m^{inc}(z)\ . \qquad (184)$$

Combining the two terms on the left of the equals sign in (184), see (166), yields Hallén's equation (60) with the asymptotic expansion of the equivalent antenna radius in the Very Thick limit (77). If the Thick slot conformal mapping solution is used to define a_o when $\frac{d}{\ell} << 1$, but $\frac{d}{w} = O(1)$, it would be possible to make (172) uniformly valid as $d \to 0$. However, because the Thick case has already been treated, and from a practical point of view because the rigorous value of a_o differs by so little from $w/4$ anyway, we can obtain a good uniformly valid approximation ($0 \leq d < \infty$) to $q_m^{\pm}(z)$ by solving (171), (172), (173), and (174) with a_o given approximately by the exterior Thin slot value

$$a_o \approx \frac{w}{4}\ . \qquad (185)$$

X. AXIAL POLARIZABILITY FOR DEEP CASE

An approximate solution of (171) and (172) can now be derived by iteration, similar to Section V. The first step is to expand the magnetic charge per unit length in the basis

$$q_m^e(z') = \sum_{n=1}^{\infty} q_{mn}^e \cos\frac{n\pi}{\ell}(z' + h) \quad , \tag{186}$$

$$q_m^o(z') = \sum_{n=1}^{\infty} q_{mn}^o \cos\frac{n\pi}{\ell}(z' + h) \quad . \tag{187}$$

Now making use of the orthogonality of $\cos\frac{n\pi}{\ell}(z + h)$ and applying the operator

$$\int_{-h}^{h} \cos\frac{m\pi}{\ell}(z + h)\, dz \quad , \tag{188}$$

to both sides of (171) and (172), the summations in the second terms (interior part of the kernel of the integral equations) of (171) and (172), as well as the summations introduced by inserting (186) and (187) into these terms, are eliminated. In other words the interior kernel is diagonal in the basis (186) and (187). The first terms (exterior part of the kernel) of (171) and (172) are broken up as in (79), with Ω_o (See (141).) replacing Ω. The dominant Ω_o part of the exterior kernel is diagonal in any basis, but the remaining part is not diagonal in the basis (186) and (187). Thus the summations introduced by insertion of (186) and (187) are not eliminated for this part of the exterior kernel. The resulting system can now be iterated by including only the interior and Ω_o parts of the kernel on the first iteration (zero order), then using this solution in the previously

discarded exterior terms to obtain the first order solution. Instead of following this straightforward but tedious iteration procedure we now introduce an alternative approximation.

We are interested in determining the polarizabilities of the Deep slot. The Thick result (86) indicates that the first order solution could have been determined by a simple zero order calculation if the expansion parameter had been selected as $\Omega' = \Omega + 2(\ell n\ 2 - 7/3)$ instead of Ω. This consideration of the Thick Case leads us to choose the expansion parameter

$$\Omega_o' = \Omega_o + 2(\ell n\ 2 - 7/3)\ , \qquad (189)$$

instead of Ω_o for the exterior kernel. A zero order calculation will now be carried out for the Deep case. This zero order calculation will actually be correct to first order in the Thick limit. When the slot becomes Very Deep the zero order distribution of magnetic charge is changed somewhat from the Thick case (for example, the Thick case has a zero order charge distribution which is linear in z, whereas the Very Deep zero order magnetic charge distribution on the transmitted side is proportional to $\sin(\frac{\pi}{\ell}z)$). This change is not significant, however, and furthermore, the choice of the "best" expansion parameter is most critical only in the Thick limit (to be more precise only in the Thin limit $d/w \to 0$) where the choice (189) does indeed produce the correct first order result. A comparison of this zero order calculation with a Galerkin numerical solution later in this section will confirm the usefulness of the choice (189).

The n even coefficients in (186) and (187) all vanish. From (171) and (172) we obtain for the n odd coefficients

$$q^{e}_{mn}\left[\frac{h\Omega'_o}{4\pi\mu_o} + \frac{h^2}{\pi\mu_o wn}\coth(\frac{n\pi}{2\ell}d)\right] = -2H_z^{inc}(\frac{\ell}{n\pi})^2 \ , \qquad (190)$$

$$q^{o}_{mn}\left[\frac{h\Omega'_o}{4\pi\mu_o} + \frac{h^2}{\pi\mu_o wn}\tanh(\frac{n\pi}{2\ell}d)\right] = -2H_z^{inc}(\frac{\ell}{n\pi})^2 \ . \qquad (191)$$

Inserting (170), (186), and (187) into (137) we determine the polarizabilities as

$$\alpha^{-}_{m,zz} = \frac{8\ell^3}{\pi^3}\sum_{m,odd}\frac{1}{m^3}\left[\frac{1}{m\Omega'_o + 2\frac{\ell}{w}\coth(\frac{m\pi}{2\ell}d)}\right.$$

$$\left. + \frac{1}{m\Omega'_o + 2\frac{\ell}{w}\tanh(\frac{m\pi}{2\ell}d)}\right] \ , \qquad (192)$$

$$\alpha^{+}_{m,zz} = \frac{16\ell^4}{\pi^3 w}\sum_{m,odd} m^3\left[m\Omega'_o\sinh(\frac{m\pi}{2\ell}d) + 2\frac{\ell}{w}\cosh(\frac{m\pi}{2\ell}d)\right]$$

$$\left[m\Omega'_o\cosh(\frac{m\pi}{2\ell}d) + 2\frac{\ell}{w}\sinh(\frac{m\pi}{2\ell}d)\right] \ . \qquad (193)$$

These expressions are identical to the heuristic results (138) and (139) except for the replacement of Ω_o by Ω'_o. Obviously, one term again gives a useful approximation

$$\alpha^{-}_{m,zz} \approx \frac{8\ell^3}{\pi^3}\left[\frac{1}{\Omega'_o + 2\frac{\ell}{w}\coth(\frac{\pi d}{2\ell})} + \frac{1}{\Omega'_o + 2\frac{\ell}{w}\tanh(\frac{\pi d}{2\ell})}\right] \ , \qquad (194)$$

$$\alpha^{+}_{m,zz} \approx \frac{16\ell^4/(\pi^3 w)}{\left[\Omega'_o\sinh(\frac{\pi d}{2\ell}) + 2\frac{\ell}{w}\cosh(\frac{\pi d}{2\ell})\right]\left[\Omega'_o\cosh(\frac{\pi d}{2\ell}) + 2\frac{\ell}{w}\sinh(\frac{\pi d}{2\ell})\right]} \ . \qquad (195)$$

The Very Deep limit of (194) and (195) gives

$$\alpha^{-}_{m,zz} \approx \frac{16\ell^3}{\pi^3(\Omega'_o + 2\frac{\ell}{w})} , \tag{196}$$

$$\alpha^{+}_{m,zz} \approx \frac{64\,\ell^4\ e^{-\pi d/\ell}}{\pi^3 w(\Omega'_o + 2\frac{\ell}{w})^2} . \tag{197}$$

The purely interior results (146) and (147) remain unchanged when we let $\Omega'_o \to 0$.

A numerical solution of the Deep case is now given. As in the Thick case, Section V, it is more convenient to work with $y^{\pm}_m$ or $y^{e\,o}_m$ where

$$\frac{\partial}{\partial z} y^{\pm}_m = q^{\pm}_m , \tag{198}$$

$$\frac{\partial}{\partial z} y^{e\,o}_m = q^{e\,o}_m , \tag{199}$$

and

$$y^{\pm}_m(\pm h) = y^{e\,o}_m(\pm h) = 0 . \tag{200}$$

The operator $\frac{\partial}{\partial z}$ is applied to (171), (172), (173), or (174), followed by integation by parts to bring the second derivative outside the integral

$$\frac{\partial^2}{\partial z^2} \int_{-h}^{h} y^{e}_m(z') \left[\frac{1}{R_{a_o}} + \frac{4}{w} \sum_{m,\text{odd}} \frac{1}{m} \coth(\frac{m\pi}{2\ell} d) \cos(\frac{m\pi}{\ell} z) \right.$$

$$\cos(\frac{m\pi}{\ell}z')\Big] \, dz' = 4\pi\mu_o H_z^{inc} \quad , \tag{201}$$

$$\frac{\partial^2}{\partial z^2}\int_{-h}^{h} y_m^o(z')\Big[\frac{1}{R_{a_o}} + \frac{4}{w}\sum_{m,odd}\frac{1}{m}\tanh(\frac{m\pi}{2\ell}d)\cos(\frac{m\pi}{\ell}z)$$

$$\cos(\frac{m\pi}{\ell}z')\Big] \, dz' = 4\pi\mu_o H_z^{inc} \quad , \tag{202}$$

and for the Very Deep case

$$\frac{\partial^2}{\partial z^2}\int_{-h}^{h} y_m^-(z')\Big[\frac{1}{R_{a_o}} + \frac{4}{w}\sum_{m,odd}\frac{1}{m}\cos(\frac{m\pi}{\ell}z)\cos(\frac{m\pi}{\ell}z')\Big] \, dz'$$

$$\sim 4\pi\mu_o H_z^{sc} \quad , \tag{203}$$

$$\frac{\partial^2}{\partial z^2}\int_{-h}^{h} y_m^+(z')\Big[\frac{1}{R_{a_o}} + \frac{4}{w}\sum_{m,odd}\frac{1}{m}\cos(\frac{m\pi}{\ell}z)\cos(\frac{m\pi}{\ell}z')\Big] \, dz'$$

$$\sim \frac{8\pi^2}{w\ell^2} e^{-\pi d/\ell}\cos(\frac{\pi}{\ell}z)\int_{-h}^{h} y_m^-(z')\cos(\frac{\pi}{\ell}z') \, dz' \quad , \tag{204}$$

where the fact that $y_m^{\pm}$ and $y_m^{e,o}$ are even in z has been used.

The Galerkin method is now identical (with the addition of $\pm$ superscripts to the appropriate quantities) to that in equations (89) through (100) of Section V except: (95),

(96), and (100) are replaced by

$$\alpha^{\pm}_{m,zz} = \pm \frac{1}{4\mu_o H_z^{inc}} \int_{-h}^{h} y^{\pm}_m(z)\, dz \ , \tag{205}$$

$$\alpha^{\pm}_{m,zz} = \pm \frac{1}{4\mu_o H_z^{inc}} \sum_{j=-N}^{N} y^{\pm}_{mj}\, H_j \ , \tag{206}$$

$$\alpha^{\pm}_{m,zz} = \frac{\pm 1}{4\mu_o H_z^{inc}} \sum_{j=1}^{N} \epsilon_j\, y^{\pm}_{mj}\, H_j \ , \tag{207}$$

$\frac{1}{R_a}$ in (93) is replaced by each of the bracketed quantities in (201) through (204) above, H_z^{inc} is replaced by H_z^{sc} when solving (203), and the right hand side $4\pi\mu_o H_z^{inc}$ of (89) and the succeeding equations is replaced by the right hand side of (204) when solving (204) for y^{+}_m. Note that when solving (204), the integral on the right hand side is simply a normalization constant which can be taken as unity in the numerical solution and then multiplied by the solution once y^{-}_m has been determined from (203).

The sums in (201) through (204) were terminated at $m \leq M$ where we chose

$$M = 10\, N \ , \tag{208}$$

and N was the upper limit of basis functions in (90).

Figures 24 through 27 show a comparison of the Galerkin results from (207), the analytical results from (192) and (193) including terms $m \leq M = 11$ with Ω_o' expansion parameter, the one term $m = M = 1$ approximations (194) and (195) with Ω_o' expansion

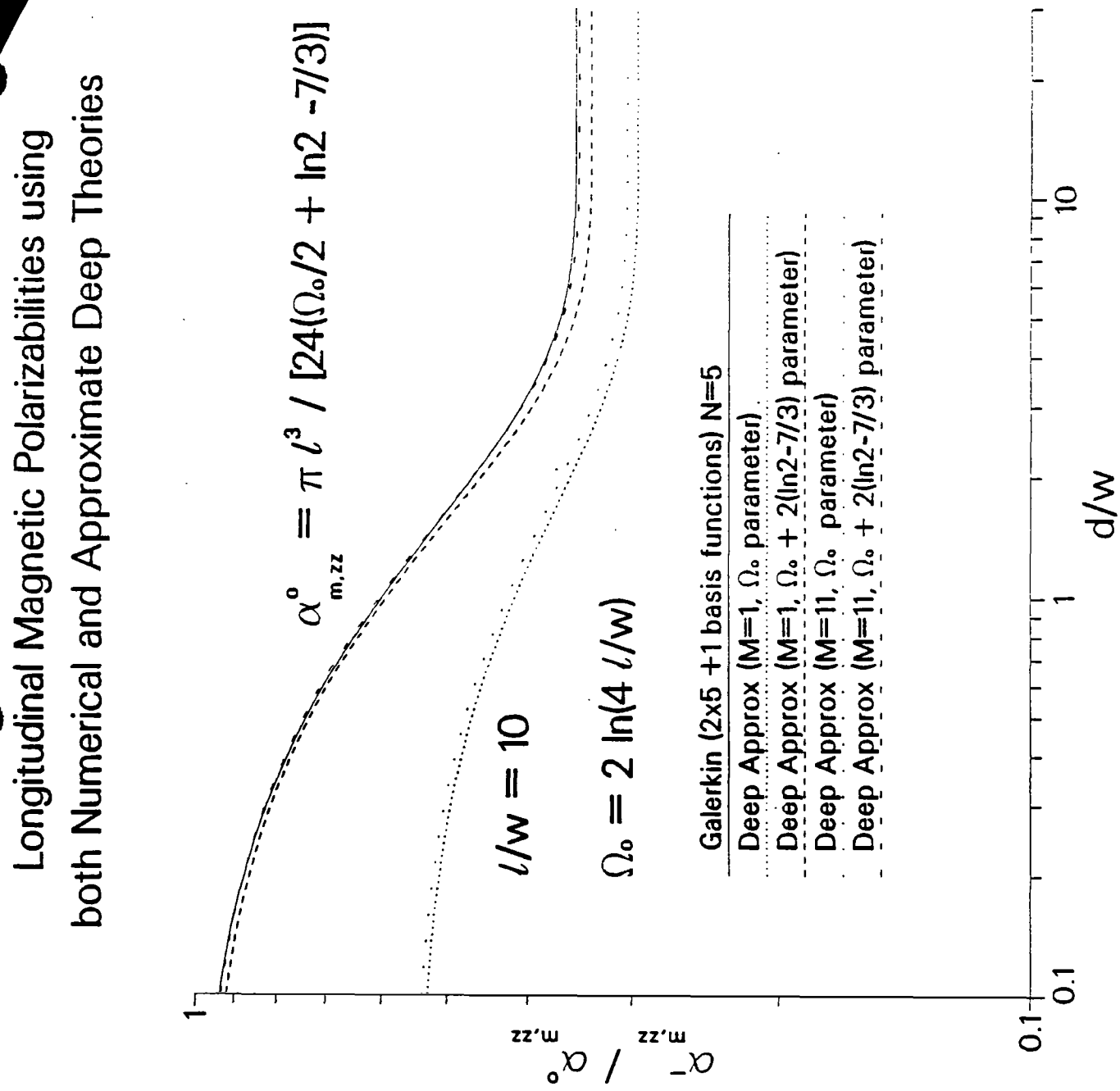

Figure 24. Longitudinal magnetic polarizability for Deep case with ℓ/w = 10. A comparison of the Galerkin solution with N = 5 (solid curve), and zero order approximations using expansion parameter $\Omega_o' = \Omega_o + 2(\ell n\ 2 - 7/3)$ (dashed curves), and zero order approximations using expansion parameter Ω_o (dotted curves), is given. The closely spaced dashed and dotted curves represent only the inclusion of the dominant interior mode. All curves are normalized by the first order result for a zero depth slot and thus depend only on the parameters ℓ/w and d/w. a) Incident side.

b) Transmitted side.

Longitudinal Magnetic Polarizabilities using both Numerical and Approximate Deep Theories

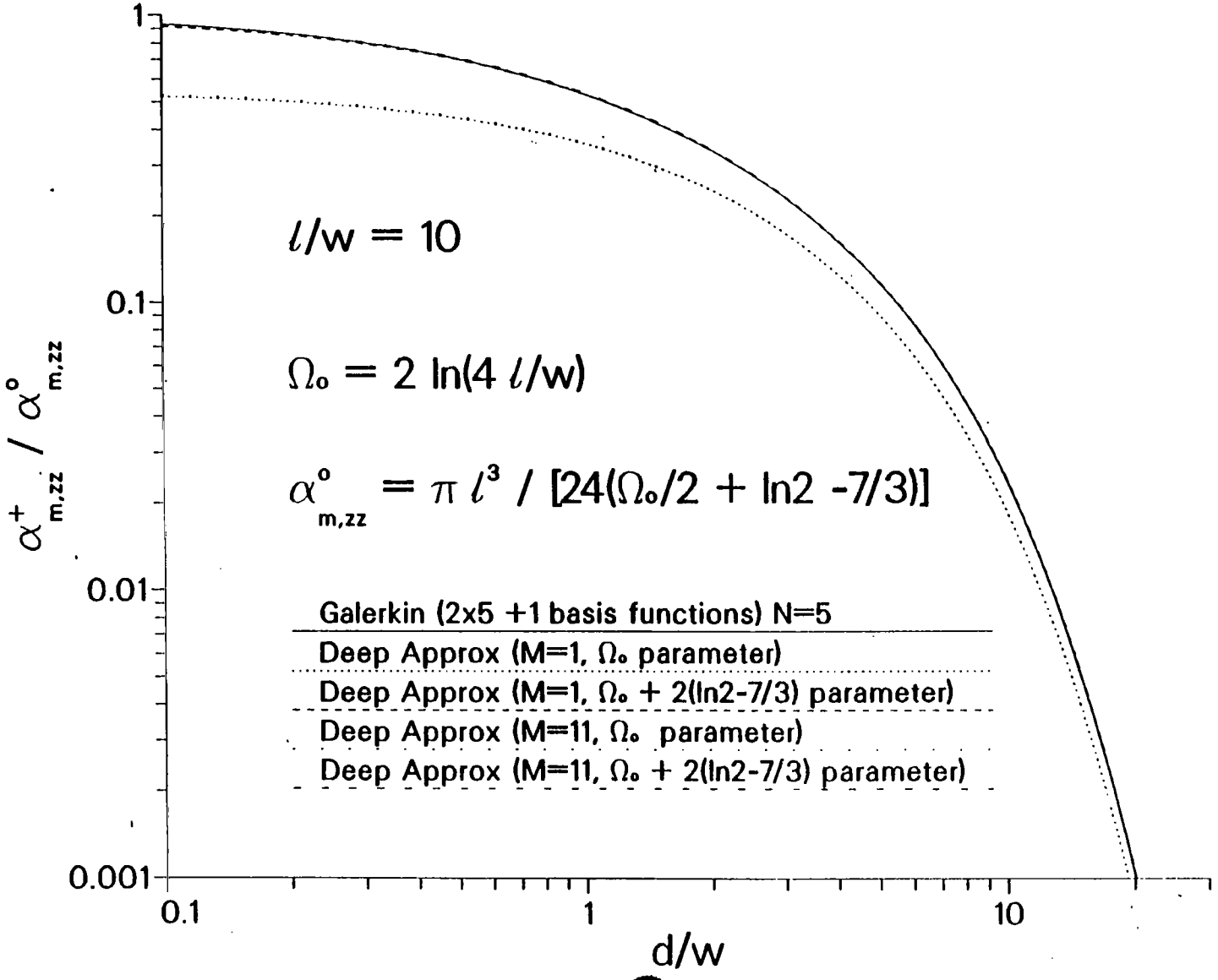

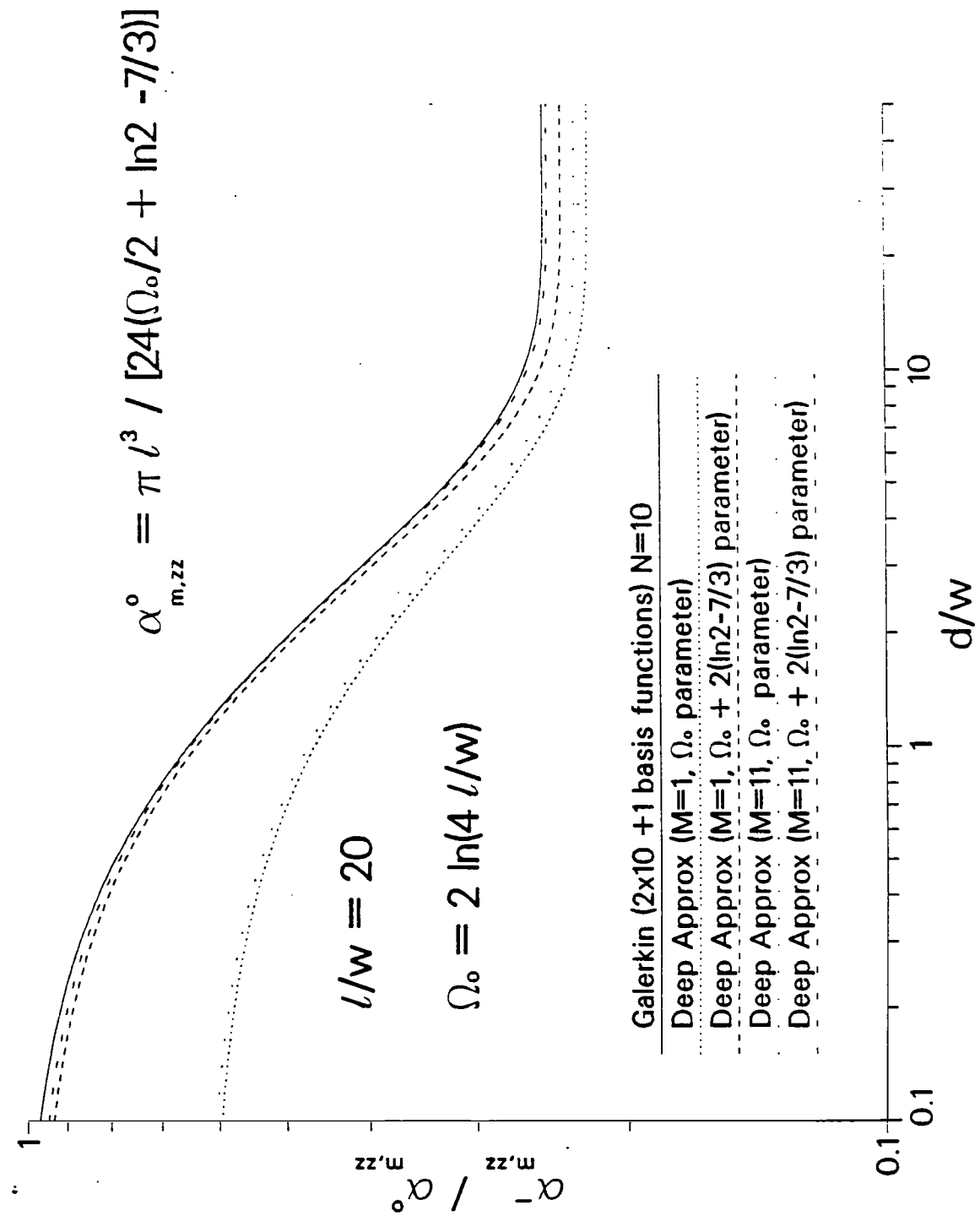

Figure 25. Same as Figure 24 except ℓ/w = 20 and N = 10 in the Galerkin results. a) Incident side.

b) Transmitted side.

Longitudinal Magnetic Polarizabilities using both Numerical and Approximate Deep Theories

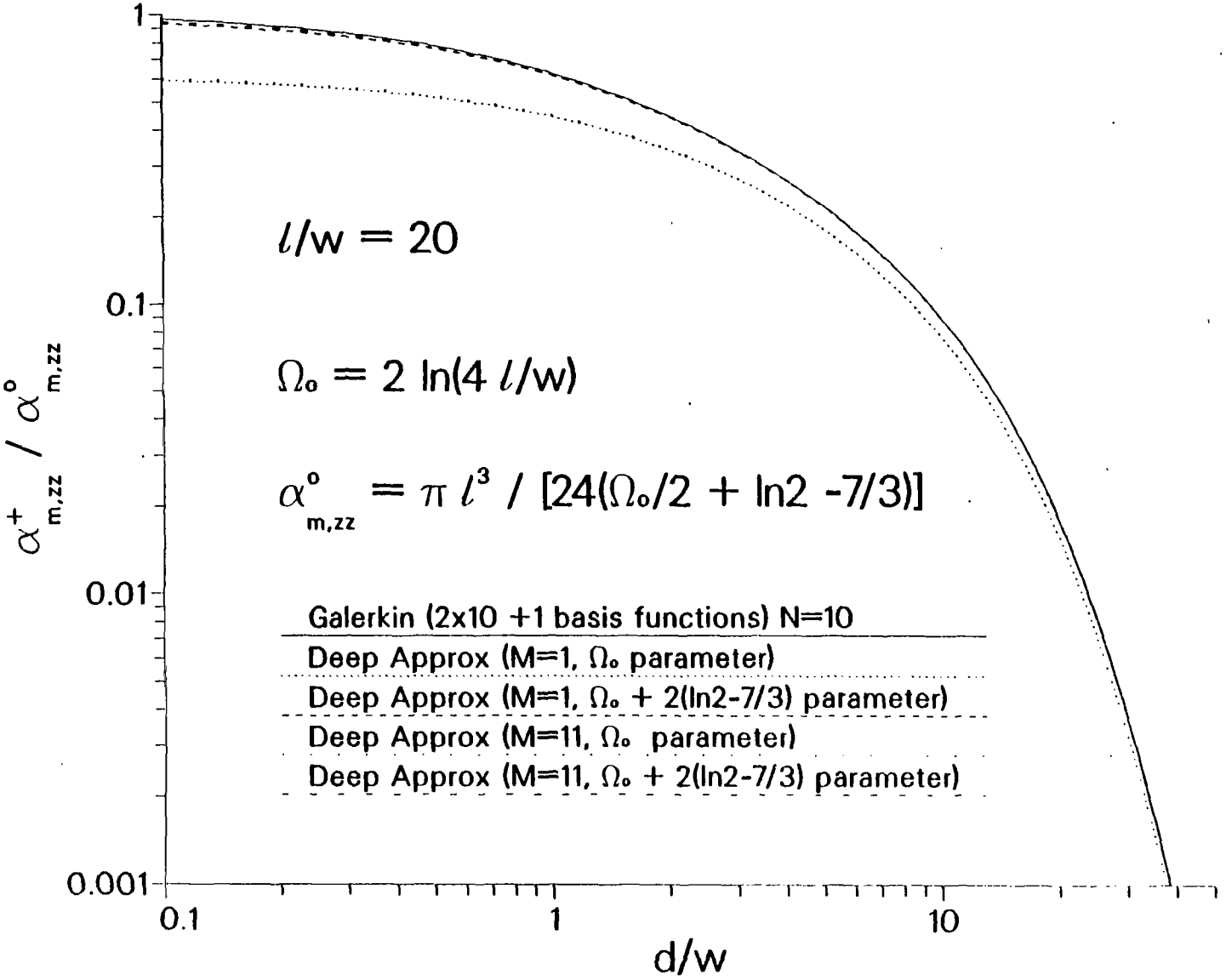

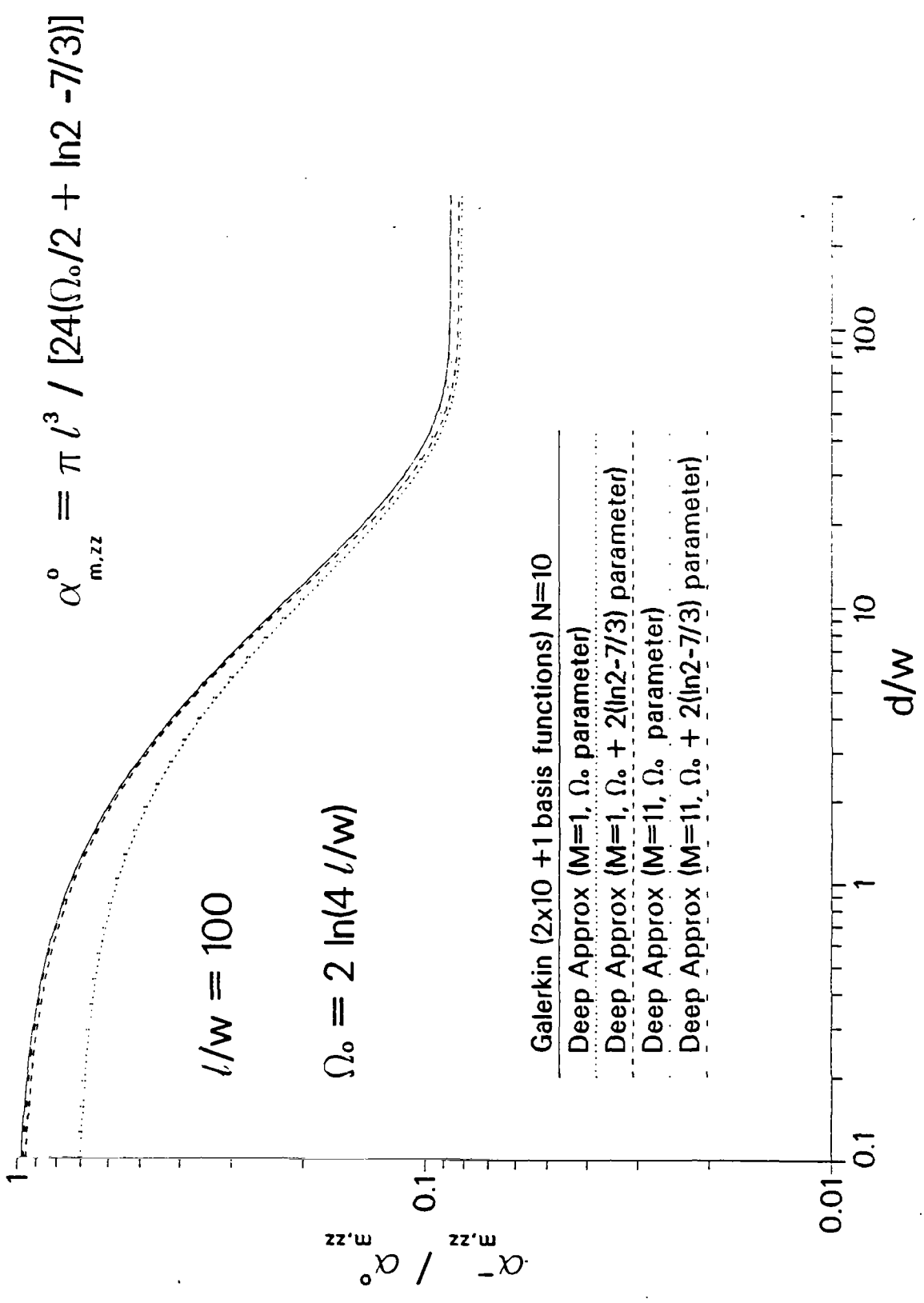

Figure 26. Same as Figure 24 except ℓ/w = 100 and N = 10 in the Galerkin results. a) Incident side.

b) Transmitted side.

Longitudinal Magnetic Polarizabilities using both Numerical and Approximate Deep Theories

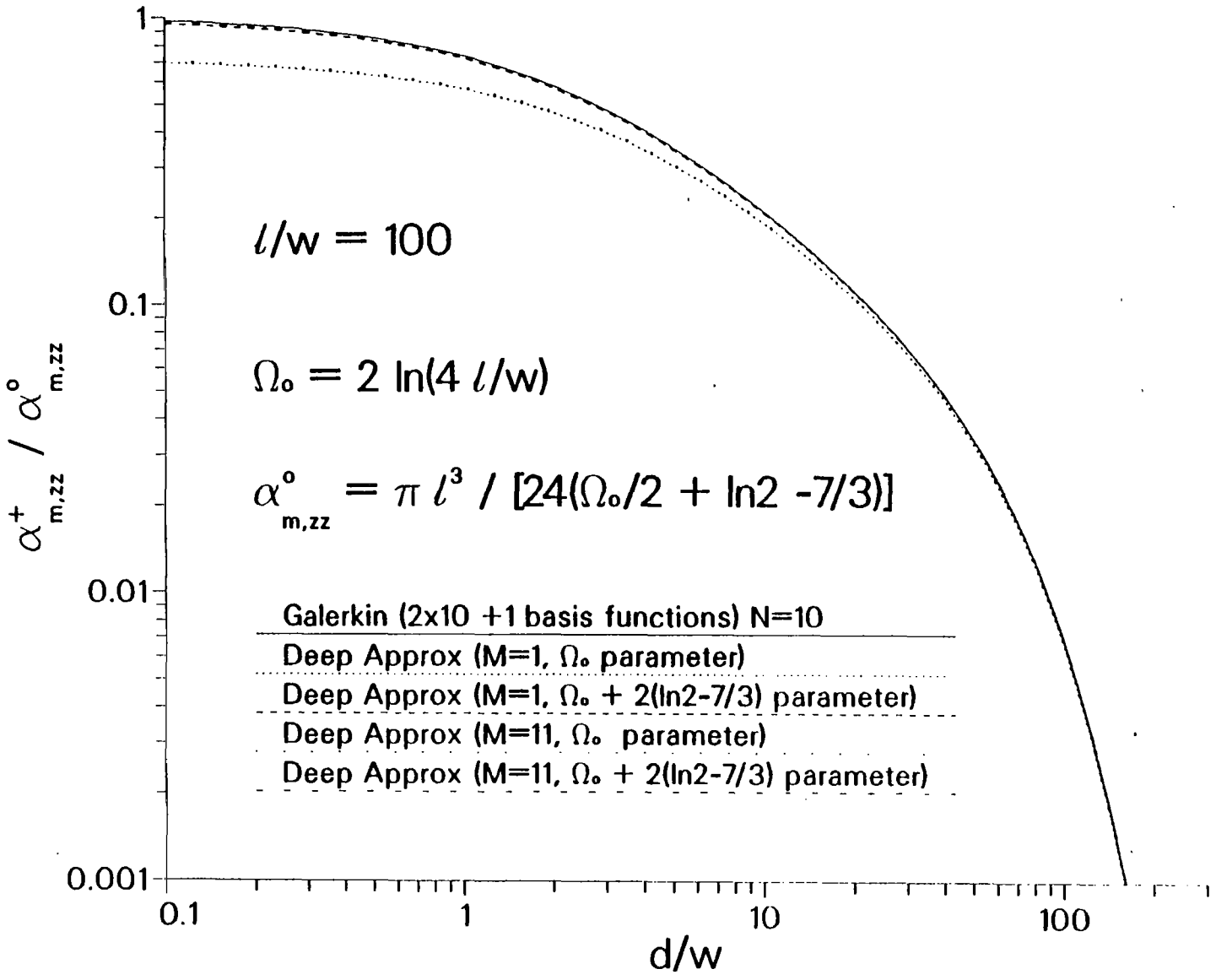

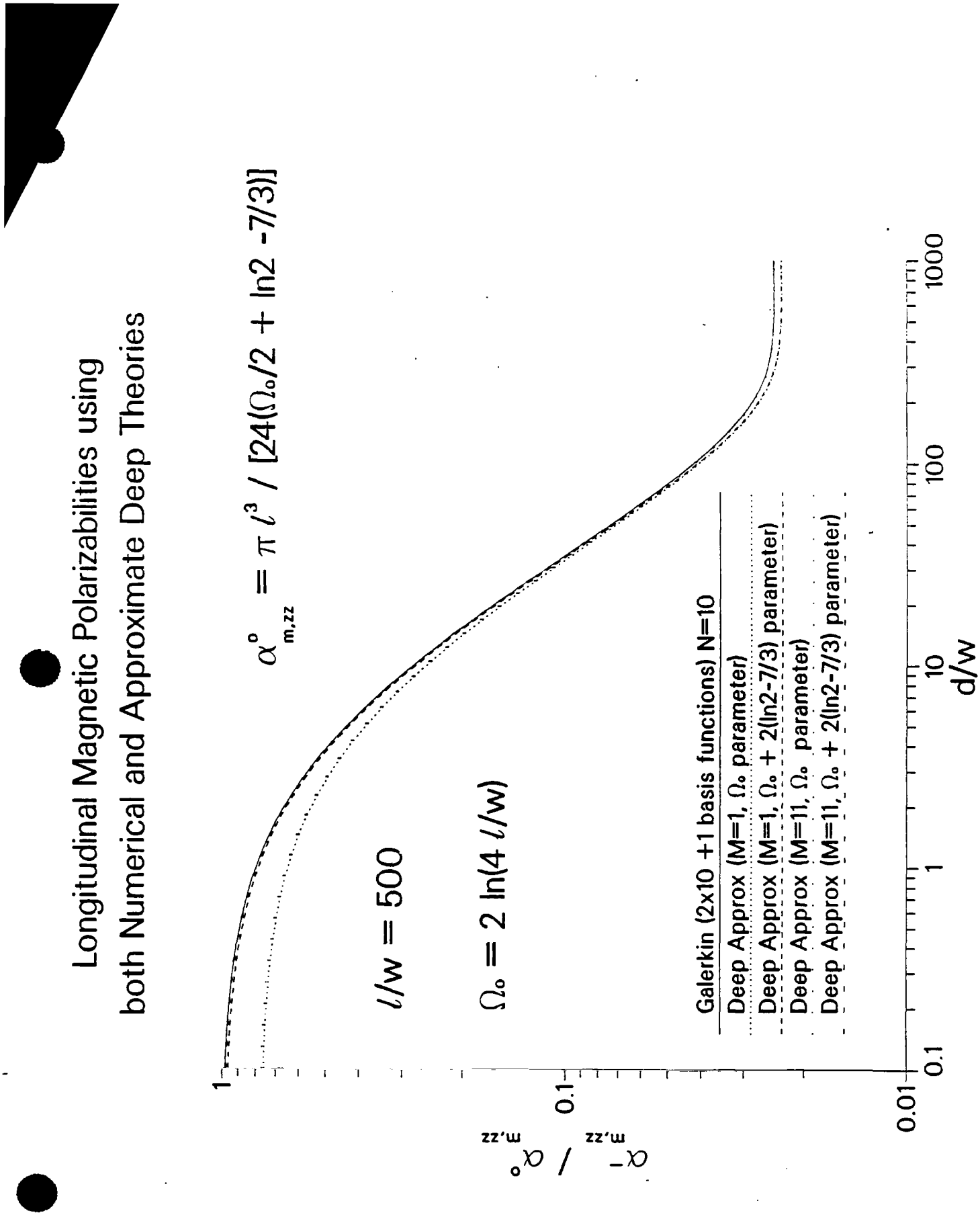

Figure 27. Same as Figure 24 except $\ell/w = 500$ and N = 10 in the Galerkin results. a) Incident side.

b) Transmitted side.

Longitudinal Magnetic Polarizabilities using both Numerical and Approximate Deep Theories

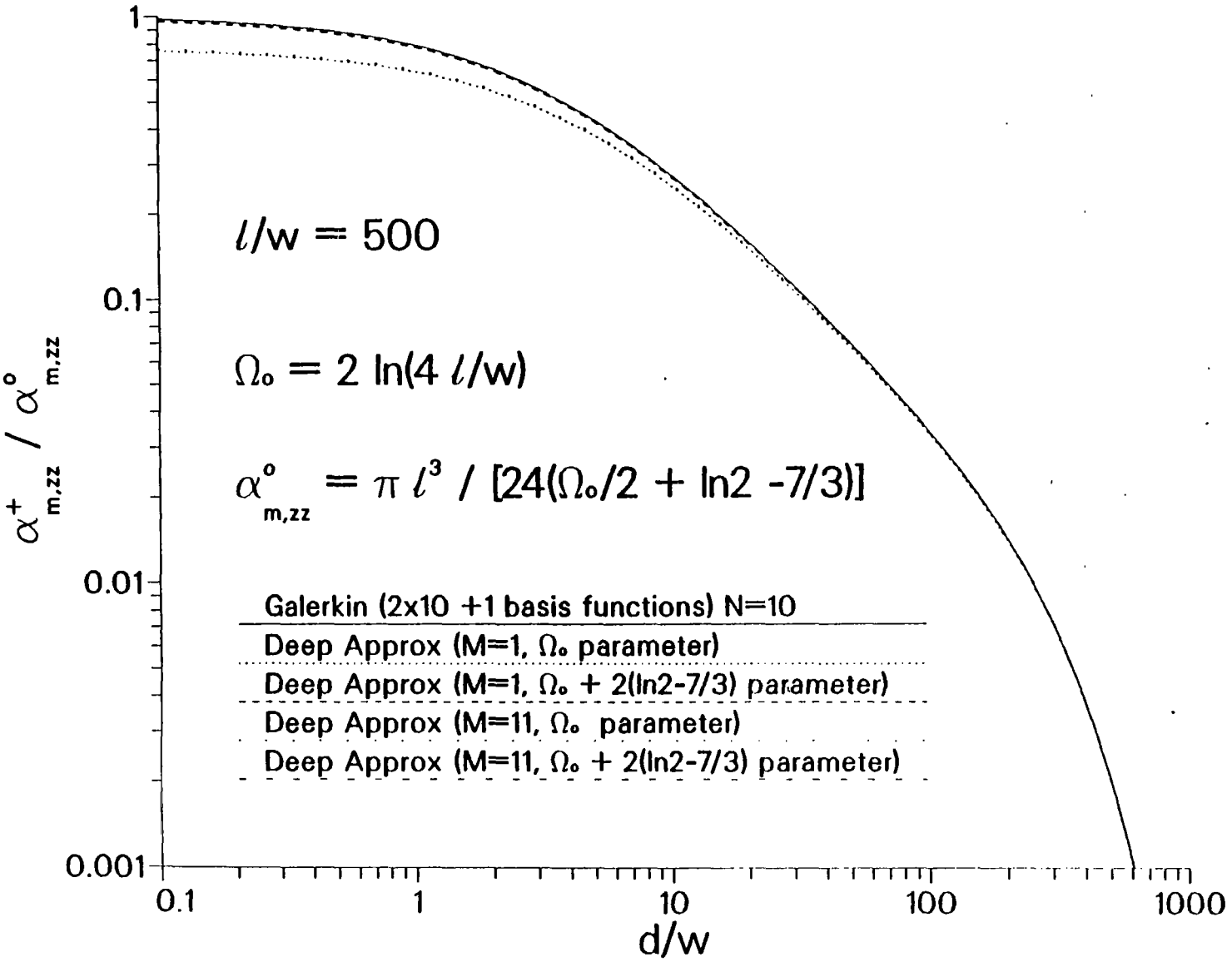

parameter, the heuristic results (138) and (139) including terms $m \leq M = 11$ with Ω_o expansion parameter, and the one term $m = M = 1$ approximations (142) and (143) with expansion parameter Ω_o. These graphs give the axial polarizabilities $\alpha^{\pm}_{m,zz}$ normalized by the first order polarizability for zero depth denoted by $\alpha^{o}_{m,zz}$. Note that the Deep equivalent radius has been taken as the approximate exterior Thin value (185) in all graphs. The basis function length Δ has again been maintained larger than approximately $4a_o$ in the graphs.

Note the good agreement of the analytical results based on the expansion parameter Ω'_o with the Galerkin solutions. The rather small, but noticeable, discrepancy of (194), for the Very Deep limit $\frac{d}{\ell} >> 1$, is explained by the discussion below (149). Nevertheless, the reasonable accuracy and simplicity of (194) and (195) distinguish them as very useful uniformly valid approximations. If greater accuracy is required than that provided by (194), a second term can be included from (192).

Figures 28 through 31 show a comparison of the Deep approximate results from (194) and (195), the Thick result (86), the Very Deep approximations (196) and (197) with expansion parameter Ω'_o, and the Very Deep (interior only) results (146) and (147). It is interesting that a crude, uniformly valid approximation is provided by an appropriate combination of the Thick and Very Deep results, switching between the two at, say, the intersection point of $\alpha^{-}_{m,zz}$

$$w\,\Omega'_o/2 \approx \ell - \pi\, d \quad . \qquad (209).$$

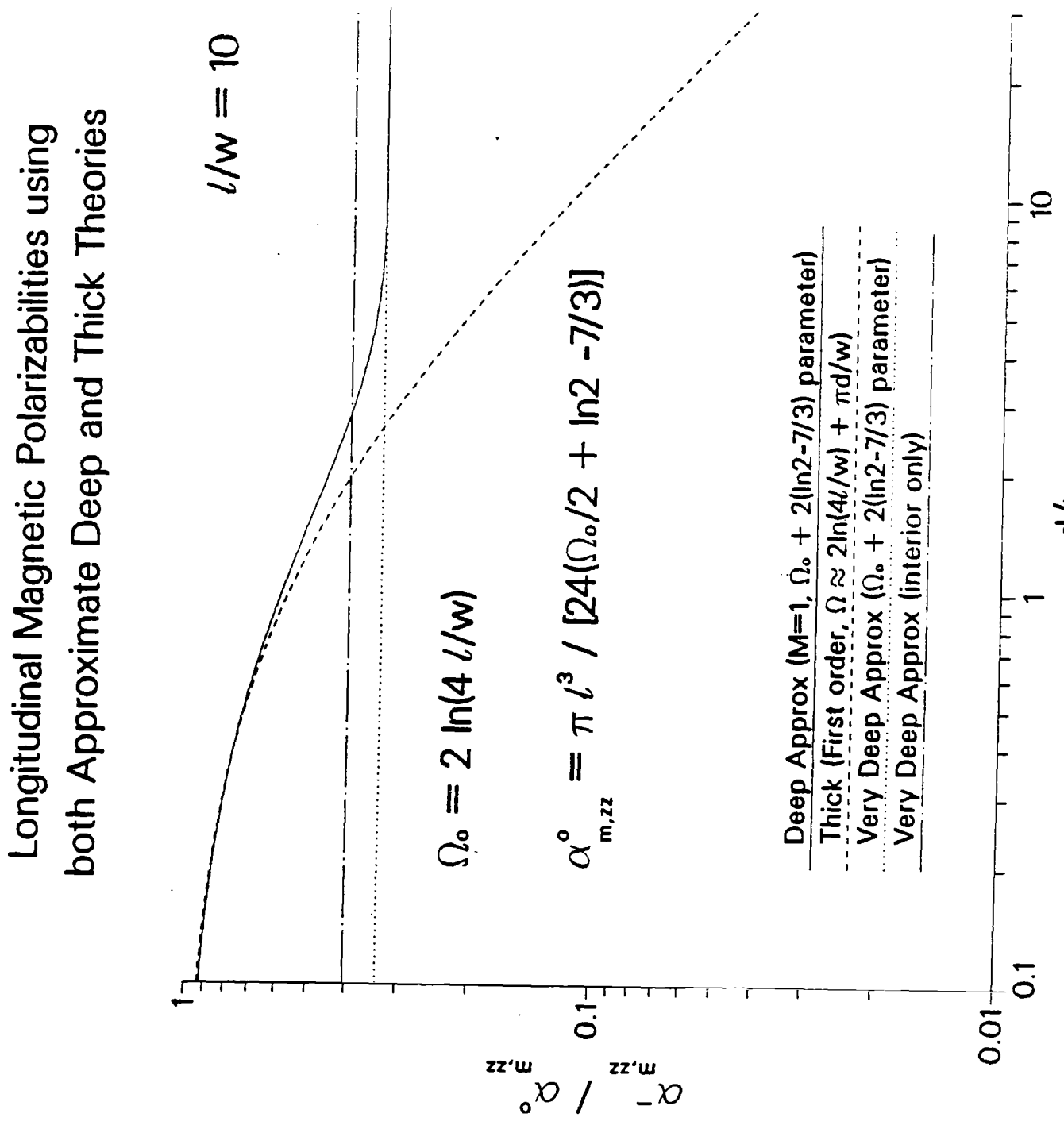

Figure 28. Longitudinal magnetic polarizabilities for the Deep case for $\ell/w = 10$. The zero order, one mode, result with expansion parameter $\Omega_o' = \Omega_o + 2(\ell n\ 2 - 7/3)$ (solid curve), the Thick result (dashed curve), the one mode Very Deep result with expansion parameter Ω_o' (dotted curve), and the one mode Very Deep result including only the slot interior (dash–dot curve), are compared. All curves are normalized by the first order zero depth result. a) Incident side.

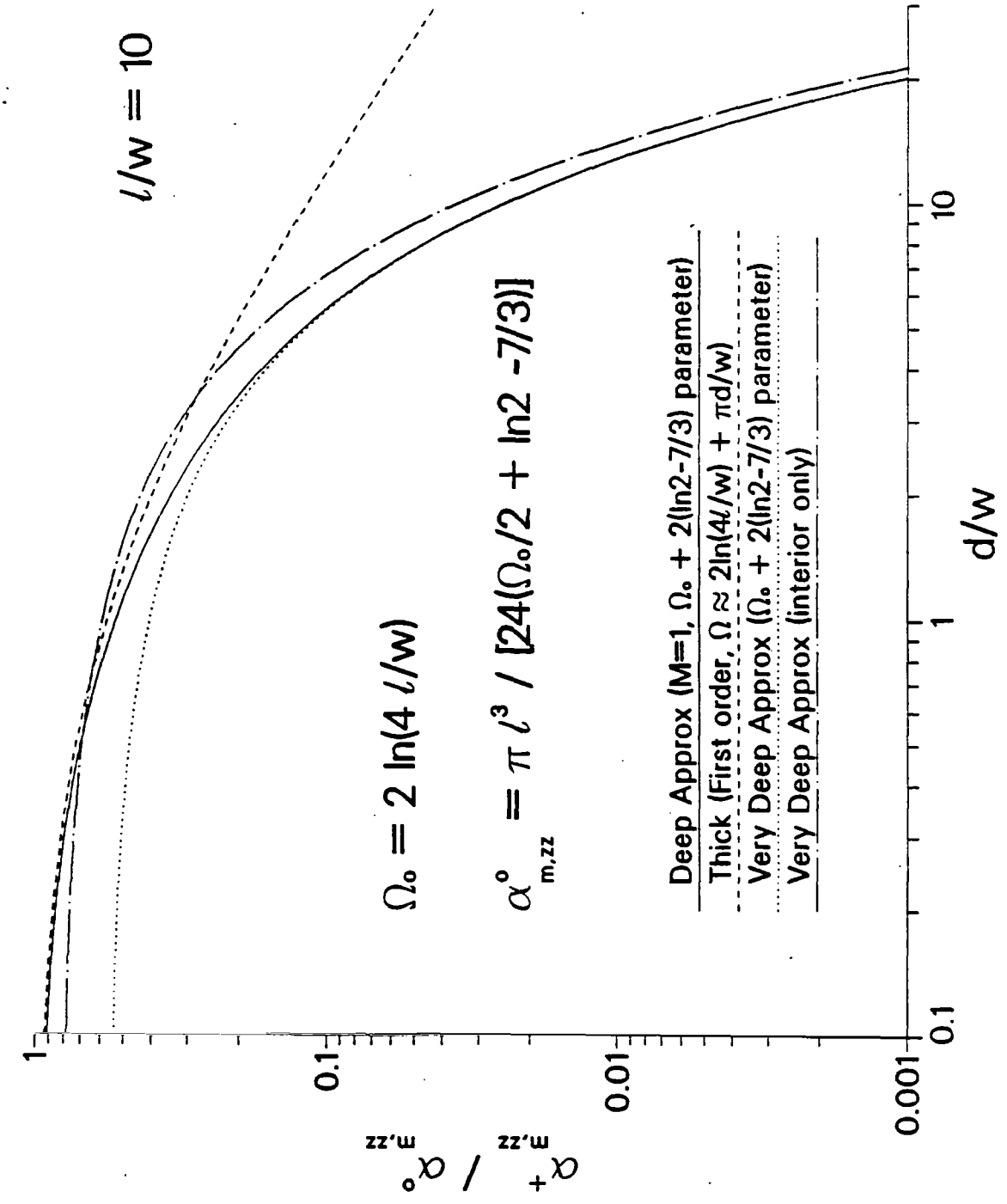

b) Transmitted side.

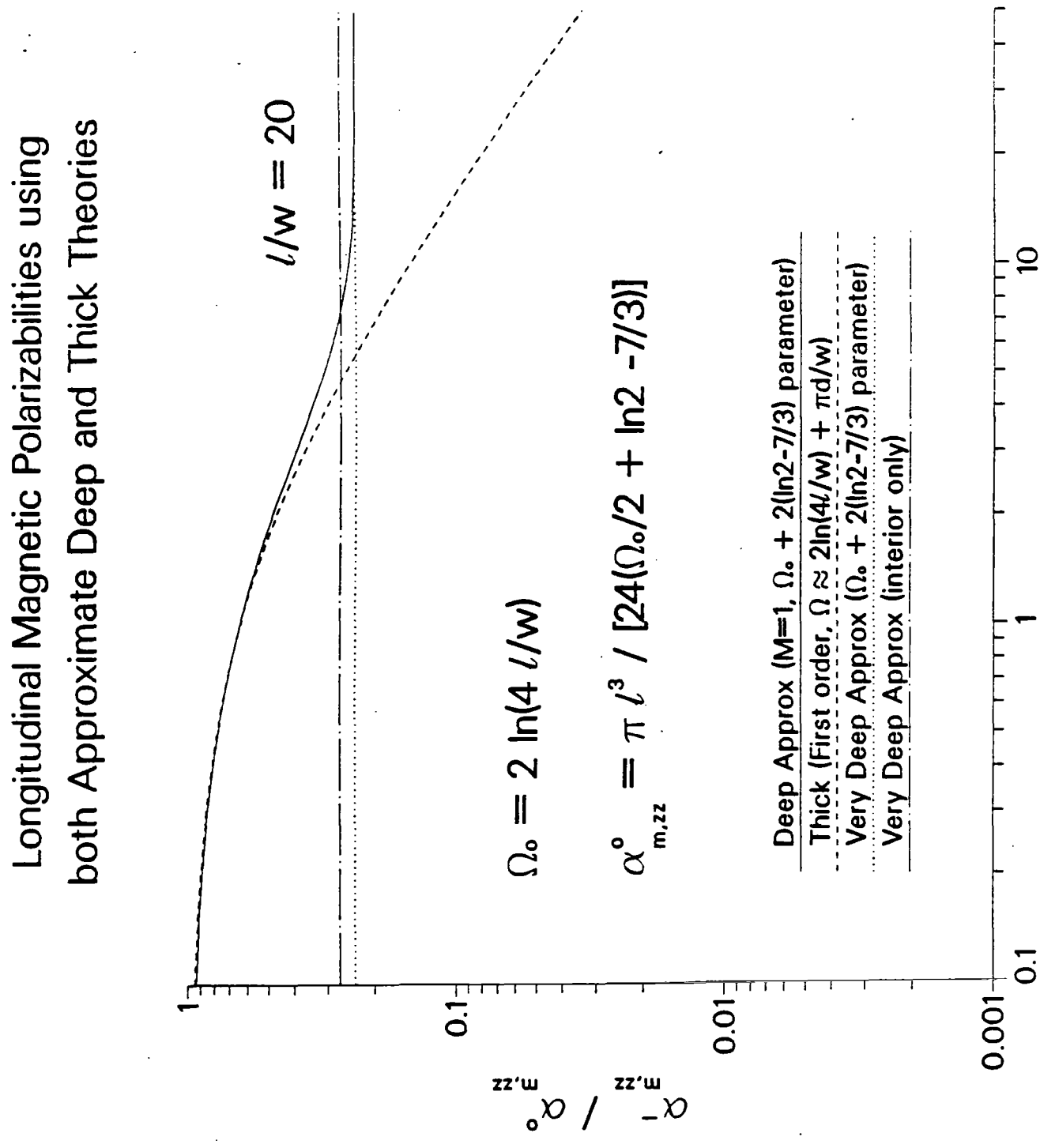

Figure 29. Same as Figure 28 except $\ell/w = 20$. a) Incident side.

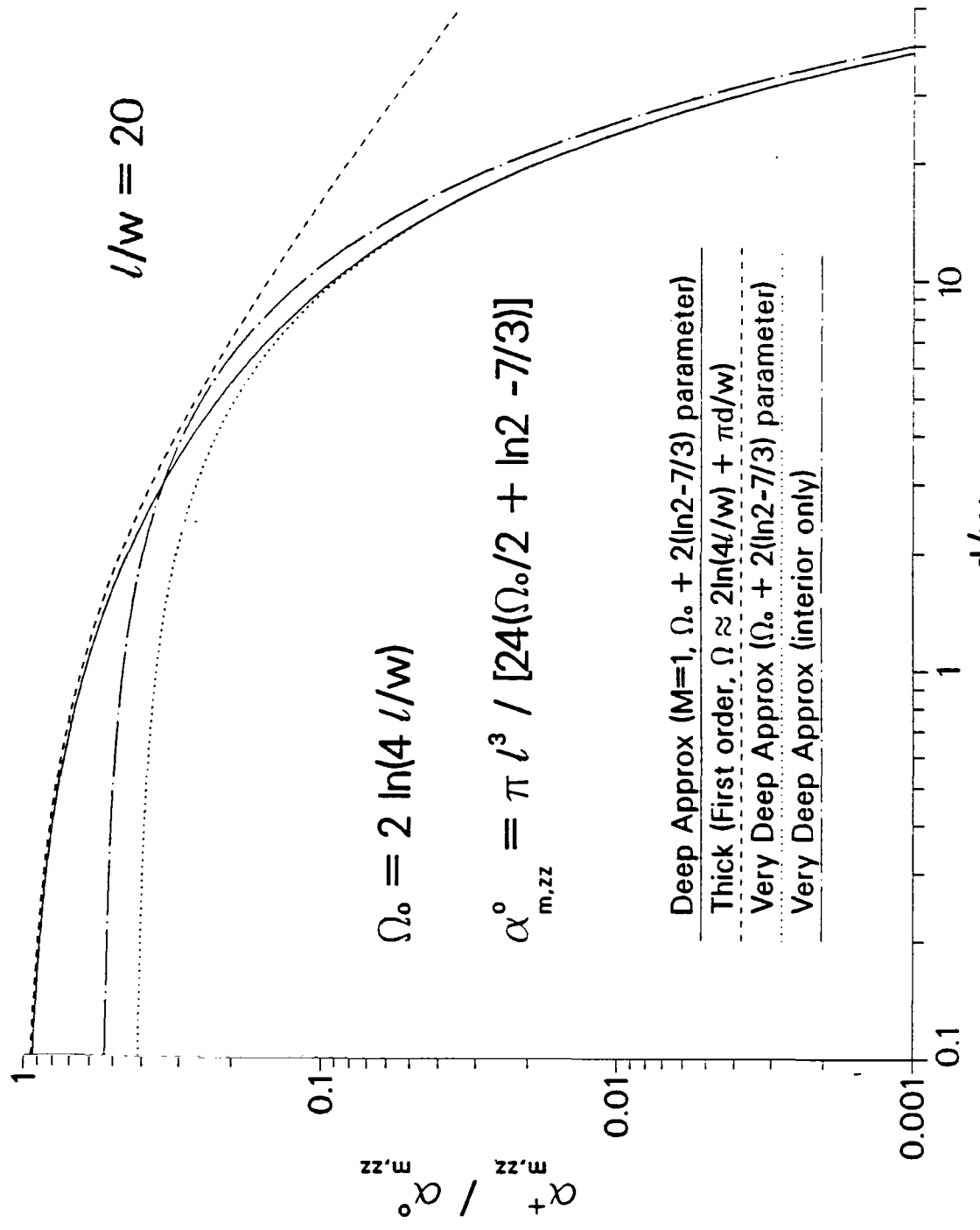

b) Transmitted side.

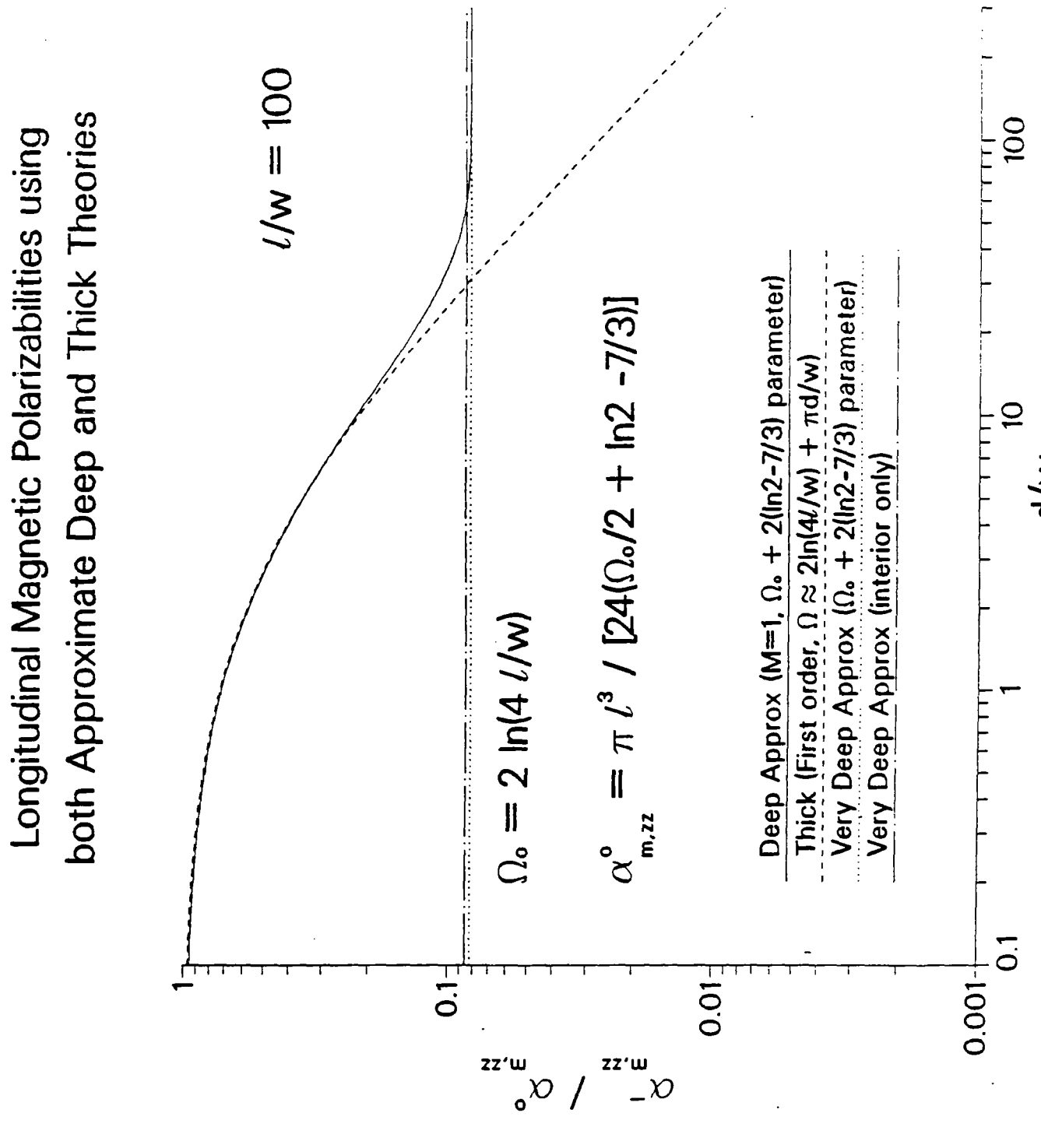

Figure 30. Same as Figure 28 except ℓ/w = 100. a) Incident side.

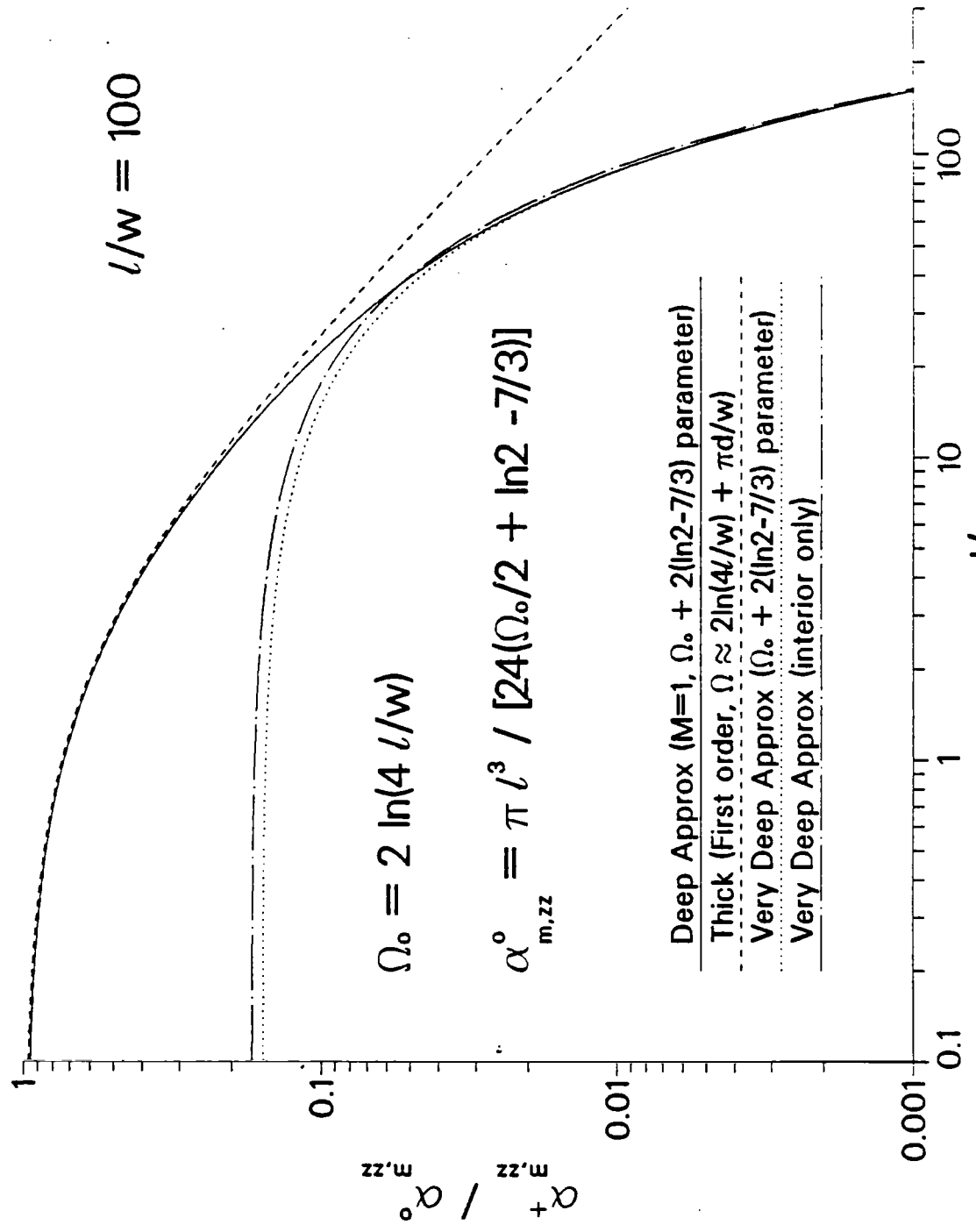

b) Transmitted side.

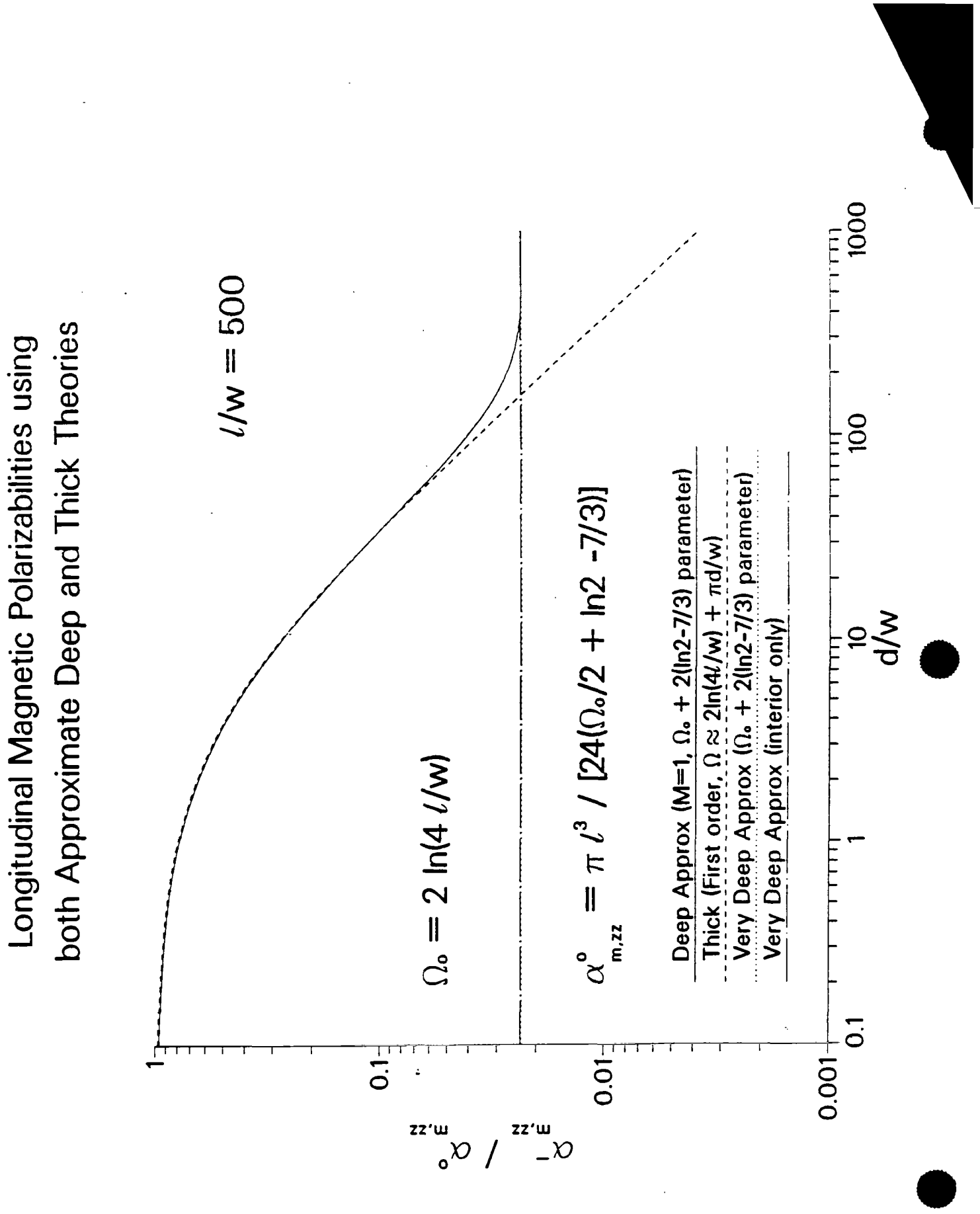

Figure 31. Same as Figure 28 except ℓ/w = 500. a) Incident side.

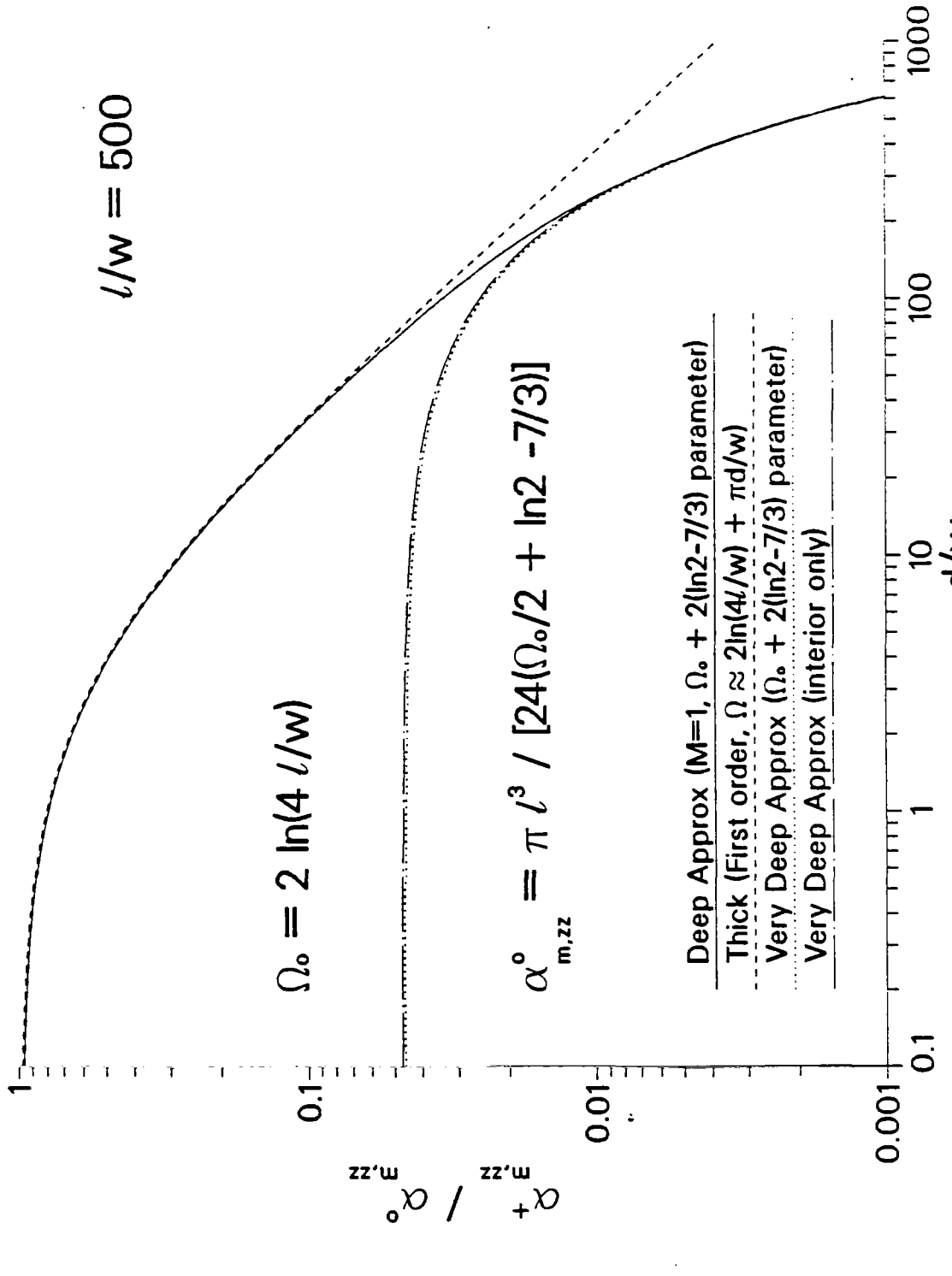

b) Transmitted side.

XI. CONCLUSIONS

The polarizabilities of a rectangular slot aperture of width w, depth d, and length ℓ. have been estimated when the slot is narrow $\ell >> w$.

The Thick case $\ell >>$ d,w is for the most part described by an equivalent antenna radius given by (75) through (78). The magnetic charge per unit length, and hence the dominant axial magnetic polarizability, is determined by solving Hallén's integral equation (60). A simple method of deriving this integral equation has been introduced in Section III. The axial polarizability is given to first order in Ω, see (80) and (81), by equation (86). This result is quite accurate as demonstrated by the numerical comparisons in Figures 12 through 14. It has been noted in Figures 16 through 18, taken from [1], that the equivalent radius concept provides an immediate generalization of existing zero depth hatch aperture polarizability formulas to the Thick case. The smaller transverse polarizabilities are given by the slot length times the line polarizabilities given in (115) through (122).

The Deep case ℓ,d >> w is described by integral equations (168) through (172) with equivalent radius (183). The Very Deep case d >> $\ell >>$ w is described by integral equations (173) and (174). A simple derivation of these integral equations is introduced in Section VIII. It is argued in Section IX that these integral equations provide a uniformly valid approximation for $0 \leq d < \infty$ if the approximate exterior equivalent radius (185) is used instead of (183). Using the accurate exterior expansion parameter (189) (see (141) for Ω_o), a simple zero order calculation yields the axial magnetic polarizabilities (192) and (193). The first terms of these sums, (194) and (195), provide reasonably accurate approximations for the axial polarizabilities as demonstrated by the comparisons with the numerical solutions given in Figures 24 through 27. The one term

Very Deep approximations, (196) and (197), and the Very Deep approximations, including only the interior waveguide region, (146) and (147), are compared with the one term Deep approximations in Figures 28 through 31. It is interesting, from these figures, that a crude, uniformly valid approximation is provided by a combination of the Thick and Very Deep results switching at the intersection point of the incident polarizabilities (209).

REFERENCES

[1] K. S. H. Lee, editor, EMP Interaction: Principles, Techniques, and Reference Data. New York: Hemisphere Pub. Corp., 1986.

[2] L. K. Warne and K. C. Chen, "Electromagnetic Penetration of Narrow Slot Apertures Having Depth," AFWL Interaction Note 464, April 1988.

[3] L. K. Warne and K. C. Chen, "Relation Between Equivalent Antenna Radius and Transverse Line Dipole Moments of a Narrow Slot Aperture Having Depth," IEEE Transactions on Electromagnetic Compatibility, Vol. 30, No. 3, August 1988.

[4] H. Kaden, Wirbelstrome und Schirmung in der Nachrichtentechnik. Berlin: Springer–Verlag, 1959, pp 236–254.

[5] L. D. Landau, E. M. Lifshitz and L. P. Pitaevskii, Electrodynamics of Continuous Media, New York: Pergamon, 1984, p17.

[6] E. C. Jordan and K. G. Balmain, Electromagnetic Waves and Radiating Systems. Englewood Cliffs, New Jersey: Prentice–Hall, Inc., 1968, Section 11.13.

[7] L. A. Vainshtein, "Symmetric Electric Oscillations of a Perfectly Conducting Hollow Cylinder of Finite Length II. Numerical Results for a Passive System," Soviet Physics – Technical Physics, Vol. 12, No. 7, January 1968, pp 857–862.

[8] F. Oberhettinger, Fourier Expansions. New York: Academic Press, 1973, p 20.

[9] S. Flugge, editor, Elektrische Felder Und Wellen. Handbuch Der Physik Band XVI. Berlin: Springer Verlag, 1958, p 75.